HISTONE METHYLATION AND METHYLTRANSFERASE ENZYME SET8 IN HEPATOCELLULAR CARCINOMA

A THESIS SUBMITTED TO
THE DEPARTMENT OF MOLECULAR BIOLOGY AND GENETICS
AND THE INSTITUTE OF ENGINEERING AND SCIENCE OF
BILKENT UNIVERSITY
IN PARTIAL FULFILLMENT OF THE REQUIREMENTS
FOR THE DEGREE OF
MASTER OF SCIENCE

BY
EYLÜL HARPUTLUGİL
AUGUST 2010

I certify that I have read this thesis and that in my opinion it is fully adequate, in scope and in quality, as a thesis for the degree of Master of Science.

Prof. Dr. Mehmet Öztürk

I certify that I have read this thesis and that in my opinion it is fully adequate, in scope and in quality, as a thesis for the degree of Master of Science.

Assist. Prof. Dr. Ali Osmay Güre

I certify that I have read this thesis and that in my opinion it is fully adequate, in scope and in quality, as a thesis for the degree of Master of Science.

Assoc. Prof. Dr. Hilal Özdağ

Approved for the Institute of Engineering and Science

Director of Institute of Engineering and Science
Prof. Dr. Levent Onural

ABSTRACT

HISTONE METHYLATION AND METHYLTRANSFERASE ENZYME SET8 IN HEPATOCELLULAR CARCINOMA

Eylül Harputlugil
MSc. in Molecular Biology and Genetics
Supervisor: Prof. Dr. Mehmet Öztürk
August 2010, 83 Pages

Hepatocellular carcinoma (HCC) is one of the most prevalent and lethal cancers worldwide. The epigenetic modifications, which are involved in virtually all cellular processes are also involved in the carcinogenic process, and this is a growing new field of investigation. HCC has also been associated with several epigenetic aberrations which include the ones in histone modifications, histone methyltransferase enzymes, and the epigenetic machinery. The transition from cirrhosis to HCC is related to senescence bypass, and the distinctions between senescence and immortality in HCC cell lines. Global levels of H3K4me3, H3K9me3, H3K27me3, H3K36me3, H3R2me2, H3R17me2 and H4K20me3 histone marks were evaluated in well-differentiated and poorly differentiated HCC cell lines in the presence and absence of TGF-β induced senescence. No prominent changes in the levels of these histone modifications were indentified in response to TGF-β induced senescence. However, H4K20me3 levels appeared to correlate with the differentiation status of the cell lines, where a loss of methylation was observed in poorly differentiated cell lines. In order to address the mechanism of this loss, H4K20 specific methyltransferases were analyzed in terms of their transcript levels, and only the expression pattern of monomethyl transferase Set8 was found to correlate with the H4K20me3 methylation patterns. A potential role played by Set8 in HCC development was investigated via overexpression and knockdown studies. But no significant role could be attributed to this enzyme in this study.

ÖZET

KARACİĞER KANSERİNDE HİSTON METİLASYONU VE METİLTRANSFERAZ ENZİMİ SET8

Eylül Harputlugil
Moleküler Biyoloji ve Genetik Yüksek Lisansı
Tez Yöneticisi: Prof. Dr. Mehmet Öztürk
Ağustos 2010, 83 Sayfa

Karaciğer kanseri (Hepatoselüler Karsinom, HSK), dünya genelindeki en yaygın ve ölümcül kanser türlerinden biridir. Hücredeki hemen hemen her olayda rol oynayan epigenetik değişimler, kanser oluşumunda da etkilidir, ve bu araştırma alanı giderek genişlemektedir. HSK da, histon modifikasyonları, histon metiltransferaz enzimleri ve epigenetik mekanizmadaki bozuklukları da içeren çeşitli epigenetik bozukluklar ile özdeşleştirilmiştir. Sirozdan karaciğer kanserine geçiş, hücre yaşlanması (senesans) durumunun aşılması ile ilintilidir, ve bu durum hücre hattı modellerinde görülen ölümsüzlük ve hücre yaşlanması durumları arasındaki farklar ile de ilişkilendirilmiştir. H3K4me3, H3K9me3, H3K27me3, H3K36me3, H3R2me2, H3R17me2 ve H4K20me3 histon işaretlerinin global seviyeleri, iyi diferansiye ve kötü diferansiye hücre hatlarında, ölümsüzlük ve TGF-β tarafından indüklenen hücre yaşlanması durumlarında incelenmiştir. TGF-β'nın indüklediği hücre yaşlanması durumunda, sözü edilen histon işaretlerinde göze çarpan bir değişiklik görülmemiştir. Buna karşın, H4K20me3 seviyelerinin hücrelerin farklılaşma durumu ile ilişkisi olduğu, ve kötü diferansiye hücre hatlarına özgü bir kayba uğradıkları saptanmıştır. Söz konusu kaybın mekanizmasını araştırmak amacıyla, H4K20 rezidüsüne özgü metiltransferazların tüm izoformlarının ifade seviyeleri hücre hatlarında incelenmiş, ve yalnızca Set8 enziminin ifade düzeninin H4K20 trimetilasyon düzeni ile örtüştüğü tespit edilmiştir. Set8 enziminin hepatoselüler karsinom oluşumunda oynadığı olası bir rolü araştırmak amacıyla enzimin ifadesini arttıran ve susturan çalışmalar yapılmıştır. Ancak sözü edilen çalışmalar sonucunda Set8 enzimine bu konuda anlamlı bir görev atfedilememiştir.

TO MY FAMILY

ACKNOWLEDGEMENTS

First of all, I would like to thank my supervisor, Prof. Dr. Mehmet Öztürk for his guidance throughout the project. He is a great scientist, and it was a privilege to work in his laboratory.

I would also like to thank Assoc. Prof. Dr. Rengül Çetin Atalay, Assoc. Prof. Dr. İhsan Gürsel and Tamer Kahraman, Assoc. Prof. Dr. Esra Erdal and İmge Kunter from 9 Eylül University, for providing me experimental support.

It was great to have people like Füsun Elvan, Bilge Kılıç and Abdullah Ünnü in the lab, with their invaluable help, they made life a lot easier.

All past and present members of our group, especially Gökhan Yıldız, Haluk Yüzügüllü, Özge Yüzügüllü, Tülin Erşahin, Ebru Bilget Güven, Mustafa Yılmaz, Şerif Şentürk, İrem Durmaz, Dr. Ayça Arslan Ergül, Dr. Sevgi Bağışlar, Dr. Mine Mumcuoğlu and Suna Pelin Gülay have been a wonderful help in the laboratory and also great friends outside.

I would like to thank all of my friends, especially İrem Gürbüz, Nilüfer Sayar and Gurbet Karahan for their endless support whenever I needed anything.

This master thesis work was supported by grants from TÜBİTAK and DPT to Mehmet Öztürk. Additionally, I was personally supported by TÜBİTAK, through BIDEB 2210 scholarship.

TABLE OF CONTENTS

LIST OF TABLES

LIST OF FIGURES

CHAPTER 1. INTRODUCTION

1.1. HEPATOCELLULAR CARCINOMA

More than 80 % of liver cancers arise from hepatocytes or hepatocyte progenitors, which are the parenchymal cells of the liver (American Cancer Society, Facts and Figures 2010). These cancers are accordingly named as hepatocellular carcinoma (HCC). HCC is highly frequent, being the fifth most frequent cancer worldwide, and has increasing rates of incidence and mortality in the West since 1980s (Bruix, J et al, 2004). HCC is also an important cause of cancer related death, with a 5 year relative survival rate of 14 % (American Cancer Society, 2010).

1.1.1 Aetiologies of hepatocellular carcinoma

There are several aetiological factors that have been associated with hepatocarcinogenesis, which include: chronic alcohol abuse, Aflatoxin B1 exposure; which might occur by the consumption of contaminated food, chronic HBV or HCV infections, non-alcoholic fatty liver disease; which is also associated with obesity, long-term oral contraceptive use in women, diabetes, and finally certain metabolic disorders such as hereditary haemochromatosis (Badvie S, et al, 2000; Farazi PA, et al, 2006). The most prevalent risk factors of HCC are variable due to regionality, for example chronic HBV and HCV infections are the major risk factors worldwide, whereas these cases constitute less than half in the US. In most western countries, the major risk factors of hepatocarcinogenesis are alcoholic cirrhosis and obesity related non-alcoholic fatty liver disease (American Cancer Society, 2010).

1.1.2 Pathogenesis of hepatocellular carcinoma

Molecular mechanisms leading to the development of HCC are quite variable, representing the variability of HCC aetiology, which results in high genetic and phenotypic heterogeneity of these tumors. HCC development occurs in chronically injured livers, in a multi-step process (Feo F, et al, 2009). Liver injury might result from one or more of the major HCC risk factors, such as chronic Hepatitis B Virus (HBV) or Hepatitis C Virus (HCV) infections, alcohol-related cirrhosis, Aflatoxin B1 exposure, or genetic disorders. The initial liver injury manifests itself as necrosis, which is followed by continuous cycles of proliferation and damage. On the one hand, these continuous cycles of proliferation and necrosis cause telomere shortening, which eventually result in hepatocyte proliferative arrest. On the other hand, liver injury provokes activation of stellate cells, which play role in the synthesis and deposition collagen. Both of these contribute to the formation of abnormal liver nodules, together with fibrous scar tissue, a state which is called cirrhosis (Feo F, et al, 2009; Farazi PA, et al, 2006). Formation of hyperplastic nodules is the next step in the pathogenesis of HCC, which are still considered as pre-malignant lesions. Together with the accumulation of genetic damage, leading to moderate genomic instability, these pre-malignant lesions progress into dysplastic nodules which have the ability of autonomous growth. Dysplastic nodules are composed of cells with altered characteristics such as increased nuclear to cytoplasmic ratio, and they tend to form mild trabecular disarrays (Feo F, et al, 2009).

Where telomere shortening is associated with chronic liver disease and cirrhosis as mentioned, telomerase reactivation is an important characteristic of HCC, together with notable genomic instability and either mutation or loss of p53 tumor suppressor. Although, the specific stages at which these changes occur is not clear, aided with these molecular changes, dysplastic nodules evolve progressively into different stages of hepatocellular carcinoma (Farazi PA, et al, 2006). HCC can be classified into four different stages, namely: well differentiated, moderately differentiated, poorly differentiated and undifferentiated. Generally, HCC arises as a well

differentiated cancer, which then dedifferentiates into the other stages through a stepwise process (Kojiro M, 2005; Yuzugullu H, et al, 2009).

1.1.3 Cellular senescence

The term senescence means "becoming old" in the general sense, and it is associated with certain morphological and gene-expression related features. The inability of cell strains to grow indefinitely in culture was first described by Hayflick, who used the term "cellular senescence" (Weinberg RA, The Biology of Cancer). Replicative senescence is characterized by irreversible cell cycle arrest due to telomere shortening, and in addition to that, there are also other immature senescence types which occur due to stress and damage (Ozturk M, et al, 2009). These stress and damage conditions that are known to induce senescence include oncogenic stress, which results in oncogene induced senescence (Bartkova J, et al, 2006; Di Micco R, et al, 2006; Mallette FA, et al, 2007) and oxidative stress, which results in Reactive Oxygen Species (ROS) induced senescence. Additionally, exposure to certain signaling molecules have also been shown to induce senescence, such as TGF-β or β-interferon in various cell types (Senturk S, et al, 2010; Moisseva O, et al, 2006).

Senescent cells exhibit certain characteristic features such as senescence-associated β-galactosidase (SABG) activity at pH 6.0, altered morphology resulting in diverse morphotypes and usually bigger cells, formation of senescence-associated DNA damage foci and senescence associated heterochromatin foci, chromosomal aberrations and polyploidy, and alterations in the expression of several genes. Although they all involve different mechanisms, all senescence pathways converge on the DNA damage response (DDR) (Ozturk M, et al, 2009). In telomere dependent senescence pathway, unprotected telomere ends resulting from telomere shortening are sensed as DNA damage. In oncogene induced senescence pathway, hyper-replication of cells which is promoted by the oncogenes result in accumulation of DNA replication errors. And finally in ROS induced senescence pathway, reactive oxygen species directly cause DNA damage themselves. Therefore, persistent DNA

damage and DDR is of pivotal importance in all senescence pathways. The DNA damage response involves activation of signaling cascades that involve the actions of ATM/ATR and CHK1/CHK2, and converge on p53 protein, which acts through $p21^{cip1}$ cyclin dependent kinase inhibitor (CDKI) activation. Alternative pathways converge on $p16^{INK4a}$ and $p15^{INK4b}$ CDKIs. Both CDKI pathways lead to the activation of retinoblastoma protein (pRb), which then plays role in the arrest of cell cycle, and thus senescence phenotype occurs (Ozturk M, et al, 2009; Senturk S, et al, 2010).

1.1.4 Senescence and hepatocellular carcinoma

Like most of the human somatic cells, hepatocytes normally do not have telomerase activity and they do not proliferate rapidly. The continuous rounds of cell division and damage cycles which pave the way to chronic liver injury and cirrhosis also play role in the shortening of telomeres. Therefore, cellular senescence which is associated with hepatocyte telomere shortening is a general characteristic of liver cirrhosis. This was illustrated by SABG staining in normal and cirrhotic livers, which revealed 84 % senescent cells in cirrhosis as opposed to only 10 % in normal liver (Wiemann SU, et al, 2002). However, in order to undergo malignant transformation, cells have to find a way to regain their ability to proliferate, and to maintain their telomeres while doing so. In that context, cellular senescence acts as a barrier in front of malignant transformation of hepatocytes to hepatocellular carcinoma. This was also supported by a study which showed 60 % SABG staining in HCC samples (Paradis V, et al, 2001).

Numerous genetic and epigenetic aberrations have been associated with hepatocarcinogenesis, that effect important actors of senescence induction, therefore help the cells to overcome the senescence barrier. These aberrations include inactivating mutations of p53, which is frequently observed in HCC (Soussi, T, 2007). Despite the lack of frequent mutations, CDK inhibitor $p16^{INK4a}$ is epigenetically silenced in half of the HCCs through promoter methylation (Ozturk

M, et al, 2009). According to a study which analyzed molecular aberrations in HCC samples from different aetiological backgrounds, 83 % of the analyzed HCC samples displayed alterations in the pRb pathway components, 31 % displayed alterations in p53 pathway components, and 30 % displayed both (Edamoto Y, et al, 2003; Ozturk M, et al, 2009).

Taken as a whole, the aberrations explained above are likely to play an important role in overcoming the senescence barrier, together with the possible involvement of telomerase reactivation. Molecular understanding of the mechanisms that drive senescence, senescence bypass, and senescence induction in cancer cells is very important since senescence induction is considered as a potential new area of anti-cancer therapy. A recent study by our group described the molecular mechanisms of TGF-β induced senescence in HCC cell lines, and showed that the specific senescence program was dependent on $p21^{Cip1}$ and $p15^{INK4b}$, but independent from p53 and $p16^{INK4a}$ (Senturk S, et al, 2010).

1.2. EPIGENETIC CHANGES AND HEPATOCELLULAR CARCINOMA

Although originally defined in a different context, the term epigenetics is currently used to mean heritable changes in the DNA or its associated proteins, which is independent from the DNA sequence information (Feinberg AP, et al, 2010). Mechanisms of epigenetic control include DNA methylation, covalent histone modifications and involvement of histone variants in the chromatin structure, which actively take role in an interplay. These factors, together with chromatin remodeling complexes and non-coding RNAs, play role in the determination of the chromatin structure. They interact in order to attain nuclear compartmentalization, as well as to establish heterochromatic and euchromatic regions of the chromatin. Epigenetic control has been shown to be involved in virtually all biological processes, which vary from embryogenesis, and cellular differentiation to learning, memory and aging (Delcuve GP, et al, 2009). As can easily be seen from this fact, errors which occur during the establishment or maintenance of the epigenetic codes play role in the

development of various diseases including cancer. Since epigenetic codes are more versatile in comparison to the genetic code, it is important to understand the mechanisms involved in the formation and upholding of these codes, in order to be able to reverse such errors, which makes epigenetic therapy an attractive new field.

1.2.1 DNA methylation

In the human genome, most of the CpG dinucleotides are methylated at the C^5 position of cytosine bases, which is commonly referred to as DNA methylation. About 50 % of the CpG dinucleotides are concentrated in promoter regions, as well as 5' untranslated regions of genes, and the remaining 50 % is located in the intragenic regions or the gene bodies (Delcuve GP, et al, 2009). These regions with concentrated CpG dinucleotides are referred to as CpG islands. DNA methylation which occurs in the CpG islands at gene promoters has generally been associated with gene silencing, in contrast to the DNA methylation in gene bodies, which might be involved in transcriptional activation (Hellman A, et al, 2007). Additionally, CpG island methylation is also observed in repetitive DNA sequences and transposable elements, and it might play a role in preventing translocations (Esteller, M, 2007).

Cancer development involves two type of aberrant DNA methylation processes, both hypermethylation and hypomethylation. The better established mode of DNA methylation alteration observed in various cancers is DNA hypermethylation found in the promoter regions in several tumor suppressors, which results in silencing of those genes. This process is responsible, at least in part, for escaping from apoptosis, loss of cell adhesion and angiogenesis, which are common features of tumors (Herceg Z, 2007). Although the direct mechanism of action has not been well established, global hypomethylation is observed in almost all types of cancers. It is hypothesized that global hypomethylation might act through several mechanisms which include: loss of imprinting, inappropriate cell type expression, genome vulnerability or the activation of endoparasitic sequences (Esteller, M, 2007).

Studies have revealed that promoter hypermethylation of tumor suppressor genes is an early event in hepatocellular carcinogenesis, given that it has been observed in non-cancerous liver tissues. The genes that have been shown to be silenced via promoter hypermethylation in HCC include: $p16^{INK4a}$, DLC1, E-Cadherin, PTEN, and many others (Wong CM, et al, 2007).

1.2.2 Histone variants and genomic imprinting

Genomic imprinting is an epigenetically regulated phenomenon, which is observed in a limited set of genes, where genes exhibit expression differences depending on whether they are paternally or maternally inherited (Jelinic P, et al, 2007). Genes which are subject to genomic imprinting appear in clusters, and the expression from those genes is coordinately regulated by imprinting control centers. DNA methylation is observed in only one allele in imprinting control centers, depending on which allele is to be expressed, additionally covalent histone modifications and recruitment of non conventional histone variants are involved in the process (Delaval K, et al, 2004). This heterochromatin structure is established in embryonic stages, and maintained in the adult organism, misregulation of which might result in loss of imprinting: one of the accepted hallmarks of cancer (Jelinic P, et al, 2007).

Genes which are subject to genomic imprinting usually have functions in embryonic development, placenta formation and adult metabolism. Some of the best studied examples of these genes include: Igf2, H19, Igf2R and Kvlqt. H19 imprinting control center is located at chromosome 11p15.5, and is responsible for the expression from Igf2 and H19 genes, which have opposite monoallelic expression (Matouk IJ, et al, 2007). Igf2 gene codes for a fetal growth factor, and H19 codes for a non translated RNA message, and anomalies of both have been associated with the pathogenesis of HCC (Boyault S, et al, 2007). In a study which compared normal liver and HCC samples, it was shown that around 40 % of the studied HCC samples displayed

abnormal genomic imprinting in at least one of these two genes, which was manifested as biallelic expression due to loss of imprinting (Wu J, et al, 2008).

Histone variants, which are low expressed, non-allelic forms of the conventional histones, serve in providing specific structural and functional characteristics to the nucleosome (Talbert PB, et al, 2010). These characteristics include gene expression control, genomic imprinting, X-chromosome inactivation and DNA repair. For example, macro-H2A1 histone variant was shown to be enriched in the inactive X-chromosome, and imprinted loci such as the Igf2/H19 imprinting control center, whereas H2ABbd histone variant was implicated in promoting gene expression (Mietton F, et al, 2009; Sha K, 2008). More interestingly, histone variants have also been implicated in processes such as senescence, specifically macro-H2A histone variant nucleosomes were found to be enriched in senescence-associated heterochromatin foci, although it is not clear that the role played by this histone variant is causative (Zhang R, et al, 2005; Bushbeck M, et al, 2010). Additionally, low levels of macroH2A histone variant were found to be in correlation with high proliferation and bad prognosis in lung cancer (Bushbeck M, et al, 2010). Taken as a whole, these cases exemplify the potential importance of histone variants in cancer.

1.2.3 Covalent histone modifications

DNA is wrapped around octameric protein structures which consist of the four so called core histones: H2A, H2B, H3 and H4. The histone octamer has a globular domain, which functions in packaging the DNA, as well as free "tail" structures which protrude out from the N-terminal ends of histone proteins. These tail regions of histones are particularly of interest, due to the importance of diverse sets of covalent modifications that they can be subjected to. At least eight different types of such modifications have been described in no less than 60 different modification sites to date, which include: acetylation of lysines, methylation of lysine and arginines, phosphorylation of serine and threonines, ubiquitylation of lysines, sumoylation of lysines, deimination of arginines, ADP ribosylation of glutamic acids,

and finally proline isomerization, which are all associated with certain biological processes (Kouzarides T, 2007; Wang GG, et al, 2007). Among all these modifications, the best studied ones are acetylations, methylations and phosphorylations.

These modifications were shown to get involved in biological processes by two mechanisms. The first mechanism is interfering with nucleosome contacts, which results in disentanglement of the chromatin structure. The second and better characterized mechanism involves interacting with and recruiting certain proteins to the nucleosome, or oppositely, detaching certain proteins from the nucleosome. Hence, histone modifications are key players of the determination of the accessibility of the chromatin, and their involvement in cancer pathogenesis is a growing new field (Kouzarides T, 2007; Wang GG, et al, 2007).

1.2.3.1 Histone acetylations, acetyltransferase and deacetylase enzymes

Several lysine residues on histone H3 and H4 tails are subject to acetylation by numerous histone acetyltransferase enzymes (HATs), some of which are: HAT1, CBP/P300, PCAF/GCN5, TIP60 and HB01 (Kouzarides T, 2007). HATs are poorly specific for their histone and non-histone substrates in the sense that they are capable of acetylating multiple residues on histones, and they also have non-histone substrates including E2F, p53 and pRb (Yang XJ, et al, 2004; Wang GG, et al, 2007).

Since the acetylation status of histone tails is of crucial importance for the formation of chromatin architecture, as well as regulation of gene expression, it is easy to deduce that misregulation of HAT activity might be involved in pathological conditions. Accordingly, disruption and misregulation of several HATs have been associated with different cancers. Mechanistically, decreased levels of histone acetylation is thought to give rise to a more compact chromatin structure, and hence transcription factors and RNA polymerases cannot access the chromatin.

Importantly, loss of acetylation in histone 4 lysine 16 has been detected in repetitive DNA sequences in many primary tumors (Wang GG, et al, 2007). However, interestingly, both aberrant activation and inactivation of HDAC enzymes were observed in malignancies (Ellis L, et al, 2009).

Histone acetylation is dynamic, and can be reversed by histone deacetylase enzymes (HDACs) which have opposing roles with HATs. HDACs are likely to function in transcriptional repression since they decrease histone acetylation levels. There are more than 10 HDACs currently identified, and they are similarly misregulated in various cancer types (Ellis L, et al, 2009). Again similarly as the HATs, HDACs are also poorly specific for their histone and non-histone substrates. Instead, the general paradigm is that they gain specificity by interacting with proteins which carry HDACs to their specific localizations. In the recent years HDAC inhibitors have emerged as a new class of anticancer drugs showing potential. Although the mechanism of action of this new class of drugs in still incompletely described, it is known that they display a variety of cellular effects. Some of these effects are induction of apoptosis, differentiation and growth arrest (Wang GG, et al, 2007).

1.2.3.2 Histone methylations, methyltransferase and demethylase enzymes

Numerous lysine and arginine residues in the N-terminal tails of histone H3 and histone H4 are subject to methylation by histone methyltransferase enzymes (HMTs). All of these residues can have mono, di or trimethyl groups attached to them. Although it was long thought that histone lysine methylation is irreversible, it is now well established that lysine methylation is also dynamically regulated through several demethylase enzymes (Trojer P, et al, 2006; Kouzarides T, 2007). A summary of HMT and demethylase enzymes acting on several residues is shown in Table 1.1.

Residues Modified	Lysine Methyltransferases	Lysine Demethylases	Arginine Methlytransferases
H3K9	SUV39H1 SUV39H2 G9a ESET/SETDB1 EuHMTase/GLP CLL8 RIZ1	JHDM2a JHDM2b JMJD2A/JHDM3A JMJD2B JMJD2C/GASC1 JMJD2D	
H3K4	MLL1 MLL2 MLL3 MLL4 MLL5 SET1A SET1B SET1	LSD1/BHC110	
H3K36	SET2 NSD1 SYMD2	JHDM1a JHDM1b JMJD2A/JHDM3A JMJD2C/GASC1	
H3K79	DOT1		
H4K20	SET8 SUV420H1 SUV420H2		
H3K27	EZH2		
H3 (R2, R17, 26)			CARM1
H4R3			PRMT4
H3R8, H4R3			PRMT5

Table 1.1: Summary of histone methyltransferases and histone demethylases. (Adapted from Kouzarides T, 2007)

Involvement of histone methylation processes in various biological phenomena is diverse. Unlike the relative uniformity of the association between histone acetylation and open chromatin conformation, the methylated residues and the degree of methylation result in dramatically different outcomes (Trojer P, et al, 2006). Generally, histone 3 lysine 4 (H3K4), histone 3 lysine 36 (H3K36), and histone 3

lysine 79 (H3K79) methylations have been associated with transcriptional activation and a more relaxed and open chromatin structure in contrast to histone 3 lysine 9 (H3K9), histone 3 lysine 27 (H3K27), and histone 4 lysine 20 (H4K20) methylations, which were found to be enriched in heterochromatic regions, and were linked with transcriptional repression, as well as a condensed chromatin state (Trojer P, et al, 2006; Wang GG, et al, 2007). Nevertheless, exceptions to this generalization do exist, and have been described by newly emerged next generation sequencing technologies which were coupled with chromatin immunoprecipitation (ChIP) technique. According to the analysis of various histone modifications on the whole genome scale, it was revealed that H3K27, H3K9, and H4K20 monomethylated forms were associated with gene activation. The trimethylated forms of H3K27 and H3K9 were confirmed to be involved in gene repression, which is in accordance with the conventional understanding. Still, trimethylated H3K79 was also implicated in gene repression (Ellis L, et al, 2009).

There are several lines of evidence showing the involvement of various histone methylations, and the enzymes functioning in histone methylation processes, in carcinogenesis, including hepatocarcinogenesis (Ellis L, et al, 2009). Some of the examples include tumor cell selective loss of global H4K20me3 levels, which is very well established (Fraga MF, et al, 2005). This was observed in numerous cancer models, including a rodent model of HCC, which was induced by methyl-deficient diet (Pogribny IP, et al, 2006). Some other HMTs and related proteins, aberrations of which have been associated with HCC include NSD1, a methyltransferase acting on H3K36, and serving in context dependent transcriptional activation or repression; HP1, a protein which binds to methylated H3K9 and has a vital role on transcriptional silencing and heterochromatin formation; and finally RIZ1/PRDM2, a family of SET-domain containing methyltransferases, acting also on H3K9 (Wang GG, et al, 2007).

1.2.3.3 Histone 4 lysine 20 methylation

Although histone H4 tail comprises 5 lysine residues, lysine 20 is the only one subject to methylation in mammals. H4K20 methylation is present in a wide variety of species, ranging from *Schizosaccharomyces pombe* (*S. pombe*) to human, with different levels of elaboration. In *S. pombe*, mono, di and trimethyl forms of H4K20 are all established by the same enzyme: Set9. Nevertheless, in humans, H4K20 methylation is more complex, resulting from the involvement of multiple methyltransferase enzymes, as well as multiple proteins which interact with H4 with different affinities depending on the degree of methylation (Yang H, et al, 2009). As can be judged from this level of elaboration, mono, di and trimethyl forms of H4K20 are likely to play distinct roles in the cell.

The cellular distribution of mono, di and trimethylated forms of H4K20 was analyzed in multiple settings such as normal and cancerous human cells, as well as drosophila, mouse and rat cells by using mass spectrometry. The analysis revealed that the dimethylated form of H4K20 was much more abundant than the other two in all cases. The results of the analysis on asynchronous HeLa (cervical cancer derived cell line) cells revealed a distribution of 10 % monomethylated, 80 % dimethylated and 5 % trimethylated H4K20 (Yang H, et al, 2009).

The sub nuclear distribution of these forms is rather contradictory. H4K20me1 has usually been associated with condensed chromatin and the inactivated X chromosome, and it was proposed that this histone modification facilitates chromatin maturation (Trojer P, et al, 2006; Scharf AND; 2009). It was proposed that, L3MBTL1 protein binds preferentially to monomethylated and dimethylated H4K20, and assists compaction of the chromatin. This interaction was shown specifically on the promoter of Cyclin E gene, where L3MBTL1 recruitment by H4K20me1 was involved in silencing of this gene (Kalakonda N et al, 2008). Nevertheless, the conclusions of the high resolution histone modification profiling study by Barski et al contradicts with those findings, since according to this study, monomethylated

form of H4K20 was associated with gene activation (Barski A, et al, 2007). Similarly, the data about H4K20me2 sub nuclear distribution is also contradictory, which might be attributed to the ubiquitous disposition of this residue (Yang H, et al, 2009).

H4K20me3 has consistently been coupled with constitutive heterochromatin including centromeric and telomeric regions, satellite and long terminal repeats, as well as imprinted genes. Nevertheless, it was not reliably associated with a certain pattern of transcriptional activity, as exemplified by the failure of genome-wide chip approaches in forming such a relationship (Yang H, et al, 2009; Barski A, et al, 2007). As mentioned earlier, Histone 4 lysine 20 trimethylation has been associated with various cancers, and loss of H4K20 trimethylation has been proposed to be a hallmark of cancer (Fraga MF, et al, 2005). Although trimethylated H4K20 levels are highly cell cycle dependent, transformed cells are subject to a specific loss. Liver tumors in rats induced by a methyl deficient diet showed a progressive decrease in H4K20 trimethylation (Pogribny IP, et al, 2006). Additionally, in human breast cancer cell lines, loss of H4K30me3 mark corresponded to more aggressive phenotypes (Tryndyak, VP, et al, 2006). Similarly, in a study of non-small cell lung cancer, cancer cells displayed loss of H4K20 trimethylation compared to normal lung cells (Broeck AVD, et al, 2008).

1.2.3.4 Histone 4 lysine 20 methyltransferases and their cellular functions

In human, there are three known enzymes which are known to act on H4K20 methylation status. Set8 (alternatively known as Setd8, Pr-Set07 or KMT5A) is the enzyme which monomethylates the unmodified H4K20. Suv4-20h1 and Suv4-20h2 enzymes use non methylated, or preferentially monomethylated H4K20 as a substrate and dimethylate or trimethylate this residue. Additional reports have argued the involvement of Ash1 and NSD1 enzymes in H4K20 methylation, but evidence is contradictory and insufficient (Yang H, et al, 2009). There are no identified demethylase enzymes that act on H4K20.

The activities of H4K20 methyltransferases are strictly regulated during the cell cycle, as well as the levels of methylated H4K20. As summarized in Figure 1.1, when newly synthesized H4 is joined into the chromatin structure during the S phase, it remains non methylated at K20 until almost the G2/M transition. With the peaking Set8 activity during the M phase, H4K20 starts to get monomethylated, which is followed by largely dimethylation and to a certain extent trimethylation by Suv4-20 activity (Yang H, et al, 2009; Trojer P, et al, 2006). Despite this paradigm, some reports have demonstrated that Set8 activity is required for cell cycle progression, especially in the S phase (Jorgensen S et. al, 2007; Yin, Y et al, 2008). It is possible however that Set8 might play its cell cycle related roles through other substrates, as evidenced by the identification of p53 as a Set8 substrate (Shi X, et al, 2007).

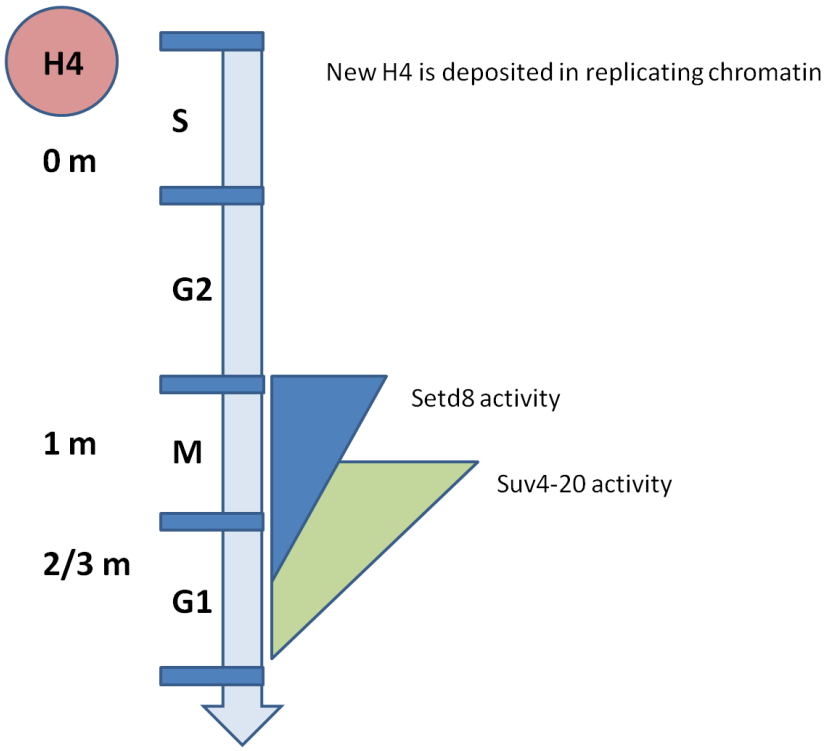

Figure 1.1: Cell cycle dependency of Set8 and Suv4-20 activities. (Adapted from Yang H, et al, 2009).

CHAPTER 2. OBJECTIVES AND RATIONALE

Despite the high mortality rate and prevalence of hepatocellular carcinoma, the available treatment options are insufficient, and there are numerous things about the pathogenesis of HCC waiting to be unraveled (Farazi PA, et al, 2006). Understanding those mechanisms, and utilizing them against HCC presents challenges. In this respect, epigenetics is a newly emerging field with lots of evidence showing the relevance and importance of several epigenetic phenomena in cancer pathogenesis, including HCC; an important example is the development of liver tumors in rodents fed with a methyl deficient diet (Pogribny IP, et al, 2006).

In a previous study performed by our group, samples from normal, cirrhotic and HCC tissues; together with senescent and immortal HuH-7 clones, were subjected to microarray analysis. According to the results of this study, epigenetic players, specifically histone modifying enzymes turned out to be promising factors that might be involved in HCC pathogenesis (unpublished data). Considering these facts, the question that if different histone methylation marks and histone modifying enzymes play roles in HCC pathogenesis came into being. Therefore, in this study, we first screened global levels of several histone methylation marks in immortal and senescent HCC cell lines. Following the identification of a marked difference of H4K20me3 levels between well differentiated and poorly differentiated HCC cell lines, and the consistent literature evidence showing the involvement of this residue in various cancer types (Yang H, et al, 2009), we decided to concentrate on trimethylated H4K20, and the methyltransferase enzymes which function in formation of this histone mark. In this context, a detailed analysis of all the transcript variants of all three enzymes involved in the H4K20 methylation process was performed. Set8 monomethyl transferase enzyme was the most prominent candidate that could play a role in HCC pathogenesis, consequently we tried to address its involvement in HCC development via overexpression and knockdown studies. The obtained results are presented and discussed in the following chapters.

CHAPTER 3. MATERIALS AND METHODS

3.1 MATERIALS

3.1.1 Reagents

Most of the chemicals used in the laboratory were purchased from Sigma-Aldrich (St. Louis, MO, USA) and Merck (Darmstadt, Germany). Additionally, Bradford reagent, Haematoxylin, Ethanol and Methanol were also from Sigma-Aldrich. ECL and ECL+ Western blot detection kits were from Amersham Pharmacia Biotech Ltd. (Buckinghamshire, UK). Fluorescent mounting medium was from Dako. Ponceau S and DMSO were from Applichem Biochemica (Darmstadt, Germany). X-Gal was from MBI Fermentas GmbH (Germany). Total RNA isolation kit: Nucleospin RNA II was from Macherey-Nagel (Duren, Germany). Standard agarose was from Sigma Biosciences (St. Louis, MO, USA). Purified recombinant human TGF-β1 was from R&D Systems (Minneapolis, USA).

3.1.2 PCR and cDNA synthesis reagents

cDNA synthesis was performed using Fermentas RevertAid First Strand cDNA synthesis kit (MBI Fermentas, Leon-Rot, Germany). Polymerase Chain Reaction (PCR) reagents; 10X Taq DNA Polymerase Buffer (+$(NH_4)_2SO_4$, -$MgCl_2$), Taq DNA Polymerase, 2 mM dNTP, 25 mM $MgCl_2$, were also purchased from Fermentas. DyNAmo HS SYBR Green qPCR Kit F-410 from Finnzymes was used for quantitative PCR reactions.

3.1.3 Nucleic acids and oligonucleotides

DNA molecular weight markers and 6x gel loading buffer were purchased from Fermentas. The primers used in PCR reactions were synthesized by İONTEK (Istanbul, Turkey). Ex-T8950-Lv06 (Set8 plasmid) was purchased from GeneCopoeia company (USA). Set8 and control siRNAs were synthesized by Eurogentec (Belgium).

3.1.4 Electrophoresis, photography and spectrophotometer

Horizontal electrophoresis was done using Thermo Electron Corporation. Power supplies Power-PAC200 and Power-PAC300, and the analysis software for agarose gel imaging were from Bio Rad Laboratories (CA, USA). Spectrophotometer used in Bradford assay for protein concentration measurements was Beckman Du640, from Beckman Instruments Inc. (CA, USA). NanoDrop used for nucleic acid concentration measurements was from Thermo Scientific (Wilmington, USA).

3.1.5 Cell culture reagents and materials

For cultivation of cell lines, Dulbecco's modified Eagle's medium (DMEM) and Roswell Park Memorial Institute (RPMI) 1640 medium were purchased from GIBCO (Invitrogen, Carlsbad, CA, USA). Additionally, Optimem medium for transfection, penicillin/streptomycin solution, trypsin-EDTA, fetal bovine serum (FBS), L-glutamine and Geneticin-G418 sulphate were also from GIBCO. All cell culture plastic ware (flasks, petri dishes, plates, cryovials) were from Corning Life Sciences Incorporated (USA). Serological pipettes and sealed-cap polycarbonate centrifuge tubes were from Costar Corporation (Cambridge, UK). Lipofectamine 2000, and Lipofectamine RNAimax were also from Invitrogen.

3.1.6 Antibodies

Working dilutions and sources for all the antibodies used in different experiments are given in Table 3.1.

Antibody	**Company and catalog number**	**Western Blot working dilution**	**Immunostaining working dilution**
H3K4me3 (rabbit polyclonal)	Abcam, ab8580	-	1:1000 (IP)
H3K9me3 (rabbit antiserum)	Upstate, 07-523	-	1:1000 (IP)
H3K27me3 (rabbit polyclonal)	Upstate, 07-449	-	1:1000 (IP)
H3K36me3 (rabbit polyclonal)	Abcam, ab9050	-	1:1000 (IP)
H3R2me2 (rabbit polyclonal)	Upstate, 07-585	-	1:600 (IP)
H3R17me2 (rabbit polyclonal)	Abcam, ab8284	-	1:900 (IP)
H3 (mouse monoclonal)	Abcam, ab24834	1:1000	-
H4K20me3 (rabbit polyclonal)	Upstate, 07-463	1:2000	1:500 (IP)
H4K20me1 (rabbit polyclonal)	Abcam, ab9051	1:5000	1:200 (FC)
HA-tag (mouse monoclonal)	Covance, MMS-101P	1:500	-
Calnexin (rabbit, polyclonal)	Sigma, C4731	1:5000	-
BrdU	DAKO, M0744	-	1:500 (IF)
Anti-mouse-HRP	Sigma, A0168	1:5000	-
Anti-rabbit-HRP	Sigma, 6154	1:5000	-
Anti-rabbit-Alexa Fluor 488	Invitrogen, A11034	-	1:100 (FC)

Anti-mouse-Alexa Fluor 568	Invitrogen, A11031	-	1:750 (IF)
Rabbit polyclonal IgG (isotype control)	Abcam, ab27472	-	1:1 (FC)

Table 3.1: Antibody dilutions. IP: immunoperoxidase staining, IF: immunofluorescent staining, FC: flow cytometry.

3.2 SOLUTIONS AND MEDIA

3.2.1 General and cell culture solutions

50x Tris Acetate EDTA (TAE): 242 g Tris base, 57,1 ml glacial acetic acid, 18,6 g EDTA in 1 liter ddH_2O (Working dilution is 1x).

Ethidium bromide: 10 mg/ml stock is dissolved in water (Working solution is 30 ng/ml).

10x Phosphate buffered saline (PBS): 80 g NaCl, 2 g KCl, 14,4 g Na_2HPO_4, 2,4 g KH_2PO_4 in 1 liter ddH_2O (Working dilution is 1x, autoclaved for use in cell culture).

DMEM/RPMI 1640 working medium: 10% Fetal bovine serum (FBS), 1% penicillin/streptomycin, 1% Non-essential amino acids were added to obtain complete medium.

3.2.2 Sodium Deodecyl Sulphate (SDS) – Polyacrylamide Gel Electrophoresis (PAGE) and immunoblotting materials and solutions

NuPAGE NOVEX pre-cast gel system from Invitrogen (CA, USA) was employed for running denaturing gels. 4-12 % gradient or 12 % Bis-Tris mini gels were used with either MES or MOPS running buffer, which were also purchased from Invitrogen.

4x sample loading buffer, 10x denaturing agent and antioxidant were also from Invitrogen, and they were used according to the manufacturer's protocols.

20x transfer buffer was also from Invitrogen, it was diluted to 1x working concentration, and used with 10 % methanol.

NP-40 lysis buffer: 150 mM NaCl, 50 mM TrisHCl (pH 8.0), 1 % NP-40, 0,1 % SDS, 1x protease inhibitor cocktail (from 25x stock) in ddH_2O.

10x Tris buffered saline (TBS): 12,19 g Trisma base, 87,76 g NaCl in 1 liter ddH_2O, pH is adjusted to 8 (Working dilution is 1x).

TBS-tween (TBS-T): 0,2 % Tween-20 was dissolved in 1x TBS.

Ponceau S solution: 0,1 % (w/v) Ponceau, 5 % (v/v) acetic acid in ddH_2O.

Blocking solution: 5 % (w/v) non-fat dry milk was dissolved in 0,2 % TBS-T.

3.2.3 Immunoperoxidase and immunofluorescence solutions

Immunoperoxidase blocking solution: 10 % FBS, 0,1% Triton-X in 1x PBS.

Immunofluorescence blocking solution: 10 % FBS in 0,2% PST-Tween 20.

4', 6-diamino-2-phenylindole (DAPI): 0,1-1 μg/ml (Working solution in ddH_2O)

DAKO EnVision™ system was used for immunoperoxidase staining (Denmark).

3.2.4 Senescence associated β-galactosidase (SABG) assay solutions

SABG buffer: 40 mM citric acid/sodium phosphate buffer (pH 6.0), 5 mM potassium ferrocyanide, 5 mM potassium ferricyanide, 150 mM NaCl, 2 mM $MgCl_2$, 1 mg/ml X-gal in ddH_2O. pH is adjusted to 6.0, and the solution is filtered prior to use.

3.2.5 BrdU incorporation assay solutions

BrdU stock solution: 10 mg/ml BrdU in ddH_2O (Working solution is 30 μM)

3.3 METHODS

3.3.1 General methods

3.3.1.1 Quantification and qualification of nucleic acids

NanoDrop ND-1000 Full-spectrum UV/Vis spectrophotometer (Thermo Fisher Scientific, Wilmington, DE, USA) was employed in order to quantify DNA and RNA. Quality and purity of nucleic acids were determined by calculation of OD_{260} to OD_{280} ratio.

3.3.1.2 Agarose gel electrophoresis of nucleic acids

DNA fragments obtained by PCR were fractioned by horizontal electrophoresis apparatus. Agarose gels were prepared using 1x TAE buffer; agarose concentration was calculated as weight / volume, and agarose was dissolved completely in 1x TAE by heating in the microwave oven. Ethidium bromide was added to a final concentration of 30 μg/ml after some cooling. All PCR products were less than 1 kb,

therefore they were separated on 2 % agarose gel with 1x TAE running buffer. Samples were prepared by the addition of 6x loading buffer from Fermentas to a final concentration of 1x. Gels were usually run at 110 V, with different time periods depending on the size of the product. Bands were visualized under UV light, and fragment sizes were estimated using Fermentas Gene Ruler DNA ladders, especially 100 bp ladder and 1 kb ladder were used for PCR products.

3.3.1.3 Computer, software and database tools

The sequences and all other information about the genes were obtained from NCBI (National Center for Biotechnology Information) website at: http://www.ncbi.nlm.nih.gov/, and Ensembl Genome Browser website at: http://www.ensembl.org/index.html. Primers were designed using the online web tool Primer3, provided by Steve Rozen and Helen J. Skaletsky (2000) at: http://frodo.wi.mit.edu/primer3/. *In silico* PCR to confirm that the primers hit only a single location in the genome was performed using UCSC (University of California, Santa Cruz) Genome Bioinformatics website, *in silico* PCR online tool at: http://genome.ucsc.edu/. The alignment of nucleic acid or protein sequences were performed by using Clustal W algorithm, provided by SDSC (San Diego Supercomputer Center) Biology Workbench website at: http://workbench.sdsc.edu/. Information about proteins was retrieved from Uniprot (Universal Protein Resource) database at: http://www.uniprot.org/.

3.3.2 Cell and tissue culture techniques

3.3.2.1 Cell lines and stable clones

15 HCC derived cell lines were used in this study, which were: HuH-7, Hep40, HepG2, Hep3B, Hep3B-TR, PLC/PRF/5, SNU-182, SNU-387, SNU-398, SNU-423, SNU-449, SNU-475, Mahlavu, FOCUS, SK-HEP-1. These cell lines were cultured as previously (Cagatay T. and Ozturk M, 2002). Briefly, HuH-7, Hep40, HepG2,

Hep3B, Hep3B-TR, PLC/PRF/5, , Mahlavu, FOCUS and SK-HEP-1cell lines were cultured in DMEM working medium, and all the SNU cell lines were cultured in RPMI 1640 working medium. SNU-475 derived stable clone SNU-475-Set8 was selected by G-418 antibiotic after 1 week of lentiviral infection. G-418 selection was performed with a concentration of 400 μg/ml in complete medium. G418 was renewed every 3 days. After 2 weeks of G-418 selection, selected cells were maintained in the presence of 100 μg/ml G-418 and G-418 was withdrawn from the medium when experiments are set-up with this clone. When a certain number of cells are needed, cells were counted by using a haemocytometer after trypsinization and resuspension in growth medium.

3.3.2.2 Thawing cells

Frozen cells in cryovials from liquid nitrogen or -80ºC freezer were taken and immediately put on ice. Vials were placed in 37 ºC water bath and waited 1-2 min to thaw. Before the cells were completely thawed, the suspension was taken into 15 ml sterile centrifuge tube with approximately 10 ml growth medium and resuspended. Cells were centrifuged at 1500 rpm for 3 minutes, supernatant was discarded, and the pellet was resuspended in 10 ml fresh growth medium to be placed into 75 cm^2 flasks or 100 mm dishes. Flasks or dishes were rocked back and forth gently in order to allow the cell suspension to mix, and they were incubated overnight at a 37ºC humidified incubator with 5 % CO_2. The next day, cells were washed with 1x PBS, and culture mediums were replaced with fresh growth mediums.

3.3.2.3 Growth conditions of cells

HCC cell lines were cultured in DMEM or RPMI 1640 mediums supplemented with 10 % FBS, 1 % penicillin/streptomycin and 1 % Non-essential amino acids as specified previously. Cells were incubated in humidified 37ºC incubators with 5 % CO_2 in the air. Cells were passaged regularly, approximately 2-3 days apart, depending on the cell type, but before reaching confluency each time. When passaging cells, old growth medium was aspirated, cells were washed with 1x PBS

once, after aspirating the PBS, trypsin-EDTA solution was added on to the cells with the amount depending on the size of the culture flask, usually 1-2 ml for 100 mm dishes were used. After waiting 1-2 minutes when trypsin removed the monolayer of the cells from the surface, fresh medium was added and cells were collected by pipetting up and down with serological pipettes several times, and therefore mixed thoroughly. Afterwards, cells were re-seeded on fresh dishes or flasks with the required dilutions. All mediums, 1x PBS and trypsin-EDTA were stored at +4ºC refrigerator. FBS stock solutions were stored at -20ºC refrigerators, thawed in 37ºC water bath, heat-inactivated at 56ºC for 30 minutes, then aliquoted into sterile 50 ml centrifuge tubes and stored at -20ºC, they were also filter-sterilized prior to use. All solutions and media were warmed at 37ºC water bath prior to use.

3.3.2.4 Cryopreservation of cells

Cells were harvested when they were approximately 60 % confluent, at their exponential growth phase. Cells were collected by trypsinization, neutralized by growth medium, centrifuged at 1500 rpm for 3 minutes and the supernatant was aspirated. The pellet was resuspended in freezing medium, which contained 8 % FBS and 8 % DMSO in growth medium, at a concentration of approximately 4 x 10^6 cells/ml. 1 ml of these cells were stored in cryovials, these were immediately placed at -20ºC for 1 hour, then stored at -80ºC overnight, then transferred into liquid nitrogen tanks for long term storage.

3.3.2.5 Transient transfection of eukaryotic cells using Lipofectamine 2000 reagent

Plasmid DNA transfection of cells were performed by using Lipofectamine 2000 reagent from Invitrogen (CA, USA), according to the manufacturer's protocols, with a DNA:Lipofectamine ratio of 1:3. OPTI-MEM reduced serum medium from GIBCO, Invitrogen was used for transfection experiments.

3.3.2.6 Transient transfection of eukaryotic cells using Lipofectamine RNAi-max reagent

Cells were transfected with siRNAs using Lipofectamine RNAi-max reagent from Invitrogen according to the manufacturer's protocols. OPTI-MEM reduced serum medium from GIBCO, Invitrogen was again used for transfection experiments. Final siRNA concentrations were determined by optimization. siRNA sequences for Set8 gene were obtained from the literature (Huen MSY, et al, 2008), similarly like control siRNAs (Shi X, et al, 2007), and synthesized by Eurogentec company (Belgium). List and sequences of the siRNAs used in this study are given in Table 3.2.

siRNA	**Sequence**
Set8-siRNA1 Sense	GCA-ACU-AGA-GAG-ACA-AAU-CTT
Set8-siRNA1 Antisense	GAU-UUG-UCU-CUC-UAG-UUG-CTT
Set8-siRNA2 Sense	GAU-UGA-AAG-UGG-GAA-GGA-ATT
Set8-siRNA2 Antisense	UUC-CUU-CCC-ACU-UUC-AAU-CTT
Set8-control siRNA	UGG-UUU-ACA-UGU-CGA-CUA-ATT
Set8-control siRNA	UUA-GUC-GAC-AUG-UAA-ACC-ATT

Table 3.2: siRNA sequences

3.3.2.7 Lentiviral Infection of eukaryotic cells

Lentiviral infection of eukaryotic cells was performed using GeneCopoeia Lenti-Pac FIV Expression Packaging Kit, according to the manufacturer's protocol. Briefly; on Day 0 packaging cells were seeded (HEK 293 cells) on 100 mm dishes. On Day 1, packaging cells were transfected with the target vector (Ex-T8950-Lv06 in this case) and the Lenti-Pac packaging mix using Endofectin transfection reagent for 14 hours at a 37^{o}C incubator. After changing the medium with growth medium supplemented with 5 % FBS and titer boost reagent, incubation was continued for an additional 24 hours, in order to let the virus particles form. Virus particles were harvested from the

supernatant of the packaging cells, filtered with a 0,2 μm filter. 1,5 ml of the collected virus containing medium was added on each well of cells to be infected (SNU-475 in this case) in 6-well plates. The next day, their medium was changed with normal growth medium, and the incubation was continued with normal growth medium until the cells approached confluency. Then they were transferred to 25 cm^2 flasks, and G-418 antibiotic selection was started within a week.

3.3.3 Extraction of total RNA from cultured cells and tissue samples

Total RNA was extracted from cultured cells and tissue samples by using Macherey-Nagel (MN) Nucleospin RNA II kit (MN, Duren, Germany) according to the manufacturer's protocol. When RNA was isolated from liver tissues, samples were first homogenized by pestle and mortar in the presence of liquid nitrogen, then the procedure was continued with the MN kit.

3.3.4 First strand cDNA synthesis

First strand cNDA was synthesized from total RNA using Fermentas RevertAid cDNA synthesis kit (MBI Fermentas, Germany) according to the manufacturer's protocols. For RNA samples from cultured cells, reactions were primed with $Oligo(dT)_{18}$ primers, and for RNA samples from tissues, reactions were primed with a 1:1 mixture of $Oligo(dT)_{18}$ and Random Hexamer primers. First strand cDNA products obtained from this kit were used directly as templates for RT-PCR reactions. First strand cDNA was synthesized from 2 μg RNA for cultured cell samples, and from 4 μg RNA for tissue samples, in total 30 μl volume, and 2 μl of this product was used as RT-PCR template. In order to check for genomic DNA contamination, RT (-) cDNA samples were also synthesized from total RNA, where no reverse transcriptase enzyme was added in the reaction, therefore the only DNA template obtained was from the possible genomic DNA contamination.

3.3.5 Primer design for gene expression analysis by RT-PCR

When primers were designed for RT-PCR reactions, forward and reverse primers were positioned on different exons. That way, it was ensured that product size would be much higher if there was amplification from genomic DNA. Difference between the melting temperatures of forward and reverse primers were set to be no greater than 1ºC, and the GC contents were no greater than 60 %. Amplicon sizes were variable; in order to differentiate between different transcript variants, different amplicon sizes were used. All primers used for gene expression analysis are listed in Table 3.3.

Primer	**Sequence**	**Tm (ºC)**	**Number of cycles**
Suv4-20h1, Variant 1	F1: TGGAGATGGGTTCTTTGGAG R1: GCTTTGCAGGCTTCTTCAGT	58	30
Suv4-20h1, Variant 2	F1: TGGAGATGGGTTCTTTGGAG R2: TGAAGTGCAGCCAAAGCTC	56	35
Suv4-20h2, Variants 1 & 2	F1: CTCACCTGCTCCTGCTCTCT R2: TCCTGATTCCTTCTGCTTCC	63	35
Suv4-20h2, Variant 3	F1: CTCACCTGCTCCTGCTCTCT R1: CTTGCGGGTTGAGTACATGA	58	35
Set8, Variants 1 & 4	F1: AGAGGCAGGAAGATGTCCAA R2: TGCCCGGTAAATACGTTCTC	60	30
Set8, Variant 3	F2: CAGTCACCCTGAGAGAAGTCCT R1: TTCCTGGCGTCTTTGATCTT	63	35
Set8, Full length	F1: AGAGGCAGGAAGATGTCCAA R3: GTCCTTTGAAGAAGGGAAAGTG	58	30
GAPDH	F: GGCTGAGAACGGGAAGCTTGTCAT R: CAGCCTTCTCCATGGTGGTGAAGA	60	21

Table 3.3: Primers and working conditions

3.3.6 Gene expression analysis by semi-quantitative RT-PCR

Firstly, before starting the gene expression analysis by RT-PCR, possible genomic DNA contamination was controlled by GAPDH RT-PCR. GAPDH primers were designed so that they amplify a 151 bp fragment from cDNA, but a 250 bp fragment from genomic DNA. Additionally, RT (-) cDNAs were also employed in order to control for possible genomic DNA contamination. When semi-quantitative RT-PCR reactions were set up, firstly 2 µl of each sample were used to setup GAPDH RT-PCR in order to do normalization. After GAPDH products were run on an agarose gel and band intensities were compared, adjustments for the cDNA amount to be used were made (if required). After then, the GAPDH RT-PCR reaction and the RT-PCR reaction for the gene of interest were set up with the adjusted amounts of cDNAs.

In order to determine the optimum cycle number for each semi-quantitative RT-PCR reaction, PCR reactions with different cycle numbers were set up and the minimum cycle number that allows the visualization of the desired product were selected.

3.3.7 Gene expression analysis by quantitative RT-PCR

Stratagene Mx 3005P system was used for quantitative PCR analysis. Reactions were performed using DyNAmo HS SYBR Green qPCR Kit F-410 from Finnzymes. Reactions were set up in a total volume of 25 µl with 2 µl cDNA for each sample. Reactions were started with 10 minutes initial denaturation at 95ºC, then amplification was performed with 40 to 45 cycles of: 30 seconds at 95ºC, 30 seconds at Tm of primer pair, 30 seconds at 72ºC. Samples were analyzed in triplicates, GAPDH reactions were performed in duplicates. Product purity was addressed by a dissociation curve. For each primer pair, prior to analysis, standard curve for the primer efficiency was obtained by setting up multiple reactions with 2 fold dilutions of selected cDNAs from 1 to 1:256. Primer efficiency was then calculated as: $E = 2^{(-}$

$^{1/slope)}$. When fold changes were calculated from the obtained data, ΔΔCt method was employed, and the primer efficiencies were also involved in the formula.

3.3.8 Crude total protein extraction from cultured cells

HCC derived cell lines were collected either by trypsinization and pelleted, or collected by scraping by a scraper in the presence of lysis buffer in order to extract protein. NP-40 lysis buffer was used for protein extraction procedures. Lysis was performed by resuspending cell pellets in twice their volume of lysis buffer, and incubating in ice for 30 minutes with gentle mixing every 5 minutes. Then the lysates were centrifuged at 11000 g for 20 minutes at +4ºC. Total protein in the supernatant form was then collected and stored at -20ºC.

3.3.9 Acid extraction of histones

In order to obtain histone extracts from cultured cells, acid extraction method was employed which was previously described (Shechter D, et al, 2007). Briefly, cells were harvested by trypsinization, lysed in triton extraction buffer (1x PBS with 0,5 % Triton-X 100 (v/v), 0,02 % (w/v) NaN_3 and 1x protease inhibitor cocktail) for 10 minutes on ice. Lysate was then centrifuged at 2000 rpm for 10 minutes at +4ºC and the supernatant was discarded. The pellet was washed with triton extraction buffer once more, and the histones were extracted in 0,2 N HCl overnight at +4ºC on rotator. The next day, samples were centrifuged at 2000 rpm for 10 minutes at +4ºC, the supernatant contained the histones, they were stored at -20ºC.

3.3.10 Western blotting

Firstly, in order to measure the concentration of protein lysates, the conventional Bradford assay was used. Sample protein concentrations were determined by comparing the absorbance values to a standard curve obtained by the absorbance values of 2-fold serial dilutions of bovine serum albumin (BSA) protein of a known

concentration. When mixed with the Bradford reagent, proteins formed blue color, which was measured by spectrophotometer at 595 nm. After quantification, equal amounts of cell lysates were used to prepare protein samples to be loaded on gels. Protein samples were prepared by mixing with 4x NuPAGE LDS Sample Buffer from Invitrogen, 10x denaturing agent from Invitrogen, and ddH_2O to complete the volume. The samples were then heated at 70ºC for 10 minutes.

NOVEX NuPAGE system from Invitrogen was used for running gels and transferring proteins to nitrocellulose membranes, according to the manufacturer's protocols. 4-12 % gradient Bis-Tris mini gels were used when working with whole cell lysates, and 12 % Bis-Tris mini gels were used when working with histone extracts, for better separation. The running buffers used were MES for histone gels, and MOPS or MES for whole cell lysate gels, depending on the size of the proteins that were being studied. The transfer buffer was used with 10 % methanol, and the gels were transferred to nitrocellulose membranes.

The obtained membranes with transferred proteins were blocked with either non fat dry milk or BSA with a 5 % concentration in 0,2 % TBS-T, depending on the suggestions for the specific antibodies used. Blocking was done for 1 hour at room temperature. Probing with the primary antibodies were either done at room temperature for one hour, or overnight at +4ºC. Membranes were washed for half an hour in 0,2 % TBS-T and incubated with HRP conjugated secondary antibodies for 1 hour at room temperature. After an additional wash of half an hour, chemiluminescent detection was performed by using ECL or ECL+ western blot detection kits from Amersham (UK), according to the manufacturer's protocols. X-ray films were exposed to the emitted chemiluminescence, duration depending on the specific antibody.

3.3.11 Immunoperoxidase staining

Cells were seeded in 6-well cell culture plates on autoclave-sterilized coverslips with such a confluency that they will be sub-confluent on the day of immunoperoxidase staining. Depending on the growth rate, size and morphology of each cell line, the exact number of seeded cells was variable. Cells were washed with 1x PBS, fixed with 4 % Formaldehyde for 10 minutes, washed once again with 1x PBS and permeabilized with 0,5 % Saponin, 0,3 % Triton-X in 1x PBS for 10 minutes. After washing three times with 1x PBS, cells were blocked with 10 % FBS, 0,1 % Triton-X in 1x PBS for 1 hour at room temperature. Primary antibody incubation was done 1 hour at room temperature, antibodies were prepared in 2 % FBS in 1x PBS, and were applied directly on coverslips. After washing once with 1x PBS and once with 1x PBS with 0,3 % Triton-X, secondary antibody (DAKO, anti mouse + anti rabbit pool) incubation was performed similarly. Cells were then stained with DAKO-DAB Chromogen solution for ~ 1 minute. The reaction was stopped with ddH_2O, and counterstaining was performed by Mayer's Haematoxylin for ~ 0,5 – 1 min. After final washes with ddH_2O, coverslips were mounted on slides using 90 % glycerol, and the images were examined under light microscope (ZEISS).

3.3.12 BrdU incorporation and immunofluorescence staining

Sub-confluent cells seeded on coverslips were labeled with 30 μM thymidine analog BrdU for 2,5 hours prior to staining with anti-BrdU antibody by immunofluorescent staining. Cells were washed with 1x PBS twice, then fixed with 70 % cold ethanol for 10 minutes. After washing with 1x PBS, cells were then incubated with 2 N HCl for 20 minutes and washed again with 1x PBS three times. Blocking was performed with 10 % FBS in 0,2 % PBS-Tween for 1 hour. Anti-BdrU primary antibody was prepared in blocking solution, and applied directly on coverslips. After washing with 0,2 % PBS-Tween three times, Alexa-568 secondary antibody was again applied directly on coverslips, for 1 hour. Cells were again washed with 0,2 % PBS-Tween three times, and nuclei were stained with DAPI for 1 minute. DAPI was washed with ddH_2O, and the coverslips were mounted on slides using DAKO fluorescent mounting medium. Cells were visualized with fluorescent microscope, and merged images were

generated with two separate filters. Several areas were counted for DAPI stained cells and BrdU positive cells manually.

3.3.13 SABG assay

SABG assay was performed as described previously (Dimri GP, et al, 1995). Briefly, cells seeded on coverslips were washed with 1x PBS, fixed with 4 % Formaldehyde for 10 minutes, washed again once with 1x PBS. Then they were incubated in SABG buffer in a 37ºC, dark and CO_2-free environment for ~18 hours.

3.3.14 Flow cytometry of histone residues

Cells were harvested by trypsinization, washed once with 1x PBS, and fixed with 4 % paraformaldehyde for 15 minutes at room temperature. Fixation was stopped by adding cold PBS, and paraformaldehyde was spinned off by centrifugation at 1500 rpm for 3 minutes. Cells were then incubated in 5 % BSA, 0,1 % Triton-X in 1x PBS for 30 minutes, which was followed by washing with incubation buffer (5 % BSA in 1x PBS) twice. 0,2 – 0,5 µg primary antibody was used for 1 million cells, similarly as the corresponding isotype control. Primary antibodies were prepared in incubation buffer, and incubation was done for 1 hour. After washing once with incubation buffer, cells were incubated with Alexa-Fluor-488 conjugated secondary antibodies; 2 µg for 1 million cells, for 1 hour. Finally, cells were washed once with incubation buffer, and resuspended in 1x PBS. Analysis was done using FACSCalibur Flow Cytometer (BD Biosciences, San Jose, CA) and Cell Quest 3.2 software.

3.3.15 Cellular growth rate measurements with Roche xCELLigence system

Cells were seeded in E-96 plates special for the apparatus, according to the manufacturer's protocols. The cell number to be seeded for the assay was optimized for the cell lines by performing the experiment with serial dilutions. For SNU-475, 1000 or 2000 cells were seeded in a total of 200 µl. Cell indexes were retrieved every 2 hours, for up to 160 hours, and calculations were done accordingly. All experiments were planned in triplicates, averages and standard deviations were calculated.

CHAPTER 4. RESULTS

4.1. Histone Methylation

4.1.1 Histone methylation levels in HCC cell lines

Global levels of histone modifications that are candidates for playing a role in HCC development or senescence were screened by immunoperoxidase staining in the presence or absence of TGF-β induced senescence. In this study, 15 HCC cell lines are used, which are divided into two subtypes by our group (Yuzugullu H, et al, 2009). These subtypes are: well differentiated and poorly differentiated, and the classification is based on characteristics such as the expression of differentiation markers like E-Cadherin and Vimentin, together with the expression of hepatocyte lineage markers. Well differentiated cell lines preserve their epithelial phenotype, and most of them respond to TGF-β treatment by undergoing senescence. Poorly differentiated cell lines are mesenchymal-like, in terms of their expression of mesenchymal markers, their high invasiveness and motility in comparison to well-differentiated cell lines, and they do not respond to TGF-β treatment by undergoing senescence (Senturk, S et al, 2010). Well differentiated cell lines include: HuH-7, Hep40, HepG2, PLC/PRF/5 and Hep3B, whereas poorly differentiated cell lines include: SNU-182, SNU-387, SNU-398, SNU-449, SNU475, Mahlavu, SK-HEP-1 and FOCUS.

The analyzed histone methylation marks are: trimethylated histone H3 lysine 27 (H3K27me3), trimethylated histone H3 lysine 4 (H3K4me3), trimethylated histone H3 lysine 9 (H3K9me3), trimethylated histone H3 lysine 36 (H3K36me3),

trimethylated histone H4 lysine 20 (H4K20me3), dimethylated histone H3 arginine 2 (H3R2me2), and dimethylated histone H3 arginine 17 (H3R17me2).

4.1.1.1 Histone H3 lysine 27 trimethylation in HCC cell lines

Global levels of H3K27me3 were the first to be compared in well and poorly differentiated HCC cell lines in the presence and absence of TGF-β induced senescence. In order to induce senescence, cells were treated with 5 ng/ml TGF-β for 72 hours, then TGF-β was withdrawn from the growth medium. On Day4 or Day8 of TGF-β treatment, senescent cells were marked with Senescence Associated β-Galactosidase (SABG) assay, which was followed by immunoperoxidase staining with H3K27me3 antibody. Nuclear counterstaining was performed using haematoxylin. The results of these staining experiments are shown in Figure 4.1.1.

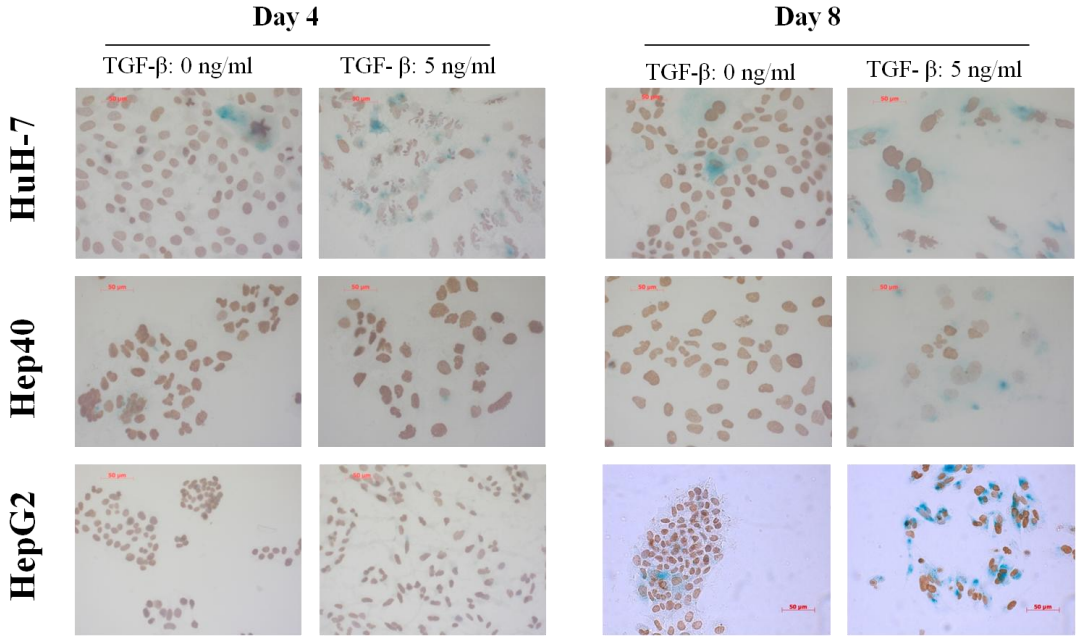

Figure 4.1.1: Global levels of H3K27me3 in HCC cell lines in the presence or absence of TGF-β induced senescence; determined by immunoperoxidase staining. Cells were seeded in 6-well tissue culture plates on coverslips with such a confluency that they will be sub-confluent on Day 4 and Day 8, when the immunostaining experiments were performed. Immunostaining was performed as explained in the Materials and Methods section. In order to avoid bias, all pairs with 0 or 5 ng/ml TGF-β treatment were visualized and photographed under same lighting conditions using 40x objective. Example positive cell was shown with a red arrow, and example negative cell was shown with a black arrow.

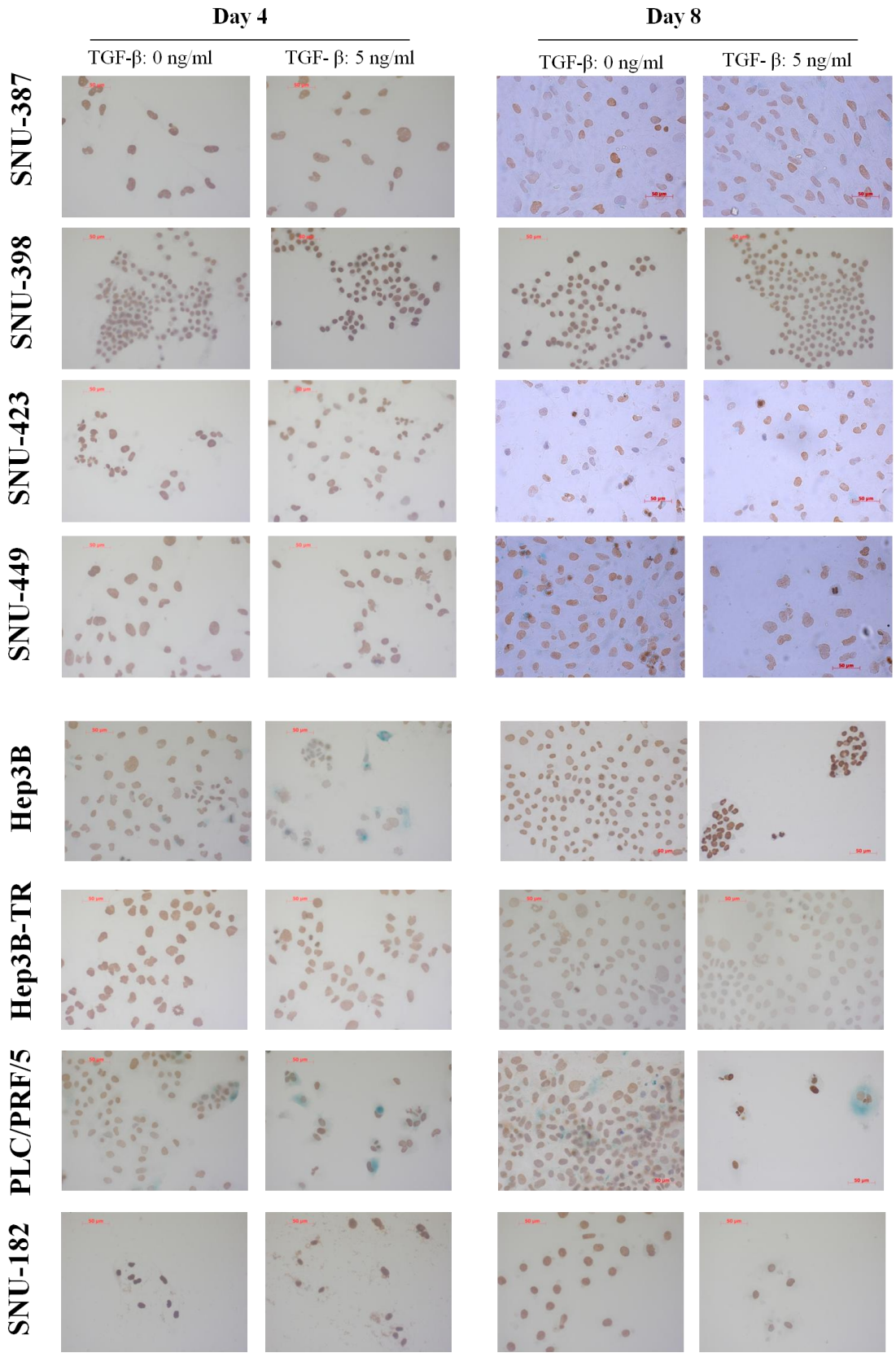
Day 4
Day 8
TGF-β: 0 ng/ml
TGF- β: 5 ng/ml
TGF-β: 0 ng/ml
TGF- β: 5 ng/ml
SNU-387
SNU-398
SNU-423
SNU-449
Hep3B
Hep3B-TR
PLC/PRF/5
SNU-182

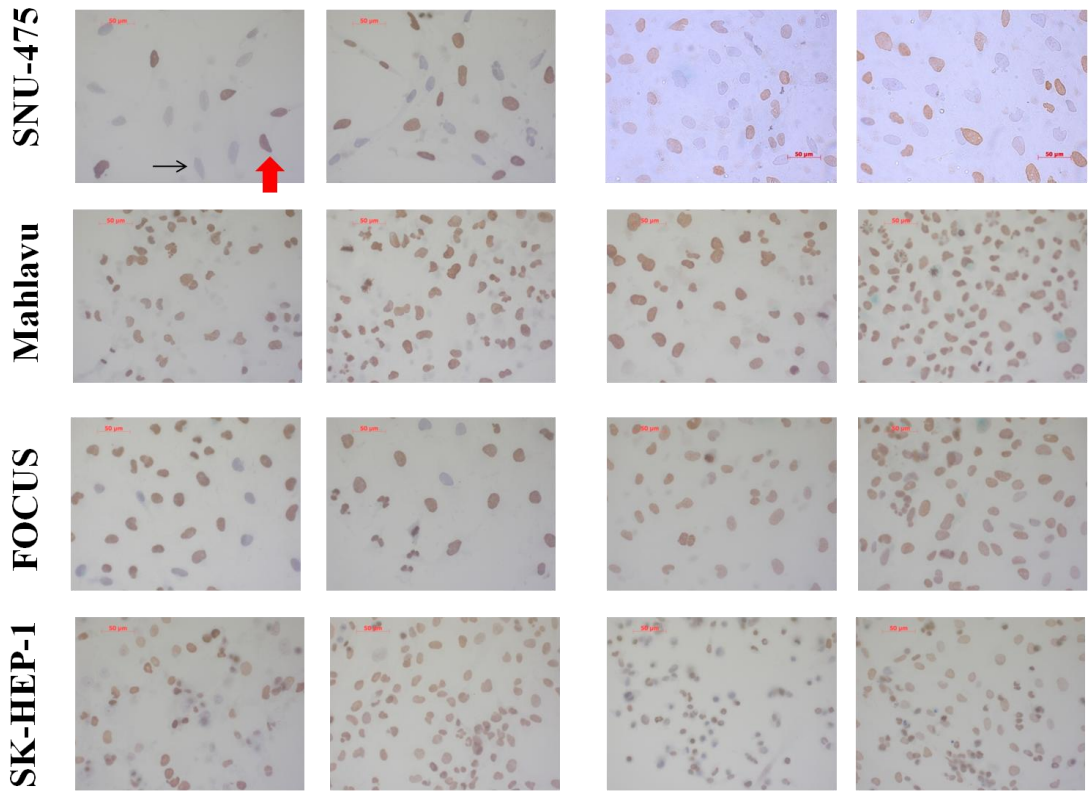

Figure 4.1.1 (continued): Global levels of H3K27me3 in HCC cell lines in the presence or absence of TGF-β induced senescence; determined by immunoperoxidase staining.

As can be seen in the above figure, most of the cell lines stained positive for H3K27me3, with the exceptions of SNU-475, SK-HEP-1, FOCUS and maybe SNU-423, which stained heterogeneously. However, we were unable to detect a significant change in global H3K27me3 levels in response to TGF-β induced senescence, when we compared the brown immunoperoxidase staining in senescent cells which are stained with SABG (light blue color) or immortal cells which are not stained with SABG. Poorly differentiated and well differentiated cells also did not seem to vary in terms of global levels of this histone mark.

4.1.1.2 Histone H3 lysine 4 trimethylation in HCC cell lines

Global H3K4me3 levels were analyzed in our 15 HCC cell lines similarly with immunoperoxidase staining. . In order to induce senescence, cells were treated with 5

ng/ml TGF-β for 72 hours, then TGF-β was withdrawn from the growth medium. On Day4 or Day8 of TGF-β treatment, cells were stained using H3K4me3 antibodies as described in the Materials and Methods section. Results of these immunostaining experiments are shown in Figure 4.1.2.

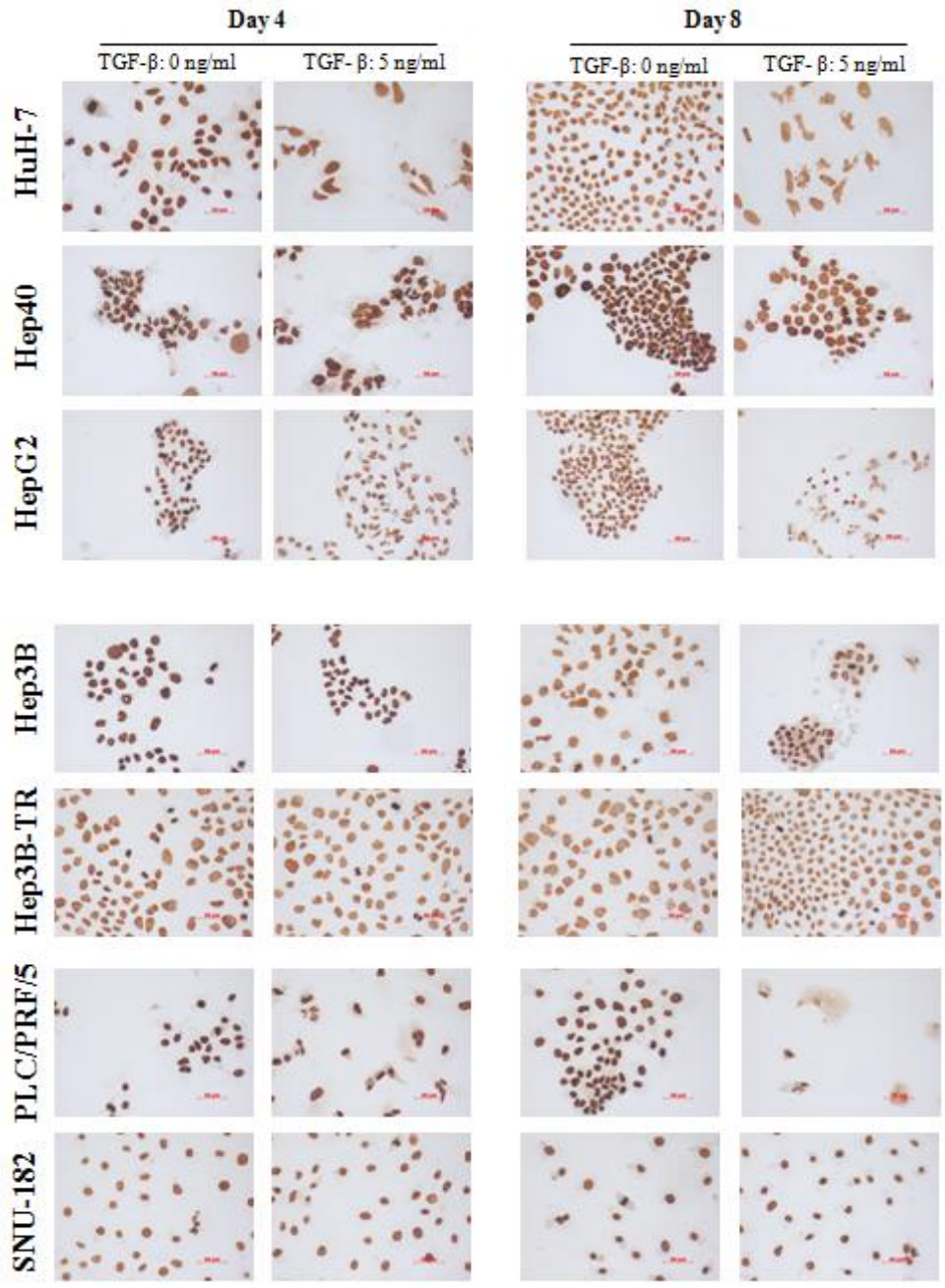

Figure 4.1.2: Global levels of H3K4me3 in HCC cell lines in the presence or absence of TGF-β induced senescence; determined by immunoperoxidase staining. Cells were seeded in 6-well tissue culture plates on coverslips with such a confluency that they will be sub-confluent on Day 4 and Day 8, when the immunostaining experiments were performed. In order to avoid bias, all pairs with 0 or 5 ng/ml TGF-β were visualized and photographed under same conditions using 40x objective. Example positive cell was shown with a red arrow, and example negative cell was shown with a black arrow.

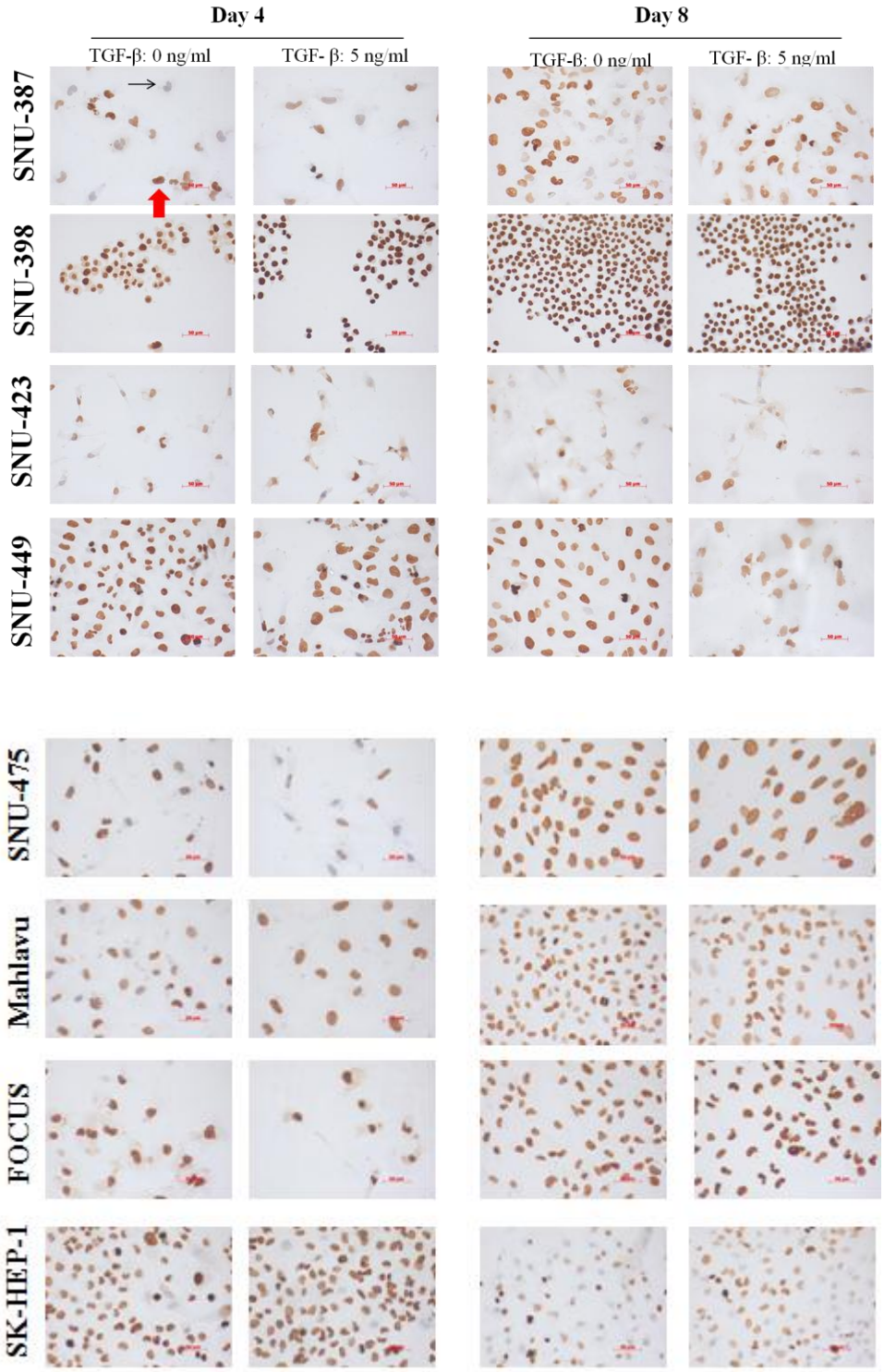

Figure 4.1.2 (continued): Global levels of H3K4me3 in HCC cell lines in the presence or absence of TGF-β induced senescence; determined by immunoperoxidase staining.

The results shown in Figure 4.1.2 indicate a strong global staining for H3K4me3 residue for most of the cell lines, with the exceptions of SNU-387 and SNU-423 which showed a slightly weaker and heterogeneous staining. In SNU-475, Day 4 samples, TGF-β treatment seemed to result in a loss of H3K4 trimethylation in a heterogeneous manner, which was not observed in Day 8 samples. Mitotic cells stained strong in all cases in that cell line. Taken as a whole, H3K4me3 modification in HCC cell lines has a strongly positive pattern with some variations among cell types; however that does not seem to be affected strongly by TGF-β induced senescence. Differentiation status of cell lines also seems to be independent from the trimethylation status of H3K4.

4.1.1.3 Histone H3 lysine 9 trimethylation in HCC cell lines

Global levels of H3K9me3 were analyzed in our 15 HCC cell line panel in the absence or presence of TGF-β induced senescence. Experimental setting for cell seeding, TGF-β treatment, and immunoperoxidase staining is as described in the previous sections. Results of these immunoperoxidase staining experiments are shown in Figure 4.1.3.

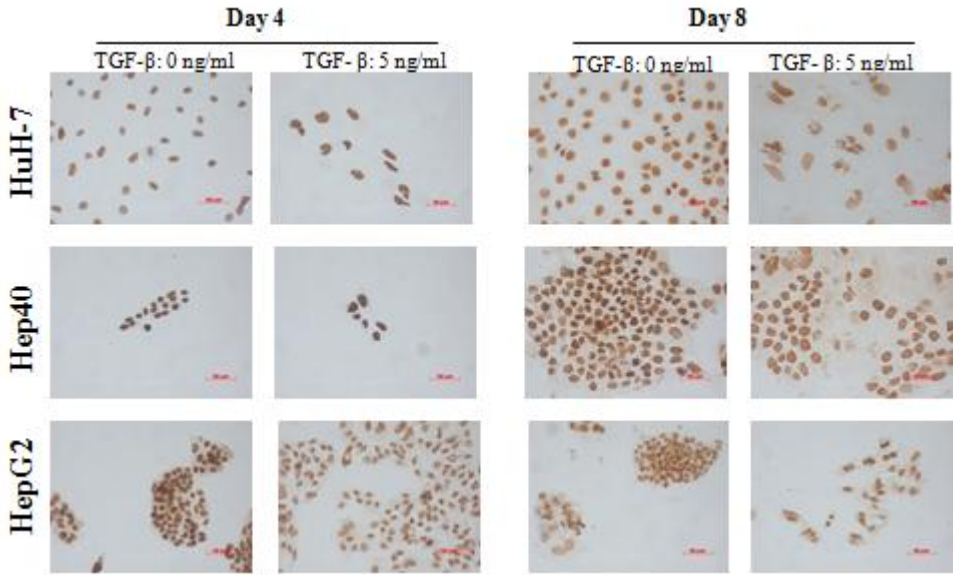

Figure 4.1.3: Global levels of H3K9me3 in HCC cell lines in the presence or absence of TGF-β induced senescence; determined by immunoperoxidase staining. Immunostaining experiments were done on Day 4 or Day 8 of 0 or 5 ng/ml TGF-β treatment. In order to avoid bias, all pairs with 0 or 5 ng/ml TGF-β were visualized and photographed under same lighting conditions using 40x objective.

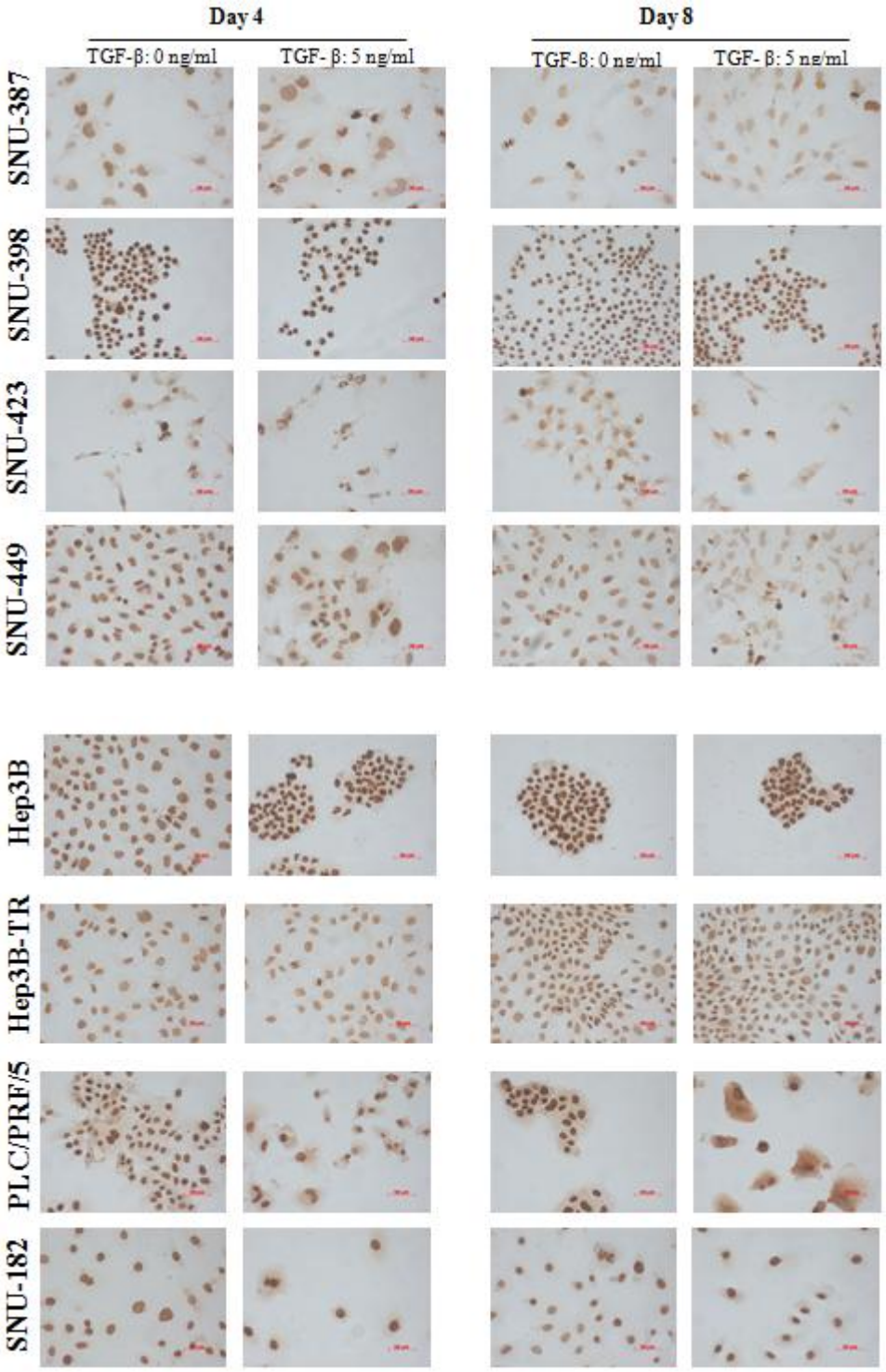
Day 4
Day 8
TGF-β: 0 ng/ml
TGF-β: 5 ng/ml
TGF-β: 0 ng/ml
TGF-β: 5 ng/ml
SNU-387
SNU-398
SNU-423
SNU-449
Hep3B
Hep3B-TR
PLC/PRF/5
SNU-182

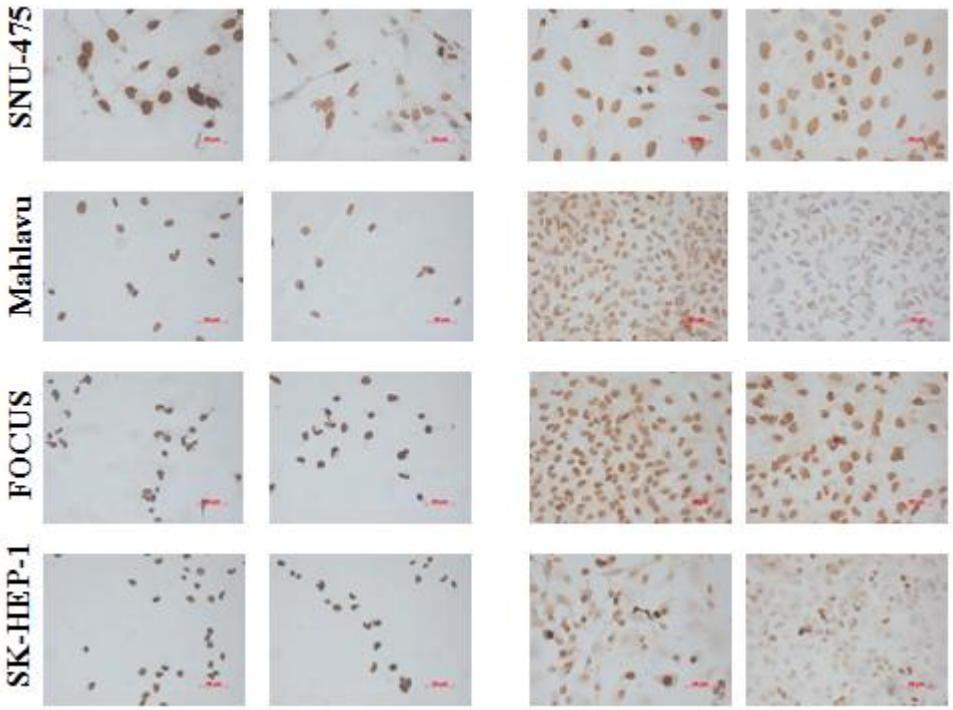

Figure 4.1.3 (continued): Global levels of H3K9me3 in HCC cell lines in the presence or absence of TGF-β induced senescence; determined by immunoperoxidase staining.

According to the results shown in Figure 4.1.3, H3K9me3 showed a strong nuclear staining pattern in most of the cell lines with some exceptions. PLC/PRF/5 contained a cytoplasmic stained fraction in addition to its nuclear positivity in Day 8 samples, and this was increased with TGF-β treatment. Cytoplasmic staining could be an artifact resulting from the staining protocol when nuclear localization of histones is considered. In SNU-387 and SNU-423 cell lines, nuclear staining patterns are observed as weak to moderately stained. In Mahlavu and SK-HEP-1 Day 8 samples, H3K9me3 staining seemed to be weaker in TGF-β positive conditions.

4.1.1.4 Histone H3 lysine 36 trimethylation in HCC cell lines

H3K36me3 levels in HCC cell lines are again determined by immunoperoxidase staining in the presence or absence of 72 hour 5 ng/ml TGF-β treatment. Cells were stained with antibodies specific to H3K36me3 modification to assess the global levels

of this histone mark on Day 4 or Day 8 of TGF-β treatment as described in the previous sections. Results of these staining experiments are shown in Figure 4.1.4.

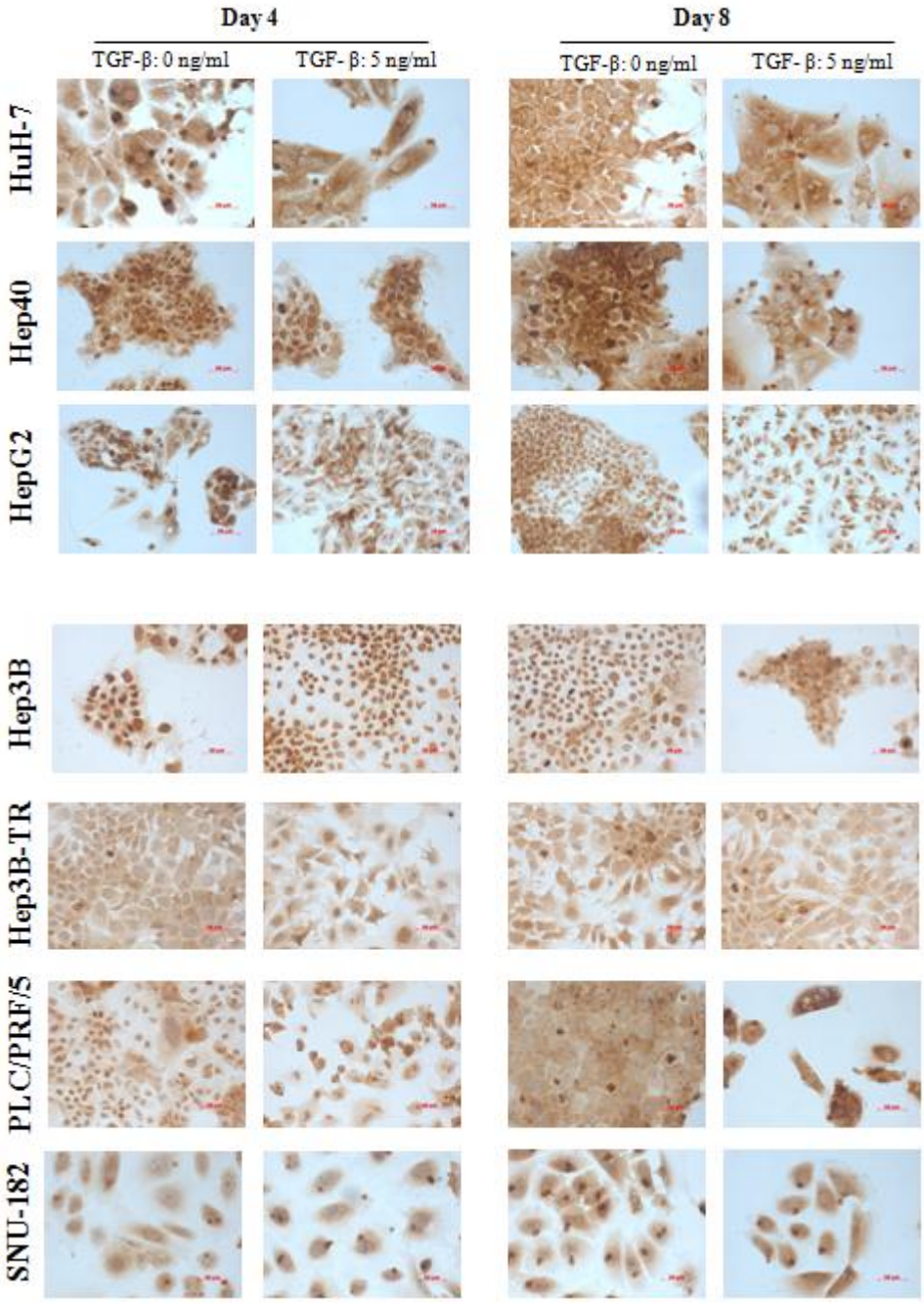

Figure 4.1.4: Global levels of H3K36me3 in HCC cell lines in the presence or absence of TGF-β induced senescence; determined by immunoperoxidase staining. Immunostaining experiments were done on Day 4 or Day 8 of 0 or 5 ng/ml TGF-β treatment. In order to avoid bias, all pairs with 0 or 5 ng/ml TGF-β were visualized and photographed under same lighting conditions using 40x objective.

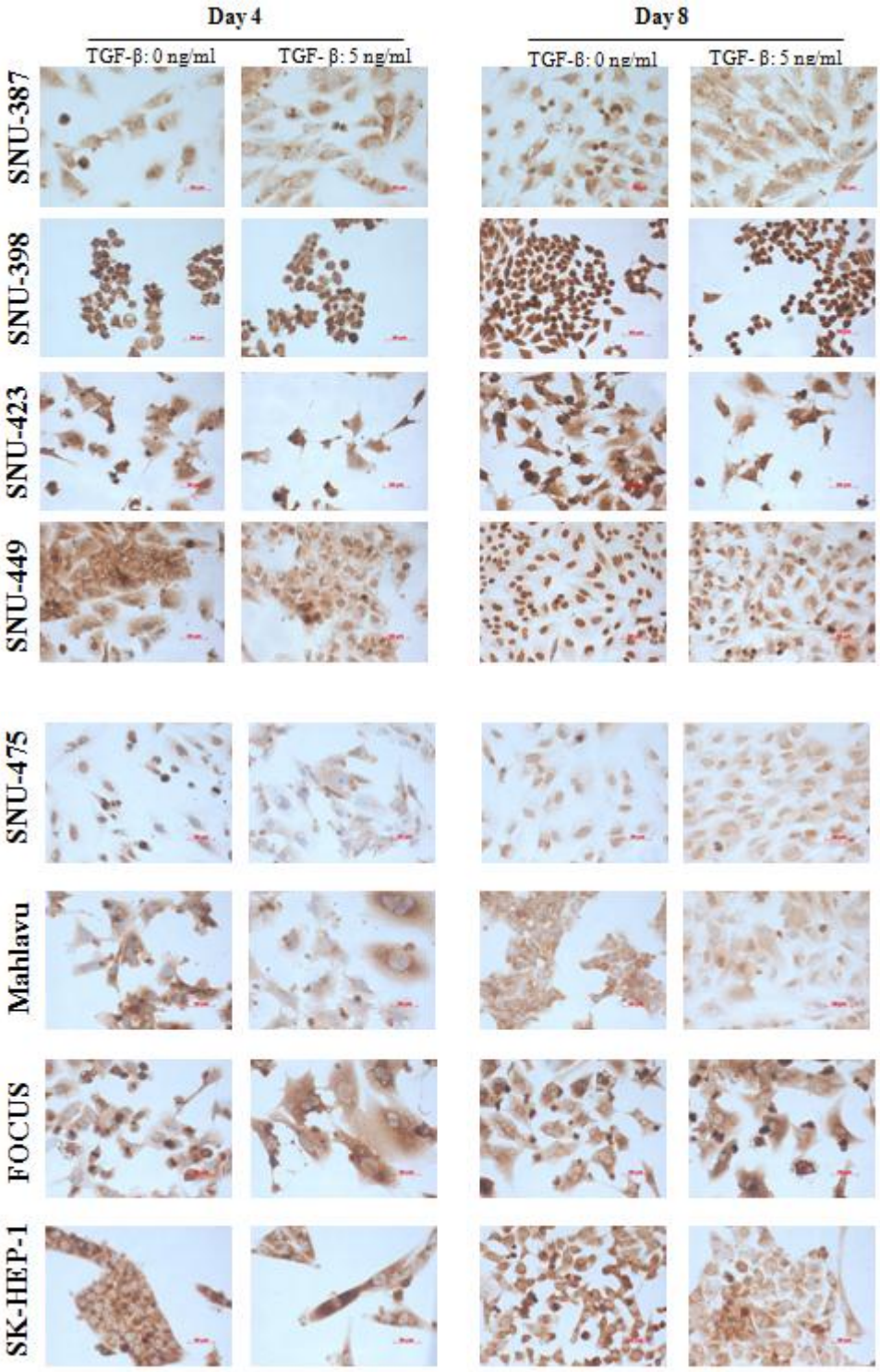

Figure 4.1.4 (continued): Global levels of H3K36me3 in HCC cell lines in the presence or absence of TGF-β induced senescence; determined by immunoperoxidase staining.

As shown in Figure 4.1.4, H3K36me3 staining in HCC cell lines revealed mostly a cytoplasmic staining pattern with a nuclear staining pattern that changed from weak to

strong. Considering the nuclear localization of histones, the cytoplasmic staining is most likely false positive, that might have resulted from nonspecific binding of the antibody. Therefore, it is not completely reliable to make comparisons or to draw conclusions from this data.

4.1.1.5 Histone H3 arginine 2 dimethylation in HCC cell lines

Global H3R2me2 levels in HCC cell lines were analyzed by immunoperoxidase staining experiments in the absence or presence of TGF-β induced senescence. Senescence was induced in specific cell lines as described in previous sections and was previously analyzed by SABG assay, therefore SABG assay was not repeated for each specific histone methylation mark. Results of these experiments are shown in Figure 4.1.5.

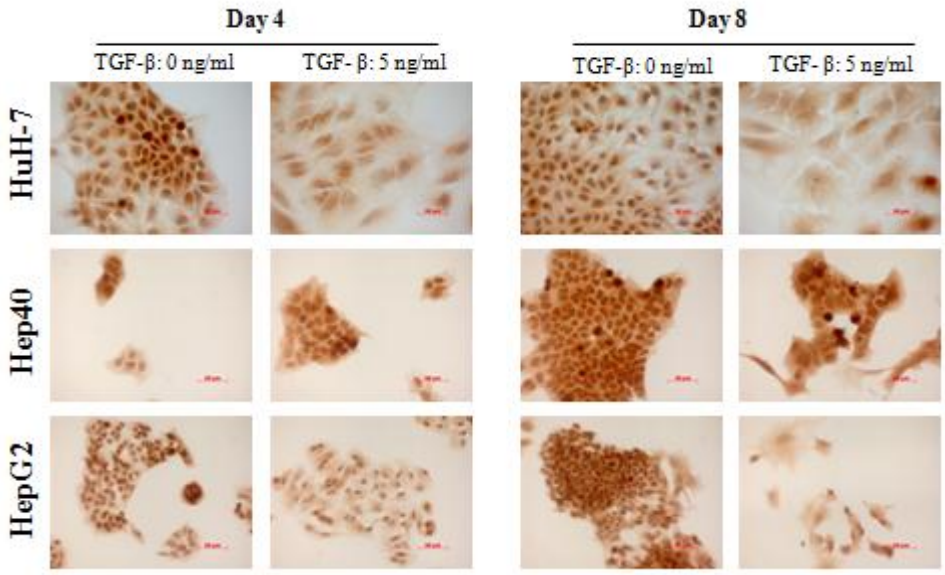

Figure 4.1.5: Global levels of H3R2me2 in HCC cell lines in the presence or absence of TGF-β induced senescence; determined by immunoperoxidase staining. Immunostaining experiments were done on Day 4 or Day 8 of 0 or 5 ng/ml TGF-β treatment. In order to avoid bias, all pairs with 0 or 5 ng/ml TGF-β were visualized and photographed under same lighting conditions using 40x objective.

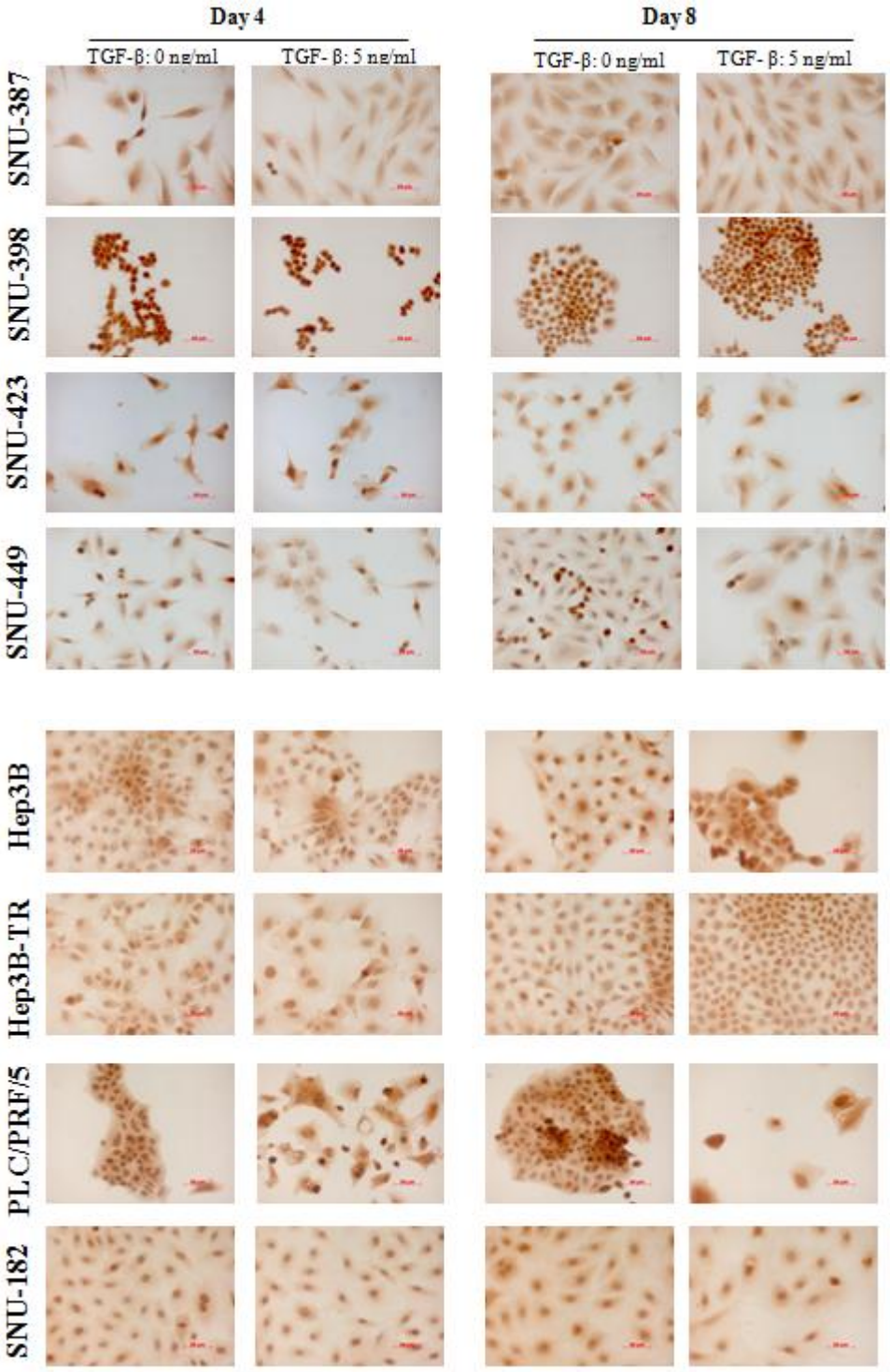
Day 4
Day 8
TGF-β: 0 ng/ml
TGF- β: 5 ng/ml
TGF-β: 0 ng/ml
TGF- β: 5 ng/ml
SNU-387
SNU-398
SNU-423
SNU-449
Hep3B
Hep3B-TR
PLC/PRF/5
SNU-182

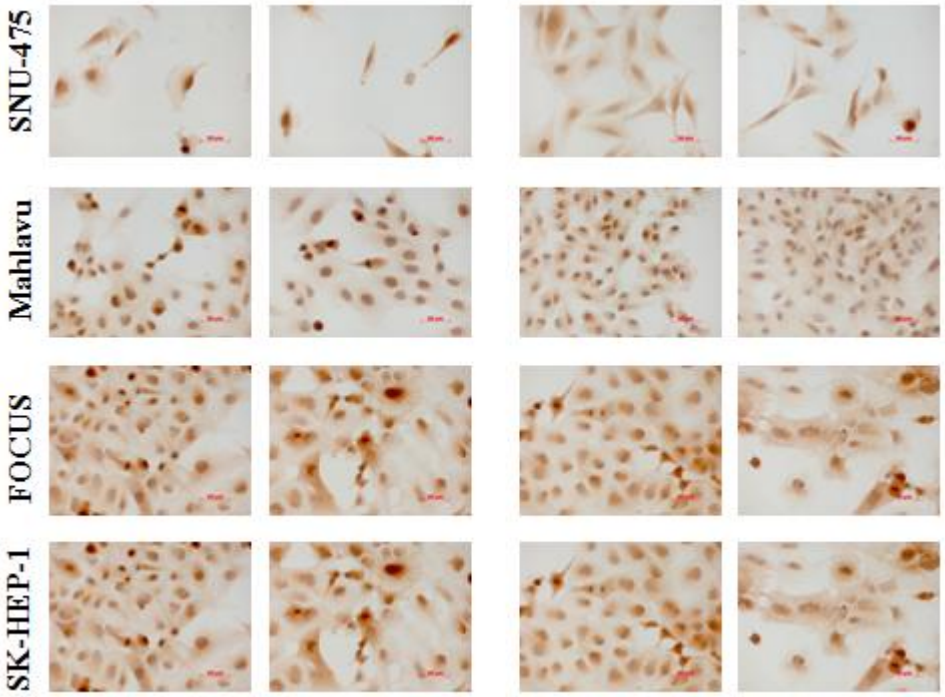

Figure 4.1.5 (continued): Global levels of H3R2me2 in HCC cell lines in the presence or absence of TGF-β induced senescence; determined by immunoperoxidase staining.

As seen in Figure 4.1.5, most of the cells were stained positive for global H3R2me2, with some amount of variation between cell lines that ranged from moderately positive to weakly positive. Slightly cytoplasmic stained parts are considered to be nonspecific. In HuH-7 cell line, H3R2me2 levels were reduced in TGF-β treated sample. In SNU-449 and Mahlavu cell lines, H3R2me2 is weakly stained, together with strongly stained mitotic cells. Other than those specified, the overall pattern of H3R2me2 staining is similar in all cell lines, irrespective of TGF-β induced senescence.

4.1.1.6 Histone H3 arginine 17 dimethylation in HCC cell lines

All cell lines were also tested against global levels of H3R17me2, similarly in the presence or absence of 5 ng/ml TGF-β treatment which induces senescence in most well-differentiated HCC cell lines. Immunoperoxidase staining experiments were

performed similarly on Day 4 or Day 8 of TGF-β treatment. The results of those experiments are shown in Figure 4.1.6

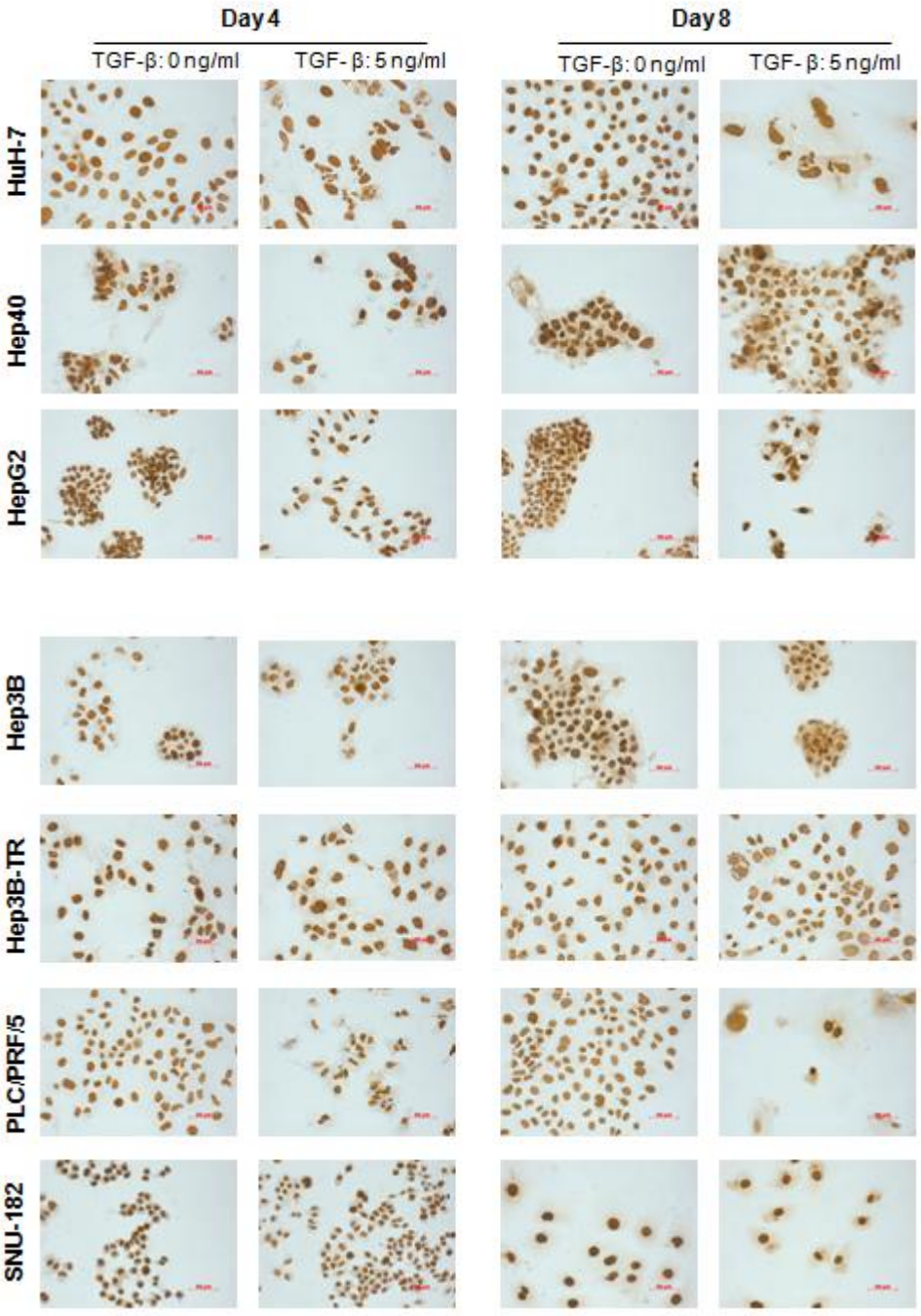

Figure 4.1.6: Global levels of H3R17me2 in HCC cell lines in the presence or absence of TGF-β induced senescence; determined by immunoperoxidase staining. Immunostaining experiments were done on Day 4 or Day 8 of 0 or 5 ng/ml TGF-β treatment. In order to avoid bias, all pairs with 0 or 5 ng/ml TGF-β were visualized and photographed under same lighting conditions using 40x objective.

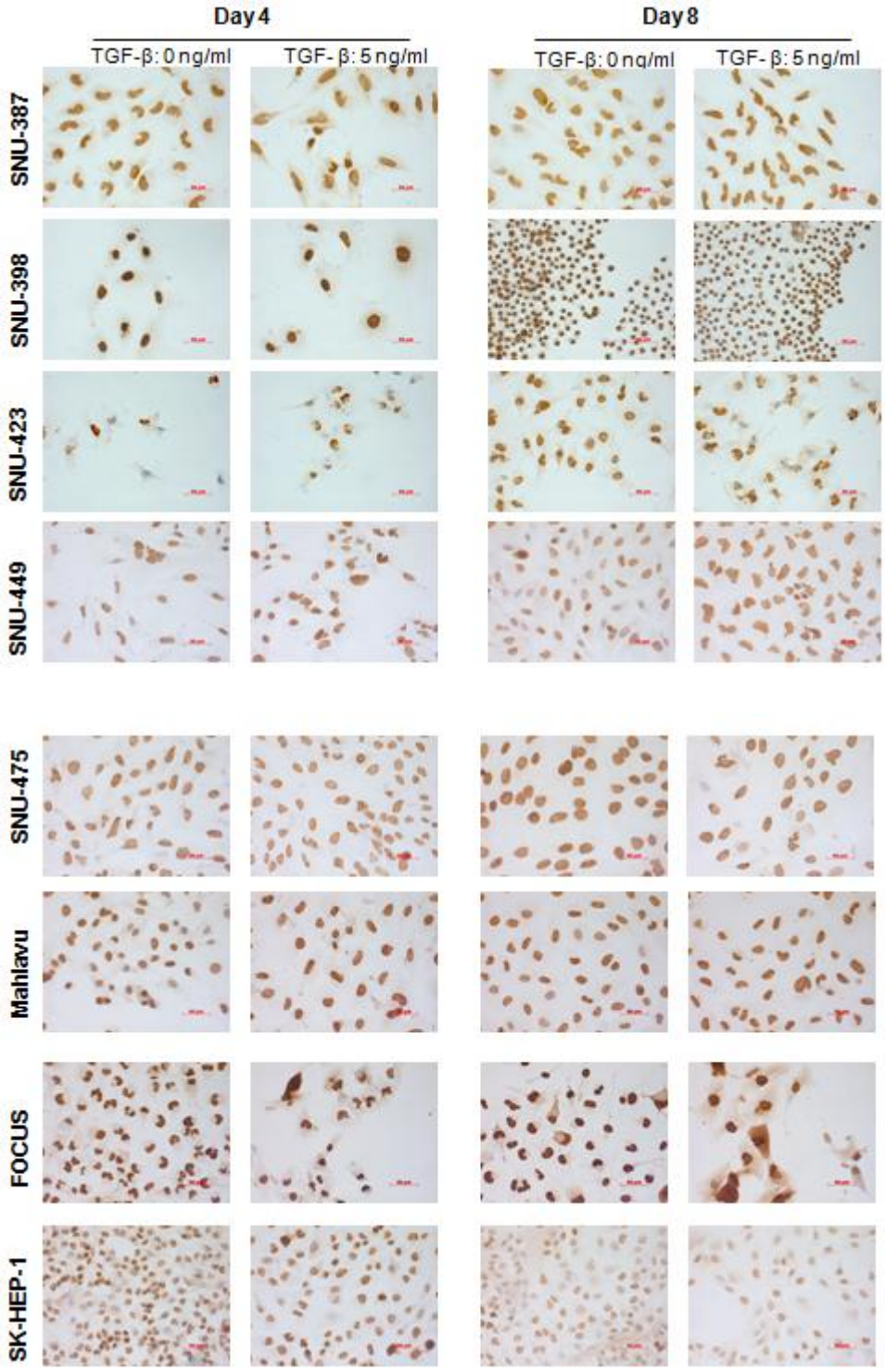

Figure 4.1.6 (continued): Global levels of H3R17me2 in HCC cell lines in the presence or absence of TGF-β induced senescence; determined by immunoperoxidase staining.

According to the results shown in Figure 4.1.6, most of the cell lines exhibited a strongly positive nuclear staining in both TGF-β conditions. PLC/PRF/5 cell line

responded to TGF-β treatment which appeared to result in a heterogeneous H3R17me2 staining in Day 8 samples. SNU-423 and SK-HEP-1 cell lines exhibited heterogeneous staining in all cases. SNU-449 cell line was stained heterogeneously, which turned into full positive staining in the TGF-β positive case.

4.1.1.7 Histone H4 lysine 20 trimethylation in HCC cell lines

As previously mentioned, Histone 4 lysine 20 trimethylation has been associated with other cancers in the literature. Loss of H4K20 trimethylation has been proposed to be a hallmark of cancer (Fraga MF, et al, 2005). Although trimethylated H4K20 levels are highly cell cycle dependent, transformed cells are subject to a specific loss. Liver tumors in rats induced by a methyl deficient diet showed a progressive decrease in H4K20 trimethylation (Pogribny IP, et al, 2006). Additionally, in human breast cancer cell lines, loss of H4K30me3 mark corresponded to more aggressive phenotypes (Tryndyak, VP, et al, 2006). Similarly, in a study of non-small cell lung cancer, cancer cells displayed loss of H4K20 trimethylation compared to normal lung cells (Broeck AVD, et al, 2008).

Since well and poorly differentiated HCC cell lines represent early and advanced stages of HCC, it was likely that these two HCC cell line subtypes could exhibit differences between H4K20me3 methylation status. Therefore, we decided to screen our cell line panel for the global H4K20me3 levels of cell lines using again immunoperoxidase staining method. TGF-β induced senescence model is also employed in this experiment. Cells were seeded in 6-well tissue culture plates on coverslips. The next day, they were subjected to 72 hours of 0 or 5 ng/ml TGF-β treatment. The immunostaining experiments were performed on Day 4 or Day 8 of TGF-β treatment. Results of these experiments are shown in Figure 4.1.7.

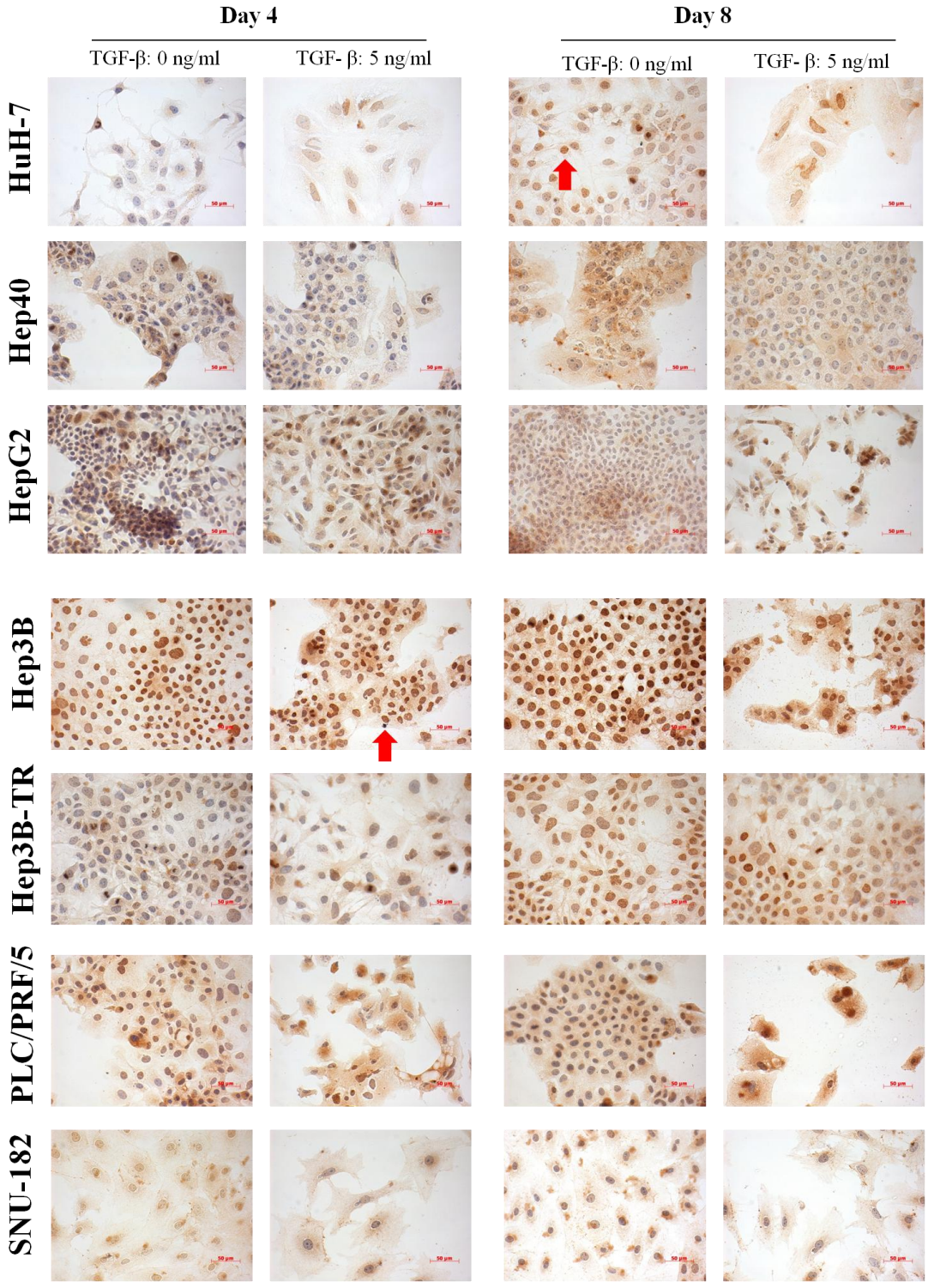

Figure 4.1.7: Global levels of H4K20me3 in HCC cell lines in the presence or absence of TGF-β induced senescence; determined by immunoperoxidase staining. Immunostaining experiments were done on Day 4 or Day 8 of 0 or 5 ng/ml TGF-β treatment. In order to avoid bias, all pairs with 0 or 5 ng/ml TGF-β were visualized and photographed under same lighting conditions using 40x objective. Example positive cells were shown with red arrows, and example negative cells were shown with black arrows.

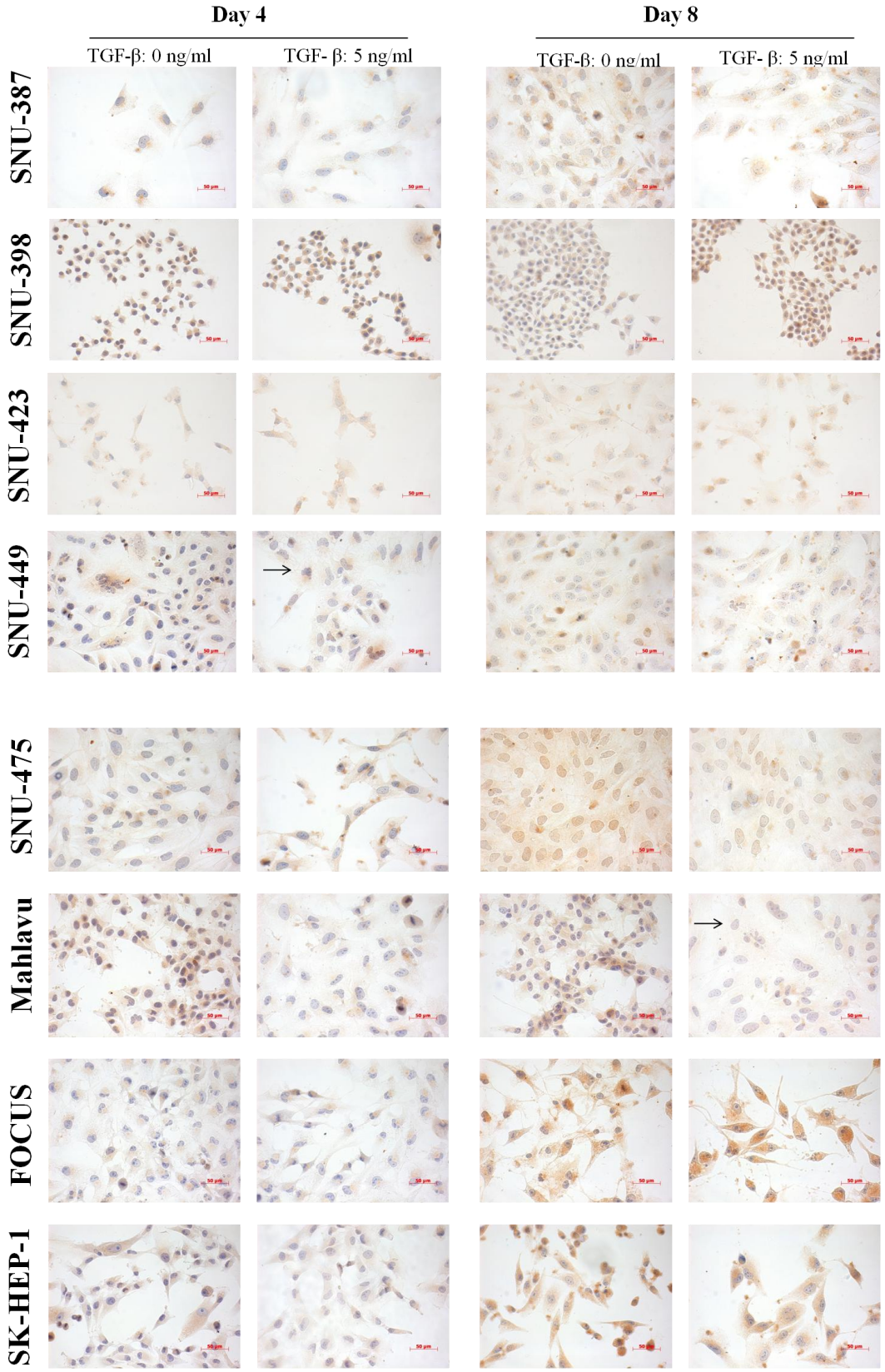

Figure 4.1.7 (continued): Global levels of H4K20me3 in HCC cell lines in the presence or absence of TGF-β induced senescence; determined by immunoperoxidase staining.

According to the results shown in Figure 4.1.7, H4K20me3 levels are low in poorly differentiated cell lines in comparison to the well differentiated cell lines. Most of the well differentiated cell lines, especially Hep3B and Hep40, also Hep3B-TR show a strong positive pattern. The difference between the staining patterns of the cell lines is more evident in Day 8 samples, and does not relate with TGF-β treatment.

In order to confirm the results obtained from the immunoperoxidase staining experiments, western blotting technique was also employed. For the western blot analysis, a smaller panel of 9 cell lines was chosen which represented the strongly stained well-differentiated cell lines and the weakly stained poorly-differentiated cell lines. Histone extracts from these cell lines were separated in SDS-PAGE, and blotted with antibodies against H4K20me3 and unmodified H3, which served as an equal loading control. Results of this western blotting experiment is shown in Figure 4.1.8.

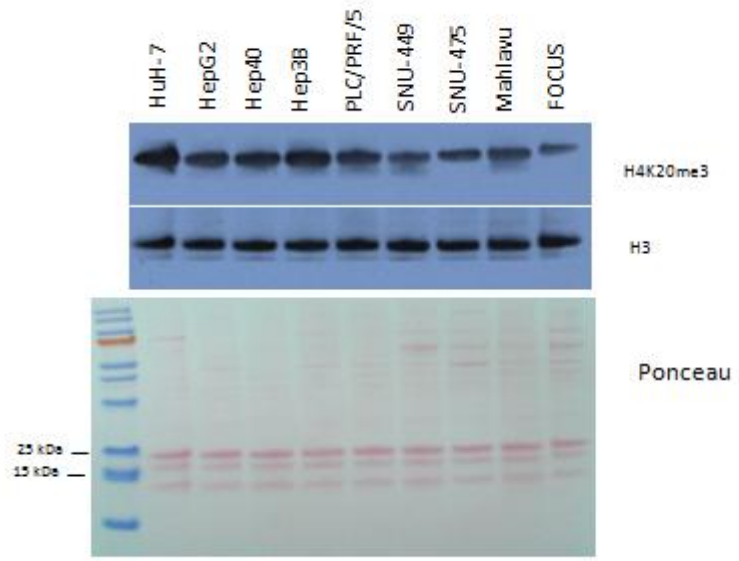

Figure 4.1.8: H4K20me3 levels in HCC cell lines; determined by western blotting. Histone lysates from all cell lines were obtained by acid extraction as explained in the Materials and Methods section. 4 μg of each lysate was loaded on a gel and blotted with H4K20me3 antibody. Unmodified H3 was used as a loading control. Ponceau S stained membrane is also shown in order to confirm equal loading.

Western blotting data confirmed the results obtained from immunoperoxidase staining. As seen in Figure 4.1.8, poorly differentiated cell lines, especially SNU-449, SNU-475 and FOCUS contained bands with weaker intensity when compared to well differentiated cell lines.

4.1.1.8 Histone H4 lysine 20 monomethylation in HCC cell lines

Immunoperoxidase and western blotting data for H4K20me3 levels let us to conclude that this histone mark was subject to a loss in poorly differentiated cell lines. H4K20me1 is the preferred substrate for the formation of trimethylated H4K20 mark, therefore, H4K20me3 levels are directly linked to H4K20me1 levels (Yang H, et al, 2009). In order to gain information on which stage histone H4 lysine 20 starts to get affected in a manner that results in the loss of its methylation status, we wanted to analyze the monomethylation levels. Monomethylated histone H4 lysine 20 levels were also analyzed by western blotting, by using acid extracted histones similarly, as shown in Figure 4.1.9.

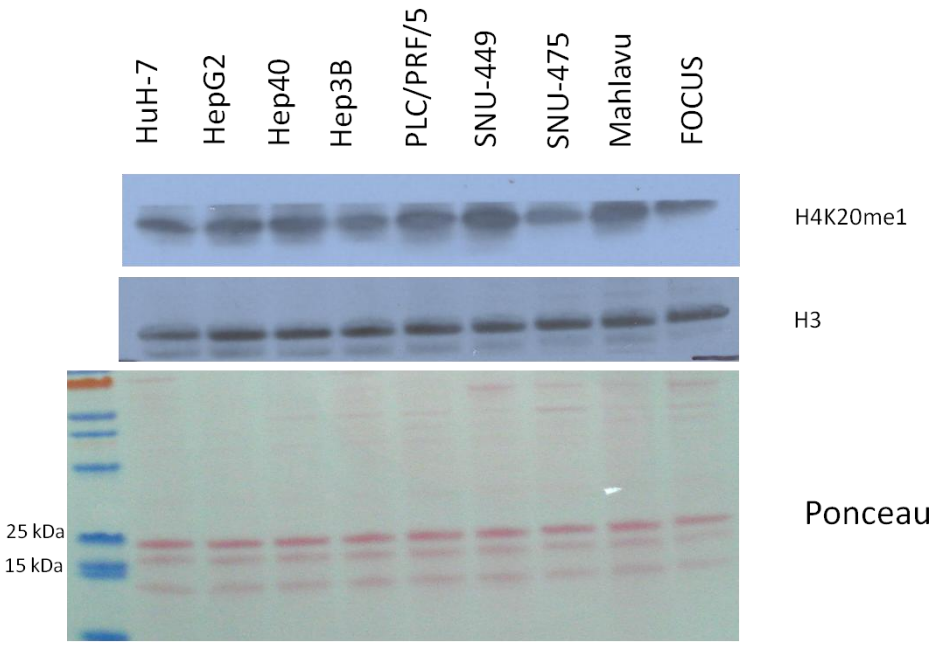

Figure 4.1.9: H4K20me1 levels in HCC cell lines; determined by western blotting. Histone lysates from all cell lines were obtained by acid extraction as explained previously. 4 µg of

each lysate was loaded on a gel and blotted with H4K20me1 antibody. Unmodified H3 was used as a loading control. Ponceau S stained membrane is also shown in order to confirm equal loading.

H4K20me1 western blotting revealed a similar pattern of H4K20 monomethylation with H4K20 trimethylation with the exception of SNU-449 cell line. These results raise the possibility that formation of the H4K20me1 mark might be affected in poorly differentiated cell lines which then results in the loss of H4K20me3. Nevertheless, they do not eliminate a possible change in the steps that lead from H4K20me1 to H4K20me3.

4.2 Histone methyltransferases that act on H4K20

There are three methyltransferase enzymes that are known to act on histone 4 lysine 20. These three enzymes are: Set8, which functions as a monomethyl transferase, Suv4-20h1 and Suv4-20h2 which both function as dimethyl transferase and trimethyl transferases. In order to address a potential role, which is played by either one of these three methyltransferases, on the loss of H4K20me3 in poorly differentiated cell lines, we wanted to characterize the expression status of all the transcript variants of these three enzymes in our HCC cell line panel. Currently, there is no identified demethylase enzyme which is known to act on H4K20, therefore we had to concentrate on the methyltransferase enzymes and the specific roles they potentially play in the phenomenon.

4.2.1 H4K20 methyltransferases Suv4-20h1 and Suv4-20h2

Dimethyl and trimethyl forms of H4K20 are both catalyzed by Suv4-20h1 and Suv4-20h2 enzymes which use the monomethylated form as the preferential substrate, and can also use the non-methylated form (Yang H, et al, 2009). Gene information for these two enzymes were retrieved from Ensembl and NCBI databases, and RT-PCR primers for all different transcript variants were designed accordingly. Exon structures, transcript variants and primer locations for these two genes are summarized in Figure 4.2.1. Suv4-20h1 gene has two isoforms. Variant 1, which is

the bigger isoform, codes for a 885 amino acid protein, with a predicted molecular weight of 99 kilo daltons. Variant 2, which is the smaller isoform, codes for a 393 amino acid protein with a predicted molecular weight of 44 kilo daltons. Suv4-20h2 gene has one canonical isoform according to Uniprot and NCBI databases, which is shown as Variant 1 in Figure 4.2.1.b, this isoform codes for a 462 amino acid protein with a predicted molecular weight of 52 kilo daltons. There is also one reported nonsense mediated decay product, according to Ensembl database, which is depicted here as Variant 2, and finally there is one other reported alternative splice product which is depicted here as Variant 3.

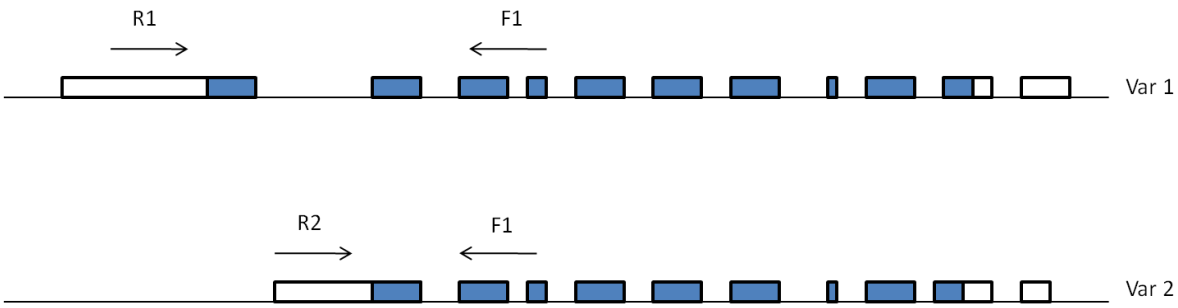

Figure 4.2.1.a: Suv4-20h1 transcript variants and RT-PCR primers. Transcript variants 1 and 2 are depicted as Var1 and Var2. All exons are shown with rectangles. Filled rectangles represent translated regions, empty rectangles represent nontranslated regions. F1 is forward primer 1, R1 is reverse primer 1, R2 is reverse primer 2. Variant 1 is analyzed by using F1 and R1 primers, Variant 2 is analyzed by using F1 and R2 primers. (Adapted from Ensembl genome browser)

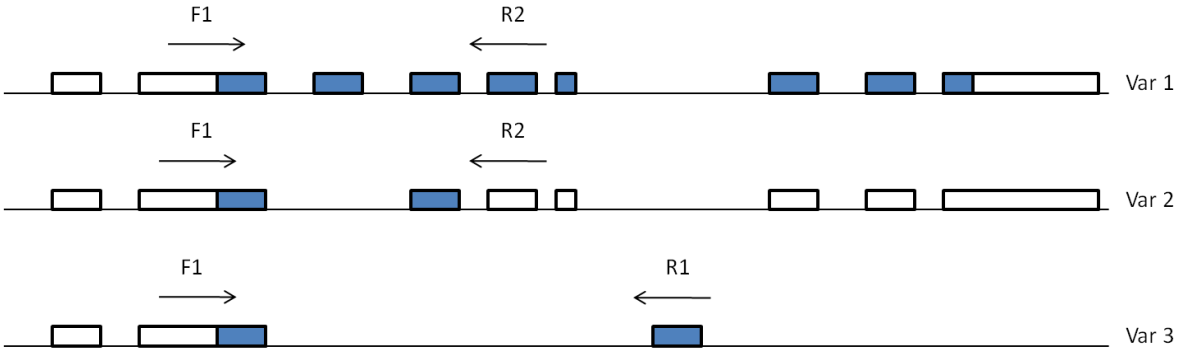

Figure 4.2.1.b: Suv4-20h2 transcript variants and RT-PCR primers. Transcript variants 1, 2 and 3 are depicted as Var1, Var2 and Var3. All exons are shown with rectangles. Filled rectangles represent translated regions, empty rectangles represent nontranslated regions. F1 is forward primer 1, R1 is reverse primer 1, R2 is reverse primer 2. Variant 1 and Variant 2 are analyzed by using F1 and R2 primers, and Variant 3 is analyzed by using F1 and R1 primers. Variant 1 is the canonical isoform. (Adapted from Ensembl genome browser)

4.2.1.1. Suv4-20h1 levels in HCC cell lines

Total RNA was isolated from our 15 HCC cell lines, and cDNAs were synthesized from all. By using these cDNAs, Suv4-20h1 levels were analyzed via RT-PCR with the primers shown in Figure 4.2.1.a. Variant 1 levels were addressed by using F1 and R1 primers, whereas Variant 2 levels were addressed by using F1 and R2 primers. In order to confirm the results obtained, RT-PCR experiments are repeated twice with two different RNA extracts. The results of these RT-PCR experiments are shown in Figure 4.2.2.

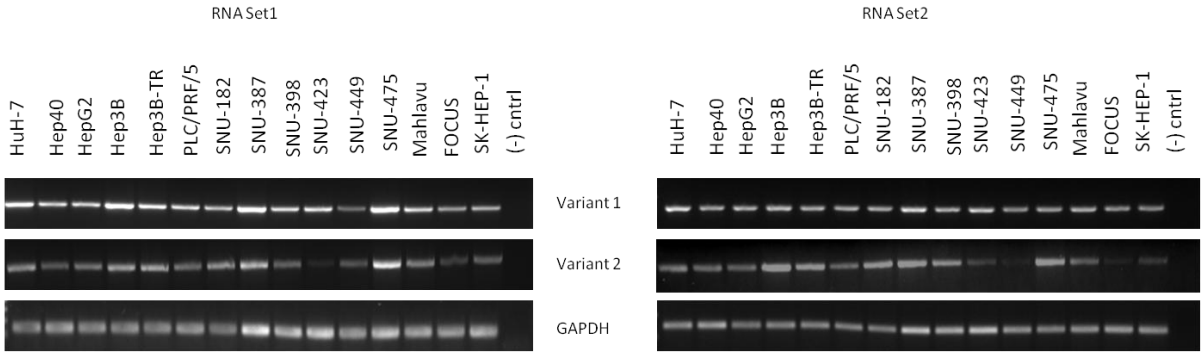

Figure 4.2.2: Suv4-20h1 levels in HCC cell lines, determined by RT-PCR. Transcript levels of Suv4-20h1 isoforms are determined by semi-quantitative RT-PCR. GAPDH (Glyceraldehyde-3-phosphate dehydrogenase) is used as an internal control. (-) cntrl stands for negative control, without cDNA, to check for any nucleic acid contamination.

According to the results shown in Figure 4.2.2, Suv4-20h1 Variant 1 is expressed in all HCC cell lines, with slight variations, for example transcript amount looks slightly more in SNU-387, and slightly less in SNU-449 when compared to GAPDH expression. Suv4-20h1 Variant 2 has more variations of expression between cell lines. Some of the poorly differentiated cell lines, such as SNU-423, SNU-449 and FOCUS have noticeably low levels of Variant 2. Differences seen between the two RNA sets might be due to differences in cell cycle profiles of the cells when pellets are collected. Since Suv4-20h1 levels are highly dependent on cell cycle stages, such slight variations are expected. Protein levels of Suv4-20h1 could not be examined in cell lines due to the lack of working antibodies.

4.2.1.2. Suv4-20h2 levels in HCC cell lines

Total RNA was isolated from our 15 HCC cell lines, and cDNAs were synthesized from all. By using these cDNAs, Suv4-20h2 levels were analyzed similarly via RT-PCR with the primers shown in Figure 4.2.1.b. Variant 1 and Variant 2 levels were addressed by using F1 and R2 primers. PCR products of Variants 1 and 2 are differentiated according to product sizes, since Variant 1 PCR product is 553 base pairs, whereas Variant 2 PCR product is 387 base pairs. Variant 3 levels were addressed by using F1 and R1 primers. In order to confirm the results obtained, RT-PCR experiments are repeated twice with two different RNA extracts. The results of these RT-PCR experiments are shown in Figure 4.2.3.

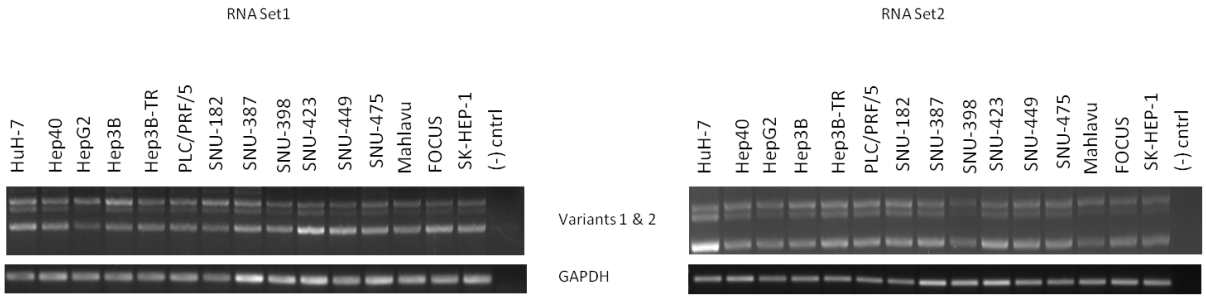

Figure 4.2.3.a: Suv4-20h2 Variants 1 and 2 levels in HCC cell lines, determined by semi quantitative RT-PCR. GAPDH is used as an internal control. (-) cntrl stands for negative control. Upper band is Variant 1 (553 bp), lower band is Variant 2 (387 bp).

Figure 4.2.3.b: Suv4-20h2 Variant 3 is not expressed in HCC cell lines, determined by semi quantitative RT-PCR. GAPDH is used as an internal control. (-) cntrl stands for negative control.

According to the results shown in Figure 4.2.3.a, Suv4-20h2 Variants 1 and 2 are expressed in all HCC cell lines, with slight variations. And according to Figure 4.2.3.b, Suv4-20h2 Variant 3 is not expressed in HCC cell lines. Therefore, Suv4-20h2 variants did not seem to be responsible for the loss of H4K20me3 mark in poorly differentiated cell lines. Protein levels of Suv4-20h2 again could not be analyzed due to the lack of a working antibody.

4.2.2 H4K20 methyltransferase Set8

Set8 is the only histone methyltransferase enzyme that is known to transfer one methyl group to unmodified histone H4 lysine 20 (Xiao B, et al, 2005; Coutre JF, et al, 2005). Since we were unable to identify a relationship between the loss of H4K20me3 mark in poorly differentiated cell lines and the status of the expression of Suv4-20h1 and Suv4-20h2 enzymes, the other candidate gene that might be involved in this process was Set8. Aberrations in Set8 expression could result in a loss of H4K20me1 levels, which in turn might result in a loss of H4K20me3 levels. The parallelism between H4K20me1 and H4K20me3 levels which were shown in Figures 4.1.8 and 4.1.9 also supports this possibility.

Information about Set8 gene was retrieved from NCBI and Ensembl databases, and RT-PCR primers were designed accordingly. Set8 gene has one canonical isoform according to NCBI database, which encodes for a protein of 352 amino acids, with a molecular weight of 39 kilo daltons. According to the Ensembl database, there are a total of 4 transcript variants, which are shown in Figure 4.2.4. Variant 1 is the mentioned canonical variant, and Variant 4 corresponds to the same protein product which only contains some difference in its nontranslated regions. Therefore variants 1 and 4 are analyzed with the same primers: F1 and R2. Variant 2 is depicted as a nonsense mediated decay product in Ensembl, therefore it was eliminated from the analysis. Variant 3 had its first exon different from the canonical isoform, and encoded for a 229 amino acid protein with a molecular weight of 34 kilo daltons, and this variant was analyzed with primers F2 and R1.

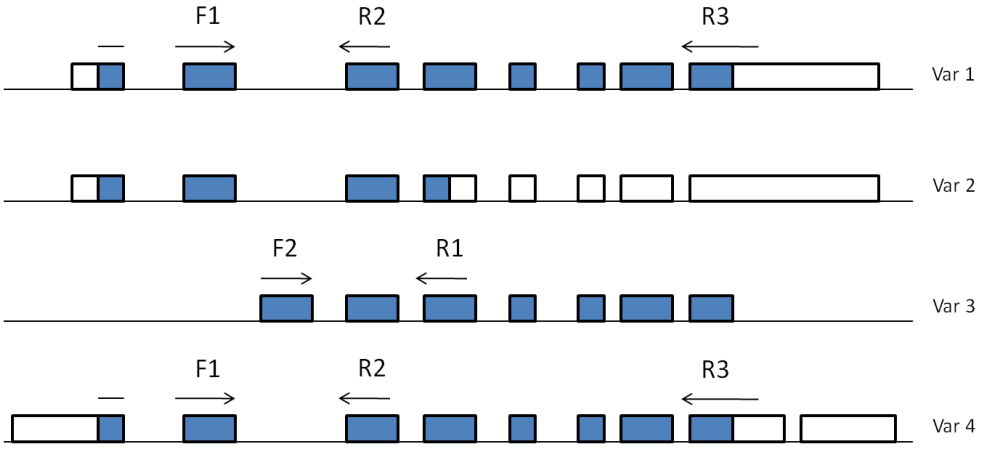

Figure 4.2.4: Set transcript variants and RT-PCR primers. Transcript variants 1, 2, 3 and 4 are depicted as Var1, Var2, Var3 and Var4. All exons are shown with rectangles. Filled rectangles represent translated regions, empty rectangles represent nontranslated regions. F1 is forward primer 1, F2 is forward primer 2, R1 is reverse primer 1, R2 is reverse primer 2, R3 is reverse primer 3. Variant 1 and Variant 4 are analyzed by using F1 and R2 primers, and Variant 3 is analyzed by using F2 and R1 primers. F1 and R3 were designed to see the full length product. Variant 1 is the canonical isoform. (Adapted from Ensembl genome browser)

4.2.2.1 Set8 Levels in HCC cell lines

In order to analyze Set8 expression patterns in HCC cell lines, total RNA was extracted from all, and cDNAs were synthesized, as described in the Materials and Methods section. Set8 levels were analyzed using primers described in Figure 4.2.4 by both semi quantitative RT-PCR and quantitative RT-PCR methods. RT-PCR experiments were repeated with 2 different sets of RNA in order to confirm the results obtained. The results of these experiments are shown in Figure 4.2.5. Additionally, in order to investigate the possibility that another alternative splice form might be expressed in HCC cell lines, F1 and R3 primers are used to set up a PCR reaction that resulted in the amplification of the full length product. For this purpose, three cell lines were chosen as representatives, and the results are shown in Figure 4.2.5.d. Since the three candidate cell lines only expressed the full length product of the expected size, this analysis was not extended to all cell lines.

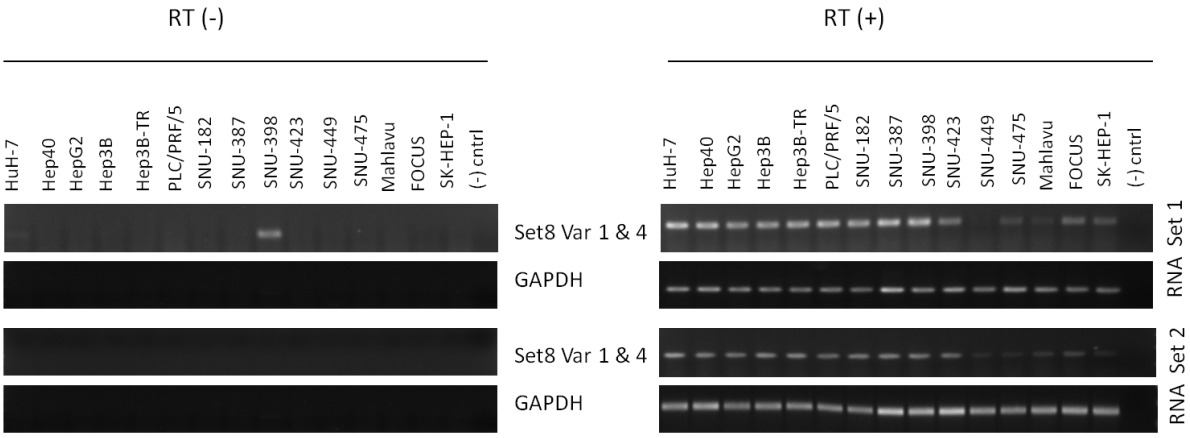

Figure 4.2.5.a: Set8 transcript variants 1 and 4 levels in HCC cell lines, determined by semi-quantitative RT-PCR. GAPDH is used as an internal control. (-) cntrl stands for negative control, to check for nucleic acid contamination in the PCR reaction. RT (-) stands for cDNAs that were synthesized without the addition of reverse transcriptase; therefore controls possible genomic DNA contamination.

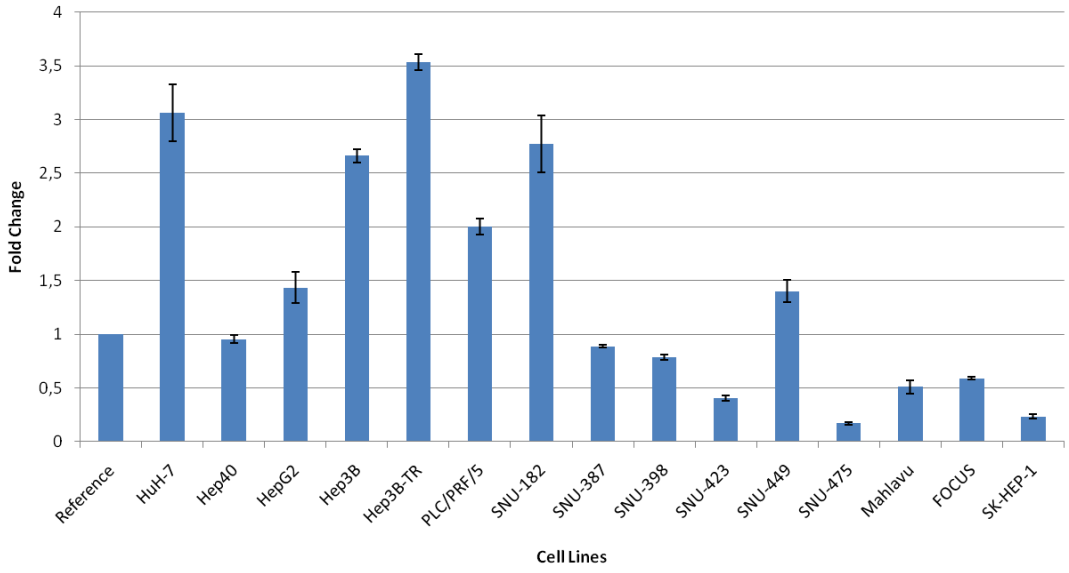

Figure 4.2.5.b: Set8 transcript variants 1 and 4 levels in HCC cell lines, by quantitative RT-PCR. F1 and R2 primers were used for Set8 amplification. Average of all cell lines was used as a reference, and fold changes were calculated with respect to that reference. Experiment was performed in triplicates, averages and standard deviations are shown.

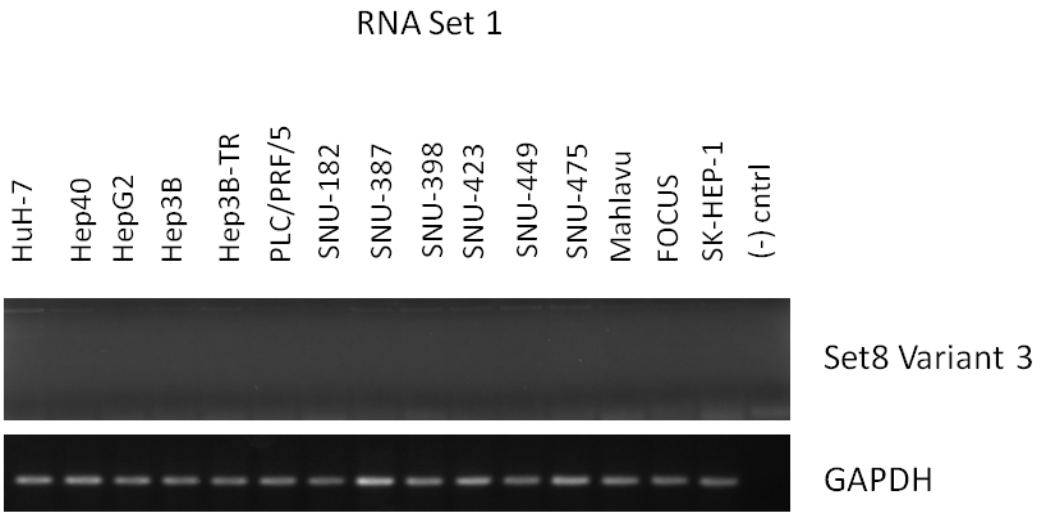

Figure 4.2.5.c: Set Variant 3 is not expressed in HCC cell lines, determined by semi-quantitative RT-PCR. GAPDH is used as an internal control. (-) cntrl stands for negative control, to check for nucleic acid contamination in the PCR reaction.

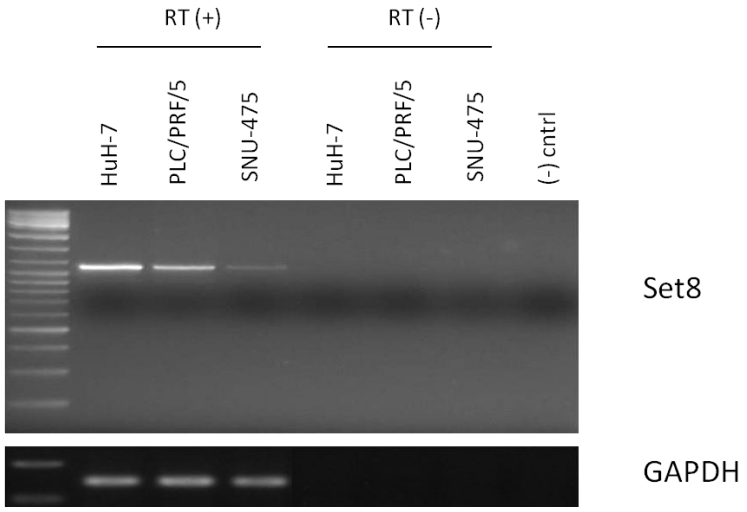

Figure 4.2.5.d: Expression of Set8 full length product in HCC cell lines, determined by RT-PCR. GAPDH is used as an internal control. (-) cntrl stands for negative control, to check for nucleic acid contamination in the PCR reaction.

As can be interpreted from the results shown in Figure 4.2.5, only the canonical variant (Variants 1 and 4) of Set8 is expressed in HCC cell lines. Set8 expression levels vary greatly between cell lines; generally highly expressed in well differentiated cell lines, and low expressed in poorly differentiated cell lines. This

pattern of expression is consistent with the levels of H4K20me3 and H4K20me1 levels in these cell lines.

4.2.2.2 Set8 levels in patient liver tissue samples

In order to gain an understanding of Set8 expression levels in human tissues, total RNA was isolated from 5 HCC-Cirrhosis paired patient tissue samples. cDNAs were synthesized from all, and Set8 canonical isoform levels were determined by quantitative RT-PCR. According to the results of this experiment, which are shown in Figure 4.2.6, Set8 expression in human tissues is quite variable. In 4 out of 5 paired tissues, Set8 expression was reduced in HCC, which was expected. In the 5th paired sample, it was the opposite.

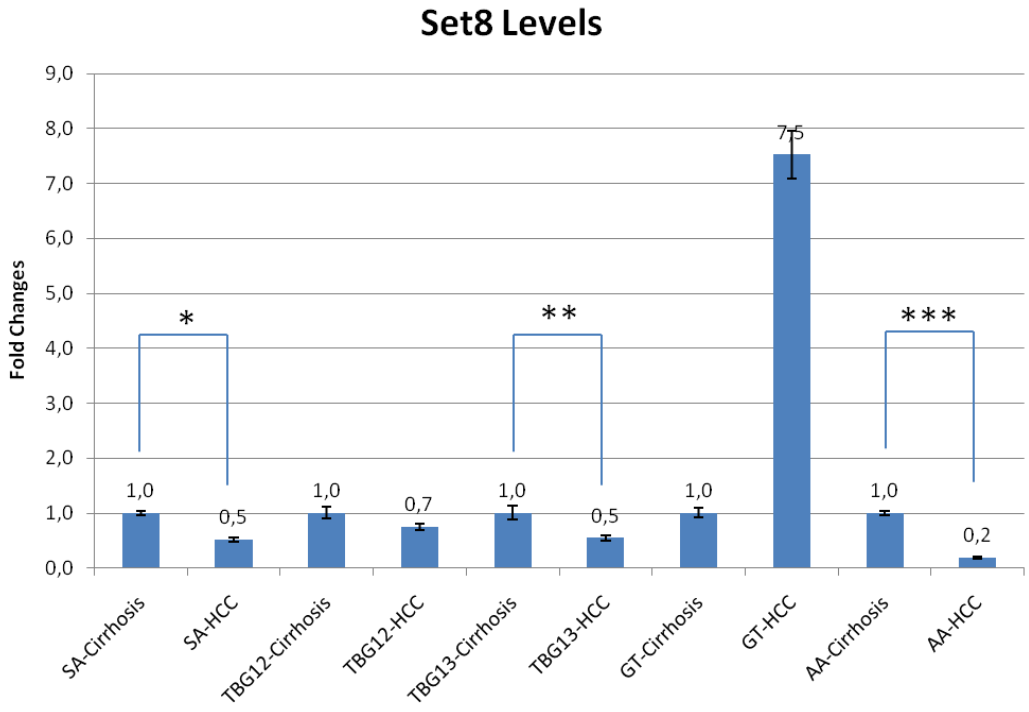

Figure 4.2.6: Set8 expression in patient liver tissue samples, determined by quantitative RT-PCR. F1 and R2 primers were used for Set8 amplification. Fold changes were calculated with respect to cirrhotic samples in each pair. Experiment was performed in triplicates, averages and standard deviations are shown. *: p-value < 0,01, **: p-value < 0,05, ***: p-value < 0,001 according to two-tailed t-test.

4.2.2.3 Set8 Overexpression in SNU-475 cell line

Since Set8 levels showed a noticeable correlation with HCC progression in both cell lines and patient tissue samples, we reasoned there could be a causative relationship between Set8 expression and HCC. Therefore we decided to employ overexpression strategy in order to search for a possible role of Set8 gene in HCC progression. SNU-475 was the cell line with the lowest expression of Set8 in our cell line panel, so it was chosen to overexpress Set8 gene. Full length Set8 vector with HA-tag at the C terminal end was purchased from GeneCopoeia company (USA), and verified by sequencing, as shown in Figure 4.2.7.

Alignment:
CLUSTAL W (1.81) multiple sequence alignment (1 Mismatch)

```
Set8-ENSEMBL-Var4               MARGRKMSKPRAVEAAAAAAAVAATAPGPEMVERRGPGRPRTDGENVFTG
Set8-NCBI                       MARGRKMSKPRAVEAAAAAAAVAATAPGPEMVERRGPGRPRTDGENVFTG
T8950-Sequencing_Result_[Tra    MARGRKMSKPRAVEAAAAAAAVAATAPGPEMVERRGPGRPRTDGENVFTG
                                ************************************************

Set8-ENSEMBL-Var4               QSKIYSYMSPNKCSGMRFPLQEENSVTHHEVKCQGKPLAGIYRKREEKRN
Set8-NCBI                       QSKIYSYMSPNKCSGMRFPLQEENSVTHHEVKCQGKPLAGIYRKREEKRN
T8950-Sequencing_Result_[Tra    QSKIYSYMSPNKCSGMRFPLQEENSVTHHEVKCQGKPLAGIYRKREEKRN
                                ************************************************

Set8-ENSEMBL-Var4               AGNAVRSAMKSEEQKIKDARKGPLVPFPNQKSEAAEPPKTPPSSCDSTNA
Set8-NCBI                       AGNAVRSAMKSEEQKIKDARKGPLVPFPNQKSEAAEPPKTPPSSCDSTNA
T8950-Sequencing_Result_[Tra    AGNAVRSAMKSEEQKIKDARKGPLVPFPNQKSEAAEPPKTPPSSCDSTNA
                                ************************************************

Set8-ENSEMBL-Var4               AIAKQALKKPIKGKQAPRKKAQGKTQQNRKLTDFYPVRRSSRKSKAELQS
Set8-NCBI                       AIAKQALKKPIKGKQAPRKKAQGKTQQNRKLTDFYPVRRSSRKSKAELQS
T8950-Sequencing_Result_[Tra    AIAKQALKKPIKGKQAPRKKAQGKTQQNRKLTDFYPVRRSSRKSKAELQS
                                ************************************************

Set8-ENSEMBL-Var4               EERKRIDELIESGKEEGMKIDLIDGKGRGVIATKQFSRGDFVVEYHGDLI
Set8-NCBI                       EERKRIDELIESGKEEGMKIDLIDGKGRGVIATKQFSRGDFVVEYHGDLI
T8950-Sequencing_Result_[Tra    EERKRIDELIESGKEEGMKIDLIDGKGRGVIATKQFSRGDFVVEYHGDLI
                                ************************************************

Set8-ENSEMBL-Var4               EITDAKKREALYAQDPSTGCYMYYFQYLSKTYCVDATRETNRLGRLINHS
Set8-NCBI                       EITDAKKREALYAQDPSTGCYMYYFQYLSKTYCVDATRETNRLGRLINHS
T8950-Sequencing_Result_[Tra    EITDAKKREALYAQDPSTGCYMYYFQYLSKTYCVDATRETNRLGRLINHS
                                ************************************************

Set8-ENSEMBL-Var4               KCGNCQTKLHDIDGVPHLILIASRDIAAGEELLYDYGDRSKASIEAHPWL
Set8-NCBI                       KCGNCQTKLHDIDGVPHLILIASRDIAAGEELLYDYGDRSKASIEAHPWL
T8950-Sequencing_Result_[Tra    KCGNCQTKLHDIDGVRHLILIASRDIAAGEELLYDYGDRSKASIEAHPWL
                                *************** ********************************

Set8-ENSEMBL-Var4               KH--------------
Set8-NCBI                       KH--------------
T8950-Sequencing_Result_[Tra    KHYASYPYDVPDYAGS
                                **
```

P: Proline R: Arginine HA-tag

Figure 4.2.7: Clustal W multiple sequence alignment of the T8950-Set8 overexpression vector with the Set8 cDNA sequences from NCBI and Ensembl. There is one mismatch between the vector and the cDNA sequences from the databases, which is a reported SNP for this gene (NCBI SNP).

SNU-475 cell line was infected with Set8 vector via lentiviral infection method, as described in the Materials and Methods section. After two weeks of G418 selection, the obtained cell line was named as SNU-475-Set8. Success of the overexpression was confirmed by both Set8 RT-PCR, and HA-tag western blotting, as shown in Figure 4.2.8. After confirming that the overexpression was successful, H4K20me1 levels were also compared between the parental cell line and over expression clone. H4K20me1 levels were determined by western blotting and a more sensitive method, flow cytometry. Results are shown in Figure 4.2.9. According to the results obtained by both methods, Set8 overexpression did not seem to affect H4K20me1 levels in SNU-475 cell line.

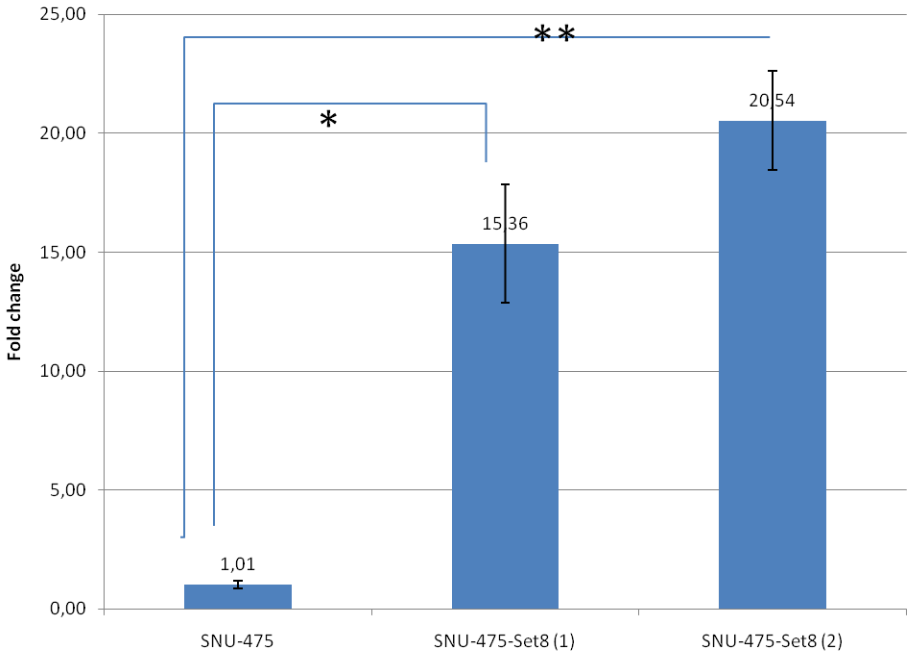

Figure 4.2.8.a: Set8 mRNA levels in parental SNU-475 and Set8 overexpression clones, determined by quantitative RT-PCR. (1) and (2) are from two cell stocks of different freezing date. Fold changes are calculated with respect to parental SNU-475, averages and standard deviations of triplicates are shown. *: p-value < 0,01; **: p-value < 0,005 according to two tailed t-test.

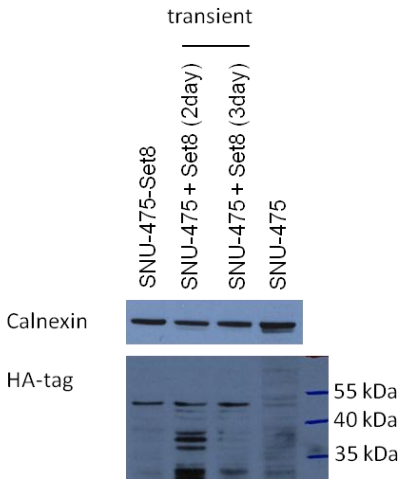

Figure 4.2.8.b: HA-tag immunoblotting in parental SNU-475, SNU-475-Set8, and transiently transfected SNU-475 in whole cell lysates. SNU-475 cells were transiently transfected with Set8 vector to use as a positive control. Calnexin is used as an internal control.

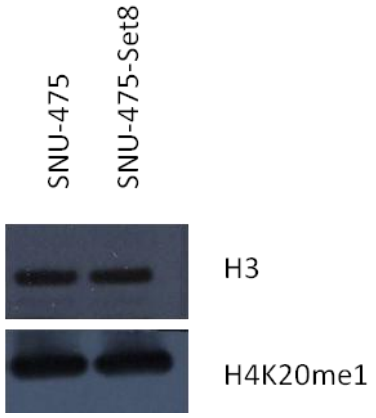

Figure 4.2.9.a: H4K20me1 levels were not affected by Set8 overexpression: western blot. Acid extracted histones were blotted with H4K20me1 and H3 antibodies. Unmodified H3 was used as an internal control.

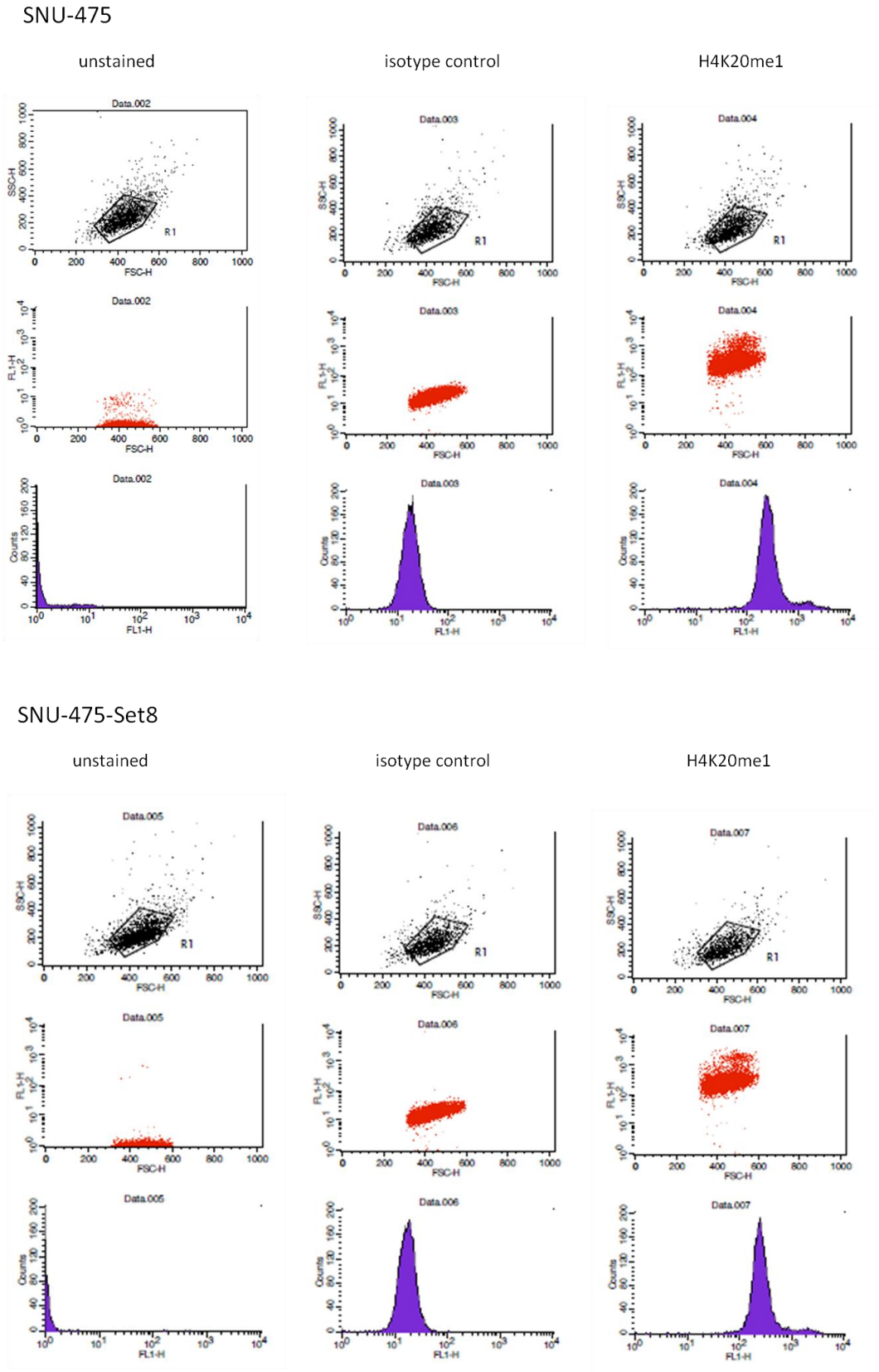

Figure 4.2.9.b: H4K20me1 levels were not affected by Set8 overexpression: flow cytometry. Rabbit IgG was used as isotype control.

4.2.2.4 Comparison of parental SNU-475 and SNU-475-Set8 overexpression clone

SNU-475-Set8 cells were morphologically identical to SNU-475. In order to address the possible effects of Set8 overexpression on cellular growth rate, SNU-475 cell line was compared with parental SNU-475, first in terms of BrdU incorporation. Sub-confluent cells were seeded on coverslips and were labeled with thymidine analog 5-bromo-2-deoxyuridine (BrdU) for 2,5 hours. Cells were then fixed and stained by immunofluorescent staining with anti-BrdU antibody. BrdU positive cells were counted in five different chosen areas under the microscope, and the results are shown in Figure 4.2.10. Although SNU-475-Set8 showed a slightly lower BrdU positivity, the difference was not significant.

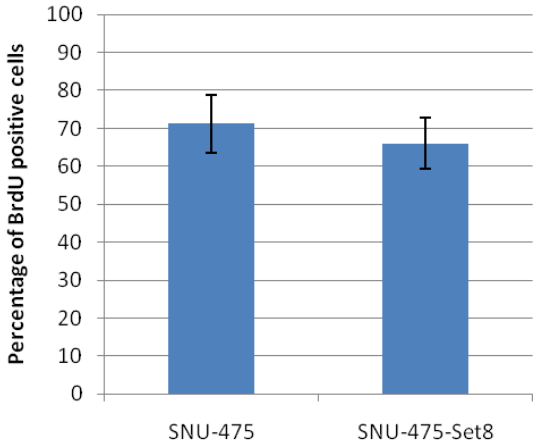

Figure 4.2.10: There is no significant difference between SNU-475 and SNU-475-Set8 in terms of BrdU incorporation. Cells were labeled with BrdU for 2,5 hours, which was followed by immunofluorescent staining of BrdU positive cells. 5 different areas for each sample were counted, averages and standard deviations are shown.

In order to measure the growth rates of the cells more sensitively, cellular growth rates were measured with Roche xCELLigence system, which allows to obtain real-time data about cell number, therefore is a powerful means to address growth rate. SNU-475 and SNU-475-Set8 growth rates were compared with this system with different cell densities and different serum concentrations. The results are shown in Figure 4.2.11.

a)

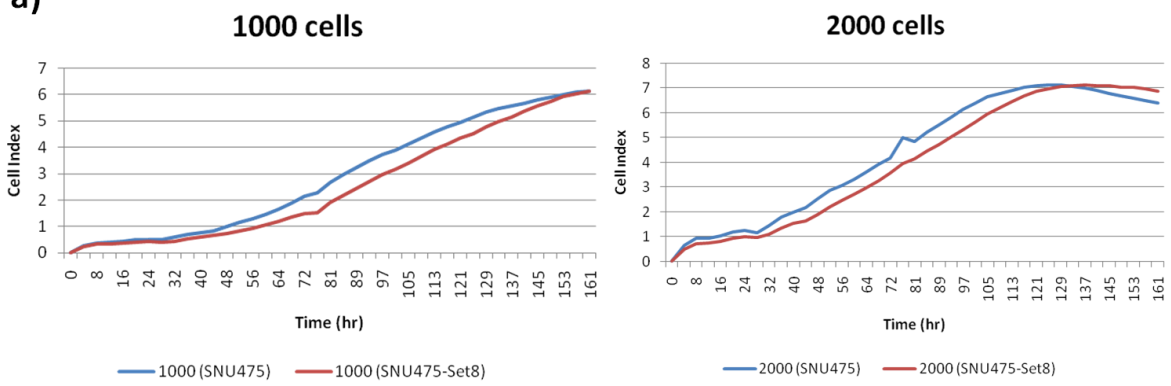

b)

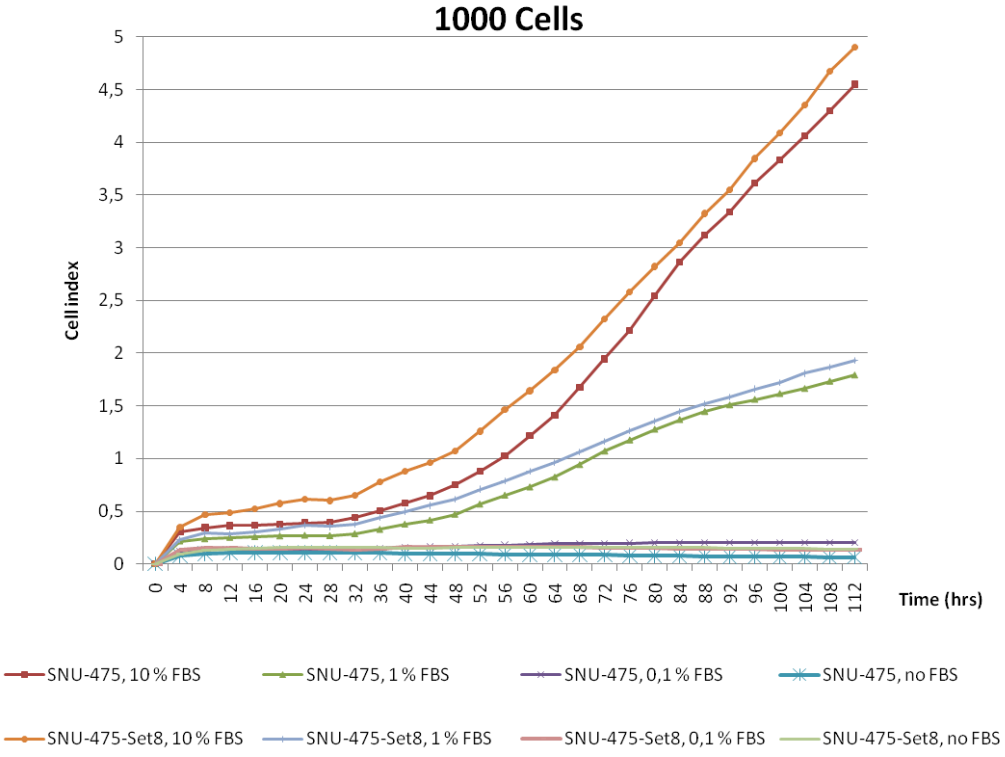

Figure 4.2.11: There is no significant difference between SNU-475 and SNU-475-Set8; determined by xCELLigence system. Two separate experiments were performed in a) and b). In a), 1000 and 2000 cells / well were seeded in complete growth medium with 10 % FBS. According to these results, SNU-475-Set8 growth rate seems slightly lower. In b), 1000 cells / well were seeded with varying serum concentrations as indicated. According to these results, SNU-475 growth rates seems slightly lower, therefore we conclude that the observed differences are not important since they could not be reproduced. There is no observed effect of serum concentration on the difference between SNU-475 and SNU-475-Set8.

4.2.2.5 Set8 siRNA knockdown

As an alternative approach to investigate the potential roles that Set8 might play in HCC development, siRNA knockdown strategy was also employed. Two different Set8 siRNAs were used with a scrambled control, and siRNAs were transfected in HuH-7 cell line which was known to express high levels of Set8. The efficiency of Set8 siRNA knockdown was confirmed by quantitative RT-PCR, and the results are shown in Figure 4.2.12.

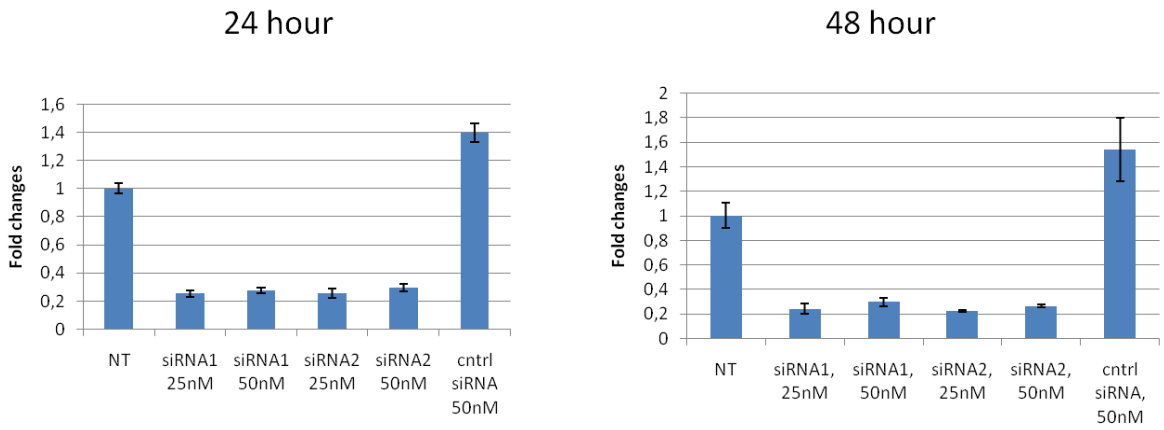

Figure 4.2.12: Set8 siRNA knockdown in HuH-7 cell line. HuH-7 cell line was transfected with the indicated siRNAs using Lipofectamine RNAi max reagent, as described in the materials and methods section. Total RNA was isolated and Set8 mRNA levels were determined by quantitative RT-PCR 24 and 48 hours post transfection. Fold changes are calculated with respect to non transfected, averages and standard deviations of triplicates are shown.

Finally, all the data obtained from immunoperoxidase staining and western blotting of histone methylation marks, and RT-PCR studies of H4K20 methyltransferase enzymes in HCC cell lines were summarized in Table 4.1.

Sub-type	Cell line	Histone Methylation Patterns															Cell line	H4K20 Methyltransferase Levels				
		H3K27me3		H3K4me3		H3K9me3		H3K36me3		H3R2me2		H3R17me2		H4K20me3		H4K20me1		Suv4-20h1		Suv4-20h2		Set8
		TGF-β (-)	TGF-β (+)	TGF-β (-)	TGF-β (+)	TGF-β (-)	TGF-β (+)	TGF-β (-)	TGF-β (+)	TGF-β (-)	TGF-β (+)	TGF-β (-)	TGF-β (+)	TGF-β (-)	TGF-β (+)	Western		Variant1	Variant2	Variant1	Variant2	Variants 1&4
WD	HuH-7	100%	100%	100%	100%	100%	100%	100% nuc + cyt	100% nuc + cyt	100% strong	100% moderate	100%	100%	100% moderate	100% moderate	**	HuH-7	***	**	**	***	***
WD	Hep40	100%	100%	100%	100%	100%	100%	100% nuc + cyt	100% nuc + cyt	100%	100%	100%	100%	100% moderate	100% moderate	***	Hep40	**	*	**	**	*
WD	HepG2	100%	100%	100%	100%	100%	100%	100% nuc + cyt	100% nuc + cyt	100% strong	100% moderate	100%	100%	100% moderate	100% moderate	**	HepG2	**	*	**	**	**
WD	Hep3B	100%	100%	100%	100%	100%	100%	100% nuc + cyt	100% nuc + cyt	100%	100%	100%	100%	100% strong	100% strong	**	Hep3B	***	**	**	**	***
WD	Hep3B-TR	100%	100%	100%	100%	100%	100%	100% nuc + cyt	100% nuc + cyt	100%	100%	100%	100%	100% strong	100% strong	not tested	Hep3B-TR	**	**	**	**	***
WD	PLC/PRF/5	100%	100%	100%	100%	100% nuc + cyt	100% nuc + cyt	100% nuc + cyt	100% nuc + cyt	100%	100%	100%	100%	100% moderate	100% strong	***	PLC/PRF/5	**	*	**	**	**
PD	SNU-182	100%	100%	100%	100%	100%	100%	100% nuc + cyt	100% nuc + cyt	100%	100%	100%	100%	100% moderate	100% moderate	not tested	SNU-182	**	**	**	**	***
PD	SNU-387	100%	100%	60%	80%	100% moderate	100% moderate	100% nuc + cyt	100% nuc + cyt	100%	100%	100%	100%	negative	negative	not tested	SNU-387	***	**	**	**	*
PD	SNU-398	100%	100%	100%	100%	100%	100%	100% nuc + cyt	100% nuc + cyt	100%	100%	100%	100%	negative	negative	not tested	SNU-398	**	*	*	*	*
PD	SNU-423	60%	60%	50%	50%	100% moderate	100% moderate	100% nuc + cyt	100% nuc + cyt	100%	100%	80%	80%	negative	100% weak	not tested	SNU-423	**	*	**	***	*
PD	SNU-449	100%	100%	100%	100%	100% moderate	100% moderate	100% nuc + cyt	100% nuc + cyt	100% weak	100% weak	90%	100%	negative	negative	***	SNU-449	*	*	**	**	**
PD	SNU-475	50%	50%	100%	100%	100%	100%	100% nuc + cyt	100% nuc + cyt	100% moderate	100% moderate	100%	100%	negative	negative	*	SNU-475	***	***	**	**	*
PD	Mahlavu	100%	100%	90%	90%	90%	60%	100% nuc + cyt	100% nuc + cyt	100% weak	100% weak	100%	100%	negative	negative	***	Mahlavu	**	**	**	**	*
PD	FOCUS	80%	80%	100%	100%	100%	100%	100% nuc + cyt	100% nuc + cyt	100% moderate	100% moderate	100%	100%	100% weak	100% weak	*	FOCUS	*	*	**	**	*
PD	SK-HEP-1	70%	90%	70%	80%	70%	60%	100% nuc + cyt	100% nuc + cyt	100% moderate	100% moderate	80%	80%	100% weak	100% weak	not tested	SK-HEP-1	*	*	**	**	*

Table 4.1: Summary of histone methylation marks and H4K20 methyltransferase levels in HCC cell lines. WD is well differentiated, PD is poorly differentiated. For the histone methylation patterns, results of immunoperoxidase staining experiments were summarized. Percentages of positive cells are indicated together with staining features. Nuc: nuclear staining, cyt: cytoplasmic staining.

CHAPTER 5. DISCUSSION

In the first part of this study, we investigated the involvement of global levels of several histone modifications in HCC pathogenesis. As mentioned earlier, senescence, which is a characteristic of liver cirrhosis, acts as a barrier in front of tumorigenesis in the liver. The transition from cirrhosis to HCC is very important to understand the pathogenesis of HCC, which necessitates to understand the mechanisms involved in senescence bypass. Additionally, non cell autonomous senescence, which is induced by various stimuli is a promising phenomenon to be utilized in anti-cancer therapy (Senturk S, et al, 2010). In order to study the differences between immortal and senescent HCC cells, we used TGF-β induced senescence as a model in our cell line panel.

It is an issue of debate whether the histone modifications in gene specific promoters are more important in biological processes, or global levels of certain histone modifications also carry information related to pathogenesis. In a recent study, global levels of H3K4me2, H3K18-ac and H3K9me2 were attributed prognostic significance in different cancer types (Seligson DB, et al, 2009). In our study, we investigated the involvement of several histone methylations, which are: H3K4me3, H3K9me3, H3K27me3, H3K36me3, H3R2me2, H3R17me2 and H4K20me3, in the development of HCC by using a cell line panel of 15 HCC cell lines, including well and poorly differentiated ones, in the case of senescence and immortality. The results we obtained however, did not reveal a prominent change in the global levels of any of these histone marks with respect to TGF-β induced senescence. This suggests global levels of the histone marks we studied are not affected by TGF-β induced senescence, although it is also a possibility that the difference might be beyond the sensitivity of immunoperoxidase staining method.

Histone 4 Lysine 20 trimethylation levels were observed to drop evidently in poorly differentiated HCC cell lines with respect to well differentiated cell lines, and this was consistently seen in both immunoperoxidase staining and western blotting experiments. This observation was in accordance with what was expected, since the loss of H4K20me3 is a common phenomenon in various cancer types, and since poorly differentiated cell lines represent advanced stages of HCC, and well differentiated cell lines represent earlier stages. Although not as obvious as trimethyl levels, monomethylated H4K20 levels also followed a similar pattern, as observed by western blotting. Therefore these data gave us a clue about the importance of H4K20 methylation in HCC.

Given that there are only three known methyltransferase enzymes which act on H4K20 residue, and there is no currently identified demethylase enzyme acting on this residue, we reasoned that one or more of the methyltransferases must be responsible for the global loss of H4K20me3 in poorly differentiated HCC cell lines. All different transcript variants of these genes were analyzed in our cell line panel by using specific primers for each. The initial analysis was performed by semi-quantitative RT-PCR. Some of the analyzed variants were not expressed in HCC cell lines, therefore only the positive variants were evaluated. According to the RT-PCR data, none of the variants of Suv4-20h1 or Suv4-20h2 correlated with H4K20me3 levels, which was quite surprising given that these are the enzymes that mediate the trimethylation of this residue. Nevertheless, the correlation between Set8 expression pattern and the H4K20 methylation pattern was impressive. After confirming this via quantitative PCR, we also analyzed Set8 expression levels in patient samples of HCC-cirrhotic paired tissues. We were unable to draw a conclusion about Set8 levels in normal tissues compared to the pathological samples, however in 4 of the 5 paired samples, HCC tissue showed lower levels of Set8 expression in comparison to the cirrhotic samples. This was also in support of what we had *in vitro*. Hence, we started to consider Set8 as a candidate to be responsible for the altered H4K20me3 levels in HCC; in our model poorly differentiated cell lines.

In order to address a potential role for Set8 in HCC development, first we decided to employ overexpression strategy and analyze the newly obtained phenotype. For this purpose, we chose SNU-475 cell line to overexpress Set8 gene, since this was the cell line with the lowest expression values according to the quantitative PCR data. We obtained SNU-475-Set8 cell line via lentiviral infection of SNU-475 cell line with Set8 overexpression vector. The success of the overexpression was evaluated via several methods. Firstly, we used HA-tag immunoblotting, since our vector contained a C-terminal HA tag. The immunoblotting confirmed the expression of HA-tag, however that did not tell us much about neither the percentage of the cells that expressed the HA-tagged Set8, nor the extent of the overexpression. We tried confirmation with a Set8 specific antibody from Abcam, however the bands recognized by this antibody did not overlap with the HA-tag bands, and the recognized protein did not migrate as expected from Set8 protein (data not shown). Therefore we concluded the antibody recognized nonspecific bands, and we did not use that data. Next, we wanted to analyze the overexpression by immunofluorescent staining with the HA-tag antibody, however this was unsuccessful and we could not address HA-tagged Set8 levels by this method as well. The final strategy that we followed was evaluating H4K20me1 levels between the parental cell line and the overexpression clone. For this purpose, we used two techniques: western blotting and flow cytometry, and both revealed no changes between H4K20me1 levels. This might stem from multiple reasons. Firstly, the overexpression of Set8 might not be as effective to result in a change in H4K20me1 levels, since histones are very ubiquitous substrates and very high amount of protein might be required to make a recognizable change, although it should always be kept in mind that histones are not the only substrates of Set8 enzyme, and there can also be other proteins that Set8 can exert its effects on. Second, it might be beyond the sensitivity of the techniques we used to recognize the obtained change. Finally, it is also possible that there might be a compensatory mechanism in the cell that counteracts the newly introduced activity of overexpressed Set8 enzyme, such as the activity of an unidentified demethylase enzyme.

Even though the confirmation we could provide for the overexpression of Set8 in SNU-475 cell line was not completely robust, we assessed the changes associated with the overexpression of this protein. There were no initial morphological changes that we could observe following the overexpression. The first phenotypic effect we wanted to analyze was cellular growth rate. This was evaluated by BrdU incorporation, and much more sensitively with xCELLigence system. Neither of the methods revealed a significant difference between the tested cells. This suggests that Set8 overexpression does not have a role on the cellular growth rate of SNU-475 cell line, although it should also be kept in mind that this could be a misinterpretation because of the ineffectiveness of the overexpression.

Alternatively, siRNA mediated knockdown was used as a new approach to the question in mind. HuH-7 cell line was chosen for the siRNA mediated knockdown due to its high expression of Set8, according to the qRT-PCR data. Although the knockdown was confirmed via qRT-PCR, confirmation at the protein level and the assessment of the effects of the knockdown remains to be worked on.

Taken as a whole, according to the data obtained from this study, we were unable to identify a specific role of Set8 methyltransferase enzyme in the development of hepatocellular carcinoma. The intriguing question of whether the loss of H4K20me3 histone mark in hepatocellular carcinoma has a causative relationship with the pathogenesis of HCC, or this is just a correlation, remains unanswered. It is also a possibility that the alterations in the methionine metabolism, rather than the methyltransferase enzymes might be responsible for the loss of H4K20me3 levels, and might be influential in the development of HCC.

CHAPTER 6. FUTURE PERSPECTIVES

First of all, when working with global histone modifications, more sensitive methods such as flow cytometry or top down mass spectrometry could be used to obtain better results with higher precision. The screening study of global histone modifications in senescent and immortal cells could be repeated with such a technique. Also, gene promoter specific histone modification changes could be addressed by using specific candidate gene sets which are known to be involved in the mechanism of cellular senescence. Since our group has an already identified senescence – immortality gene set, that might be utilized in this respect.

In order to further address the potential roles played by the Set8 gene, the siRNA knockdown study should be completed, first by proper confirmation of the knockdown in the protein level. The levels of H4K20me1 and H4K20me3 can still be unaffected from this knockdown, because the Suv4-20h enzymes can also use the monomethylated form as a substrate, and they might compensate for the loss of Set8. Nevertheless, the big question regarding the issue of the histone code hypothesis also applies here: is it the particular histone modifications that are more important, or is it the enzymes that mediate these effects? Even though the siRNA knockdown ends up not affecting the histone modification levels, Set8 enzyme knockdown, even to a limited extent might reveal other important roles of Set8 enzyme, when it acts through other substrates.

Additionally, Set8 stable over expression could be repeated to obtain more clones, and the most efficiently overexpressed clone can be selected. Therefore, a more powerful model will be obtained. Taken as a whole, Set8 enzyme is worth investigating more as a candidate gene to be involved in hepatocarcinogenesis.

CHAPTER 7. REFERENCES

American Cancer Society, (2010). Cancer Facts & Figures 2010. Atlanta: American Cancer Society

Badvie, S. (2000). Hepatocellular carcinoma. *Postgrad. Med.J*., 76, 4–11

Barski, A., Cuddapah, S., Cui, K., Roh, T. Y., Schones, D. E., Wang, Z.,… Zhao, K., (2007). High-Resolution Profiling of Histone Methylations in the Human Genome. *Cell,* 129, 823-837

Bartkova, J., Rezaei, N., Liontos, M., Karakaidos, P., Kletsas, D., Issaeva, N.,… Gorgoulis, V. G., (2006). Oncogene-induced senescence is part of the tumorigenesis barrier imposed by DNA damage checkpoints. *Nature*, 444, 633-637

Boyault, S., Rickman, D. S., de Reyniès, A., Balabaud, C., Rebouissou, S., Jeannot, E.,… Zucman-Rossi J., (2007). Transcriptome Classification of HCC Is Related to Gene Alterations and to New Therapeutic Targets. *Hepatology*, 45, 42-52

Bruix, J., Boix, L., Sala, M. & Llovet, J. M., (2004). Focus on hepatocellular carcinoma. *Cancer Cell*, 5, 215-9

Buschbeck, M., Di Croce, L., (2010). Approaching the molecular and physiological function of macroH2A variants. *Epigenetics*, 5, 118-23

Cagatay, T. & Ozturk, M., (2002). P53 mutation as a source of aberrant beta-catenin accumulation in cancer cells. *Oncogene*, 21, 7971-80

Delaval, K., Feil, R., (2004). Epigenetic regulation of mammalian genomic imprinting. *Current Opinion in Genetics & Development*, 14, 188-195

Delcuve, G. P., Rastegar, M. & Davie, J. R., (2009). Epigenetic Control. *J. Cell. Physiol.,* 219, 243-250

Di Micco, R., Fumagalli, M., Cicalese, A., Piccinin, S., Gasparini, P., Luise, C.,… d'Adda di Fagagna, F., (2006). Oncogene-induced senescence is a DNA damage response triggered by DNA hyper-replication. *Nature*, 444, 638-642

Dimri, G. P., Lee, X., Basile, G., Acosta, M. *et al*., (1995). A biomarker that identifies senescent human cells in culture and in aging skin in vivo. *PNAS*, 92, 9363-7

Ellis, L., Atadja, P. W. & Johnstone, R. W., (2009). Epigenetics in cancer: Targeting chromatin modifications. *Mol Cancer Ther*., 8, 1409-1420

Esteller, M., (2007). Cancer epigenomics: DNA methylomes and histone-modification maps. *Nature Reviews Genetics*, 8, 286-298

Farazi, P. A. & DePinho, R. A., (2006). Hepatocellular carcinoma pathogenesis: from genes to environment. *Nature Reviews Cancer* , 6, 674-687

Feinberg, A. P., (2010). Genome-scale approaches to the epigenetics of common human disease. *Virchows Arch*., 456, 13-21

Feo, F., Frau, M., Tomasi, M. L., Brozzetti, S., & Pascale, R. M., (2009). Genetic and Epigenetic Control of Molecular Alterations in Hepatocellular Carcinoma. *Exp Biol Med*, 234, 726-36

Fraga, M., Ballestar, E., Villar-Garea, A., Boix-Chornet, M., Espada, J., Schotta, G.,.... Esteller, M., (2005). Loss of acetylation at Lys16 and trimethylation at Lys20 of histone H4 is a common hallmark of human cancer. *Nature Genetics*, 37, 391-400

Hellman, A. & Chess, A., (2007). Gene body-specific methylation on the active X chromosome. *Science*, 315, 1141-1143

Herceg, Z., (2007). Epigenetics and cancer: towards an evaluation of the impact of environmental and dietary factors. *Mutagenesis*, 22, 91-103

Hubbard T. J. P., Aken B. L., Beal K., Ballester B., Caccamo M., Chen L., … Bimey E., (2007). Ensembl. *Nucleic Acid Res*., 35, 610-617

Huen, M. S. Y., Sy, S. M. H., van Deursen, J. M. & Chen, J., (2008). Direct interaction between SET8 and proliferating cell nuclear antigen couples H4-K20 methylation with DNA replication. *Journal of Biological Chemistry*, 283, 11073-11077

Jelinic, P., Shaw, P., (2007). Loss of imprinting and cancer. *Journal of Pathology*, 211, 261-268

Jørgensen, S., Elvers, I., Trelle, M. B., Menzel1, T., Eskildsen, M., Jensen, O. N.,… Sørensen, C. S., (2007). The histone methyltransferase SET8 is required for S-phase progression. *JCB*, 179, 1337-1345

Kalakonda, N., Fischle, W., Boccuni, P., Gurvich, N., Hoya-Arias, R., Zhao, X.,… Nimer SD. (2008). Kalakonda, N et. al, Histone H4 lysine 20 monomethylation promotes transcriptional represion by L3MBTL1. *Oncogene*, 27, 4293-4304

Kojiro M., (2005). Histopathology of liver cancers. *Best Pract Res Clin Gastroenterol*, 19, 39-62.

Kouzarides T., (2007). Chromatin Modifications and Their Function. *Cell*. 128, 693-705

Maglott, D., Ostell, J., Pruitt, K. D., and Tatusova, T. (2005). Entrez gene: gene-centered information at ncbi. *Nucleic Acids Res*, 33(Database issue)

Mallette, F. A., Gaumont-Leclerc, M. F. & Ferbeyre, G. (2007). The DNA damage signaling pathway is a critical mediator of oncogene-induced senescence. *Genes Dev*., 21, 43-48

Matouk, I. M., DeGroot, N., Mezan, S., Ayesh, S., Abu-lail, R., Hochberg, A., Galun, E., (2007). The H19 non-coding RNA is eseential for human tumor growth. *Plos One*, 2, e845

Mietton, F., Sengupta, A. K., Molla, A., Picchi, G., Barral, S., Heliot, L.,… Dimitrov, S., (2009). Weak but unifrom enrichment of histone variant macroH2A1 along the inavtive X chromosome. *Molecular and Cellular Biology*, 29, 150-156

Ozturk, M., Arslan-Ergul, A., Bagislar, S., Senturk, S. & Yuzugullu, H., (2009). Senescence and immortality in hepatocellular carcinoma. *Cancer Lett.*, 286, 103-13

Paradis, V., Youssef, N., Dargère, D., Bâ, N., Bonvoust, F., Deschatrette, J., Bedossa, P., (2001). Replicative Senescence in Normal Liver, Chronic Hepatitis C, and Hepatocellular Carcinomas. *Hum Pathol.*, 32, 327-32

Pogribny, I. P., Ross, S. A., Tryndyak, V. P., Pogribna, M., Poirier, M. A. & Karpinets, T. V., (2006). Histone H3 lysine 9 and H4 lysine 20 trimethylation and the expression of Suv4-20 and Suv-39h1 histone methyltransferases in hepatocarcinogenesis induced by methyl deficiency in rats. *Carcinogenesis*, 27, 1180-1186

Rhead B., Karolchik D., Kuhn R. M., Hinrichs A. S., Zweig A. S., Fujita P., …, Kent W. J., The UCSC Genome Browser database: update 2010. *Nucleic Acids Res*. 2010 Jan;38(Database issue):D613-9. Epub 2009 Nov 11

Rozen S, Skaletsky H (2000) Primer3 on the WWW for general users and for biologist programmers. In: Krawetz S, Misener S (eds) Bioinformatics Methods and Protocols: Methods in Molecular Biology. *Humana Press, Totowa, NJ*, pp 365-386

Scharf, A. N. D., Meier, K., Seitz, V., Kremmer, E., Brehm, A. & Imhof A., (2009). Monomethylation of lysine 20 on histone h4 facilitates chromatin maturation. *Molecular and Cellular Biology*, 29, 57-67

Seligson, D. B., Horvath, S., McBrian, M. A., Mah, V., Yu, H., Tze, S. (2009). Global levels of histone modifications predict prognosis in different cancers. Am J Pathol., 174, 1619-28

Senturk, S., Mumcuoglu, M., Gursoy-Yuzugullu, O., Cingoz, B., Akcali, K. C. & Ozturk M. (2010). Transforming growth factor-beta induces senescence in hepatocellular carcinoma cells and inhibits tumor growth. *Hepatology*, [Epub ahead of print]

Sha, K., (2008). A Mechanistic view of genomic imprinting. *Annu. Rev. Genom. Human Genet.*, 9, 197-216

Shechter, D., Dormann, H. L., Allis, D. C. & Hake, S. B., (2007). Extraction, purification and analysis of histones. *Nature Protocols*, 2, 1445-1457

Shi, X., Kachirskaia, I., Yamaguchi, H., West, L. E., Wen, H., Wang, E. W.,… Gozani, O., (2007). Modulation of p53 Function by SET8-Mediated Methylation at Lysine 382. *Molecular Cell*, 27, 636–646

Soussi, T., (2007). p53 alterations in human cancer: more questions than answers. *Oncogene*, 26, 2145-56

Subramaniam, S. (1998) The Biology Workbench--a seamless database and analysis environment for the biologist. *Proteins*, 32, 1-2

Talbert, P. B & Henikoff, S., (2010). Histone variants — ancient wrap artists of the epigenome. *Nature Reviews Molecular Cell Biology*, 11, 264-275

The UniProt Consortium (2010). The Universal Protein Resource (UniProt) in 2010. Nucleic Acids Research, 38, D142-D148

Trojer, P. & Reinberg, D., (2006). Hypothesis Histone Lysine Demethylases and Their Impact on Epigenetics. *Cell*, 125, 213-217

Tryndyak, V. P., Kovalchuk, O. & Pogribny, I. P., (2006). Loss of DNA methylation and histone H4 lysine 20 trimethylation in human breast cancer cells is associated with aberrant expression of DNA methyltransferase 1, Suv4-20h2 histone methyltransferase and methyl-binding proteins. *Cancer Biology & Therapy*, 5, 65-70

Wang, G. G., Allis, C. D. & Chi, P., (2007). Chromatin remodeling and cancer, part I: covalent histone modifications. *Trends in Molecular Medicine*, 13, 363-372

Weinberg, R. A. (2006). The Biology of Cancer. *Garland Science*

Wiemann, S. U., Satyanarayana, A., Tsahuridu, M., Tillmann, H., Zender, L., Klempnauer, J.,… Rudolph, K. L., (2002). Hepatocyte telomere shortening and

senescence are general markers of human liver cirrhosis. *The FASEB Journal*, 16, 935-942

Wong, C. M., Ng, I. O. L., (2007). Molecular pathogenesis of hepatocellular carcinoma. *Liver Internationa*l, 28, 160-174

Wu, J., Qin, Y., Li, B., He, W. Z., Sun, Z. L. (2008). Hypomethylated and hypermethylated profiles of *H19*DMR are associated with the aberrant imprinting of *IGF2* and *H19* in human hepatocellular carcinoma. *Genomics*, 91, 443-450

Van Den Broeck, A., Brambilla, E., Moro-Sibilot, D., Lantuejoul, S., Brambilla, C., Eymin, B., Khochbin, S. & Gazzeri, S., (2008). Loss of histone H4K20 trimethylation occurs in preneoplasia and influences prognasis of non-small cell lung cancer. *Clinical Cancer Research,* 14, 7237- 7245

Yang, H., Mizzen, C. A., (2009). The multiple facets of histone H4-lysine 20 methylation. *Biochem. Cell Biol.*, 87, 151-161

Yang, X. J., (2004). The diverse superfamily of lysine acetyltransferases and their roles in leukemia and other diseases. *Nucleic Acids Research*, 32, 959-976

Yin, Y., Yu, V. C., Zhu, G., Chang, D. C., (2008). SET8 plays a role in controlling G_1/S transition by blocking lysine acetylation in histone through binding to H4 N-terminal tail. *Cell Cycle*, 7, 1423-1432

Yuzugullu, H., Benhaj, K., Ozturk, N., Senturk, S., Celik, E., Toylu, E.,..., Ozturk, M., (2009). Canonical Wnt signaling is antagonized by noncanonical Wnt5a in hepatocellular carcinoma cells. *Molecular Cancer*, 8:90

Zhang, R., Poustovoitov, M. V., Ye, X., Santos, H. A., Chen, W., Daganzo, S. M.,… Adams, P. D., (2005). Formation of MacroH2A-Containing Senescence-Associated Heterochromatin Foci and Senescence Driven by ASF1a and HIRA. *Dev Cell*., 8, 19-30